Molecular elucidation of the physiological significance of Ca^{2+} channelsome in neuronal function

Yoshinori Takada

2015

Preface

The studies presented in this thesis have been carried out under the direction of Professor Yasuo Mori at the Laboratory of Molecular Biological Chemistry, Department of Synthetic Chemistry and Biological Chemistry, Graduate School of Engineering, Kyoto University during April 2010 to September 2015. This thesis aims to elucidate the significance of Ca^{2+} channel complexes in neuronal function.

It is the greatest pleasure to me to express my sincere gratitude to Professor Yasuo Mori for his guidance, valuable suggestion and encouragement throughout these studies.

I am also deeply grateful to Professor Toshihisa Ohtsuka, Department of Biochemistry, Graduate School of Medicine/Faculty of Medicine, University of Yamanashi, Associate professor Shigeki Kiyonaka, Associate professor Masayuki X Mori, Assistant professor Tomohiro Numata, Assistant professor Tatsuki Kurokawa, Assistant professor Reiko Sakaguchi, Department of Synthetic Chemistry and Biological Chemistry, Graduate School of Engineering, Kyoto University.

I sincerely appreciate Dr. Isao Shimizu, Dr. Takeo Ishiyama, Dr. Kazuhito Ikeda, Dr. Ryu Nagata and Dr. Yoshihiro Oyamada, Drug Research Division, Sumitomo Dainippon Pharma Co., Ltd, giving an opportunity to study this research at Kyoto University.

The accomplishments described in this thesis could not have been achieved without the efforts of many colleagues. I should be emphasized that the contribution of Dr. Yoshitsugu Uriu, Mr. Hiroshi Nakajima, Mr. Mitsuru Hirano, Mr. Yoshifumi Ueda, Mr. Kazuma Yamaguchi, and Ms. Keiko Nakahara, who participated in some work presented here, are greatly appreciated. I should be also express great gratitude to Dr. Nobuaki Takahashi, Dr. Akito Nakao, and Mr. Seishiro Sawamura for heartwarming assistance.

I owe all members of Professor Mori’s laboratory a great depth of gratitude for their constant encouragement throughout this work.

I express great gratitude to my family and friends who had supported me to complete my thesis, for their kind understanding of my career decision and heartwarming assistance.

Yoshinori Takada

Laboratory of Molecular Biological Chemistry

Department of Synthetic Chemistry and Biological Chemistry

Graduate School of Engineering

Kyoto University

Contents

General Introduction 1

Chapter 1 Physical and functional interaction of the active zone protein CAST /ERC2 and the β-subunit of the voltage-dependent Ca^{2+} channel 6

Chapter 2 Functional impacts of Munc18-1 on gating properties of voltage-dependent Ca^{2+} channels 29

Chapter 3 Rab3 interacting molecule 3 mutations associated with autism alter regulation of voltage-dependent Ca^{2+} channels 52

Chapter 4 Tankyrase contributes to the risk of spinocerebellar ataxia type 6 by binding of the C-terminal of voltage-dependent Ca^{2+} channels 78

General Conclusion 102

List of Publications 104

General Introduction

Physiological significance of Ca^{2+}

Various inorganic ions have different composition inside and outside cells. Among them, the concentration of Ca^{2+} inside the cell is tightly regulated, which is ten thousand times lower than one outside the cell [1]. Ca^{2+} influx across the plasma membrane plays a vital role in regulating diverse cellular processes, ranging from ubiquitous activities like gene expression to tissue-specific functions such as neurotransmitter release and muscle contraction, by controlling the intracellular free Ca^{2+} concentration [2]. By contrast, the dysregulation of this Ca^{2+} homeostasis leads to various pathological conditions, for example ischemic cell death, neural degeneration, cerebellar ataxia, mental retardation and heart failures. Therefore, Ca^{2+} ion is essential for cell fate. This Ca^{2+} influx from the extracellular compartment are mediated by three groups of channels: voltage-dependent Ca^{2+} channels (VDCCs), ligand-gated Ca^{2+} channels (neurotransmitter receptors), and non-classical Ca^{2+} channels belonging to neither group (Fig. 1).

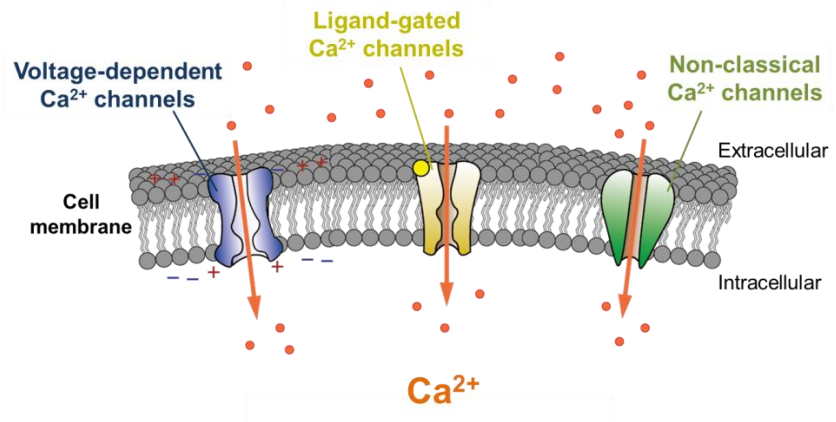

Fig. 1 Classes of Ca^{2+}-permeable ion channels.

Ca^{2+} channelsomes

As mentioned above, Ca^{2+} entry channels play essential biological roles primarily through the transportation of Ca^{2+} ions from extracellular to intracellular compartment. In addition to the role as ion transportation, Ca^{2+} channels also play roles to integrate and coordinate biological functions at different levels, ranging from the subcellular to multicellular scales. This is underpinned by efficient functional coupling within molecular

assemblies of channels, various cytomatrix proteins, small molecules and lipids (Fig. 2). These molecular assemblies, called as “channelsomes”, can be considered as physiological functional units [3].

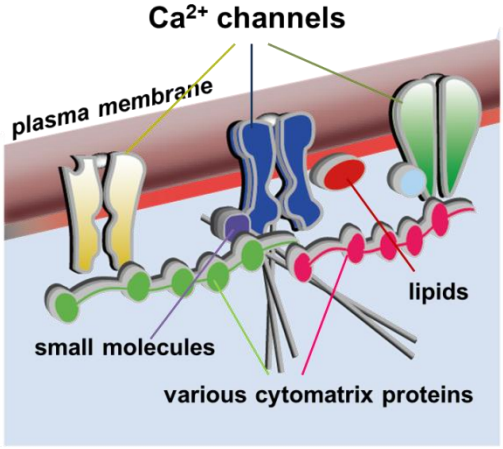

Fig. 2 Ca^{2+} channelsomes.

Ca^{2+} channelsomes involved in neurotransmission

Neurotransmitter release is regulated by presynaptic Ca^{2+} influx after membrane depolarization. Especially, Ca^{2+} influx into presynaptic nerve terminals via VDCC is an essential step in neurotransmitter release [4]. The predominant Ca^{2+} channel species in synaptic nerve terminals are P/Q-type $Ca_V2.1$ and N-type $Ca_V2.2$ channels, with their relative levels of expression varying across the nervous system [5]. The different distributions of these two channels are reflected in their distinct physiological and pathological roles. However, their activity is regulated by common mechanisms, and these channels function as part of larger signaling channelsomes that enable their precise regulation and subcellular targeting.

VDCCs

Multiple types of VDCCs are distinguished on the basis of biophysical and pharmacological properties [6]. In neurons, high voltage-activated VDCC types such as N-, P/Q-, R-, and L-types are essential for neurotransmitter release from presynaptic terminals [7-9]. Furthermore, presynaptic VDCCs are considered to serve as the regulatory node in a dynamic, multilayered signaling network that exerts short-term control of neurotransmission in response to synaptic activity [10]. Biochemically, VDCCs are known as

heteromultimeric protein complexes composed of the pore-forming α_1, designated as Ca_V, and auxiliary subunits α_2/δ, β, and γ (Fig. 3A) [11]. The Ca_V α_1-subunit is encoded by ten distinct genes, whose correspondence with functional types has already been largely elucidated (Fig. 3B) [6]. β-subunit, which is encoded by four distinct genes, interacts with α_1 from the cytoplasmic side to enhance functional channel trafficking to the plasma membrane [12, 13] and to modify multiple kinetic properties (Fig. 3C) [14, 15]. Considering the cytoplasmic disposition of β-subunits, it is intriguing to investigate whether β-subunits are involved in targeting specific subcellular machinery to VDCC channelsomes at presynaptic subcellular structure called the active zone for neurotransmitter release through as yet unidentified protein interactions.

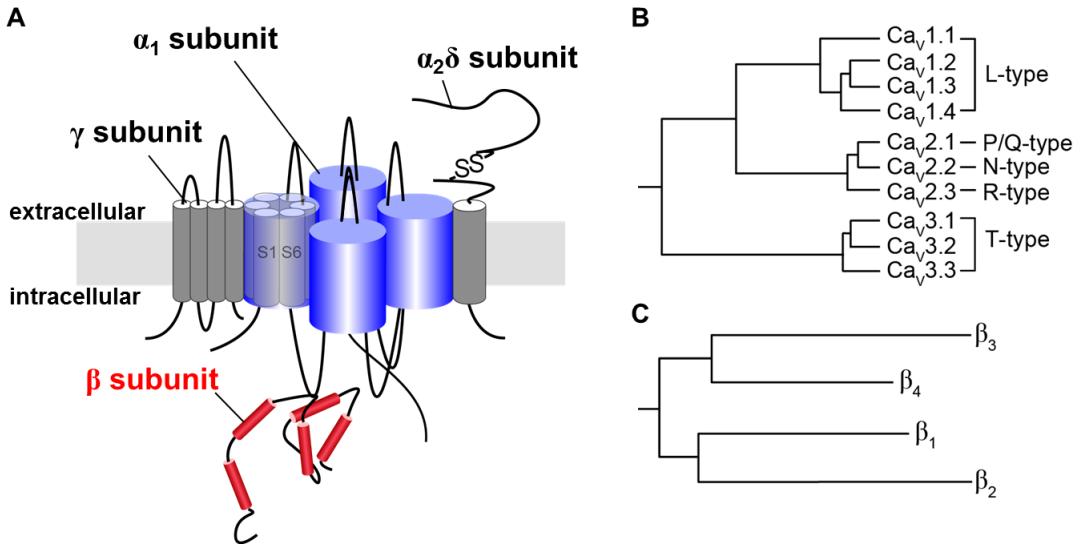

Fig. 3 Voltage-dependent Ca^{2+} channel. (A) Schematic model of VDCC complex. (B) Phylogenic tree of α_1-subunits. (C) Phylogenic tree of β-subunits.

Ca^{2+} signaling involved in neuronal disorders

Several genetic approaches have revealed that mutations in VDCC genes are implicated in the neuronal disorders. Timothy syndrome, characterized by physical malformations including heart QT-prolongation, heart arrhythmias, and autism spectrum disorders, is caused by mutations in *CACNA1C*, the gene encoding L-type $Ca_V1.2$ [16]. Missense mutations in *CACNA1A* gene encoding $Ca_V2.1$ underlie several neurological disorders, including familial hemiplegic migraine, episodic ataxia type 2, and spinocerebellar ataxia type 6 [17-19]. These disorders seem to be involved with the functional dysregulation in cellular Ca^{2+} signaling, yet the

precise pathological mechanisms have been elusive.

Survey of this thesis

This thesis consists of four chapters on VDCCs. The first two chapters describe the physiological role of novel VDCC complexes in neurotransmission, focused on VDCC-β interacting proteins. The second two chapters describe the physiological role of VDCC complexes in neuronal pathological conditions.

Reference

[1] Clapham, D. E. (1995) *Cell*, **80**, 259-268

[2] Berridge, M. J., Lipp, P., and Bootman, M. D. (2000) *Nat. Rev. Mol. Cell Biol.*, **1**, 11-21

[3] Mori, Y., Kiyonaka, S., and Kanai, Y. (2011) *Channels (Austin)*, **5**, 387-390

[4] Reid, C. A., Bekkers, J. M., and Clements, J. D. (2003) *Trends Neurosci.*, **26**, 683-687

[5] Ishikawa, T., Kaneko, M., Shin, H., and Takahashi, T. (2005) *J. Physiol.*, **568**, 199-209

[6] Tsien, R. W., Ellinor, P. T., and Horne, W. A. (1991) *Trends Pharmacol. Sci.*, **12**, 349-354

[7] Takahashi, T., and Momiyama, A. (1993) *Nature*, **366**, 156-158

[8] Wheeler, D. B., Randall, A., and Tsien, R. W. (1994) *Science*, **264**, 107-111

[9] Catterall, W. A. (1998) *Cell Calcium*, **24**, 307-323

[10] Catterall, W. A., and Few, A. P. (2008) *Neuron*, **59**, 882-901

[11] Ertel, E. A., Campbell, K. P., Harpold, M. M., Hofmann, F., Mori, Y., Perez-Reyes, E., Schwartz, A., Snutch, T. P., Tanabe, T., Birnbaumer, L., Tsien, R. W., and Catterall, W. A. (2000) *Neuron*, **25**, 533-535

[12] Mori, Y., Friedrich, T., Kim, M. S., Mikami, A., Nakai, J., Ruth, P., Bosse, E., Hofmann, F., Flockerzi, V., Furuichi, T., Mikoshiba K., Imoto K., Tanabe T., and Numa S. (1991) *Nature*, **350**, 398-402

[13] Bichet, D., Cornet, V., Geib, S., Carlier, E., Volsen, S., Hoshi, T., Mori, Y., and De Waard, M. (2000) *Neuron*, **25**, 177-190

[14] Varadi, G., Lory, P., Schultz, D., Varadi, M., and Schwartz, A. (1991) *Nature*, **352**, 159-162

[15] Lacerda, A. E., Kim, H. S., Ruth, P., Perez-Reyes, E., Flockerzi, V., Hofmann, F., Birnbaumer, L., and

Brown, A. M. (1991) *Nature*, **352**, 527-530

[16] Splawski, I., Timothy, K. W., Sharpe, L. M., Decher, N., Kumar, P., Bloise, R., Napolitano, C., Schwartz, P. J., Joseph, R. M., Condouris, K., Tager-Flusberg, H., Priori, S. G., Sanguinetti, M. C., and Keating, M. T. (2004) *Cell*, **119**, 19-31

[17] Ophoff, R. A., Terwindt, G. M., Vergouwe, M. N., van Eijk, R., Oefner, P. J., Hoffman, S. M., Lamerdin, J. E., Mohrenweiser, H. W., Bulman, D. E., Ferrari, M., Haan, J., Lindhout, D., van Ommen, G. J., Hofker, M. H., Ferrari, M. D., and Frants, R. R. (1996) *Cell*, **87**, 543-552

[18] Yue, Q., Jen, J. C., Nelson, S. F., and Baloh, R. W. (1997) *Am. J. Hum. Genet.*, **61**, 1078-1087

[19] Zhuchenko, O., Bailey, J., Bonnen, P., Ashizawa, T., Stockton, D. W., Amos, C., Dobyns, W. B., Subramony, S. H., Zoghbi, H. Y., and Lee, C. C. (1997) *Nat. Genet.*, **15**, 62-69

Chapter 1

Physical and functional interaction of the active zone protein CAST/ERC2 and the β-subunit of the voltage-dependent Ca^{2+} channel

Abstract

In the nerve terminals, the active zone protein CAST/ERC2 forms a protein complex with the other active zone proteins ELKS, Bassoon, Piccolo, RIM1 and Munc13-1, and is thought to play an organizational and functional role in neurotransmitter release. However, it remains obscure how CAST/ERC2 regulates the Ca^{2+}-dependent release of neurotransmitters. Here, we show an interaction of CAST with voltage-dependent Ca^{2+} channels (VDCCs) which are essential for regulating neurotransmitter release triggered by depolarization-induced Ca^{2+} influx at the active zone. Using a biochemical assay we showed that CAST was coimmunoprecipitated with the VDCC β_4-subunit from the mouse brain. A pulldown assay revealed that the VDCC β_4-subunit interacted directly with at least the N- and C-terminal regions of CAST. The II-III linker of VDCC α_1-subunit also interacted with C-terminal regions of CAST, however the interaction was much weaker than that of β_4-subunit. Furthermore, coexpression of CAST and VDCCs in baby hamster kidney (BHK) cells caused a shift in the voltage dependence of activation toward the hyperpolarizing direction. Taken together, these results suggest that CAST forms a protein complex with VDCCs, which may regulate neurotransmitter release partly through modifying the opening of VDCCs at the presynaptic active zones.

Introduction

The presynaptic active zone is a specialized site for neurotransmitter release in the nerve terminals, which is characterized by its high-electron density under electron microscopy [1]. Recent biochemical and molecular biological approaches have identified active zone-specific proteins including CAST/ERC2 [2, 3], ELKS [3, 4], Bassoon [5], Piccolo/Aczonin [6, 7], Munc13-1 [8] and Rab3 interacting molecules (RIMs) [9]. Among them, CAST and ELKS consist of a small family containing several coiled-coil domains and a unique C-terminal three amino acid motif (Ile-Trp-Ala, IWA) [2, 3]. CAST forms a large molecular complex through direct binding to ELKS, Bassoon, Piccolo and RIM1, and indirect binding to Munc13-1 [10], which might be the molecular basis for the electron density of the active zone cytomatrix [11].

Disruption of the CAST and Bassoon or RIM1 interaction significantly impairs synaptic transmission in cultured ganglion neurons [10]. In *Drosophila*, knockdown of Bruchpilot (Brp), a homologue of the ELKS/CAST family, results in the disappearance of the active zone cytomatrix, also called T-bar, and significantly perturbs evoked neurotransmission [12, 13]. The family member ELKS has also been reported to regulate exocytosis. For instances, overexpression of ELKS causes a significant increase in stimulated exocytosis of human growth hormone in PC12 cells [14], which is mediated at least in part via the RIM1-Munc13-1 pathway. In addition, using total internal reflection fluorescence microscopy, it has been shown that disruption of the ELKS and Bassoon binding reduces the docking and fusion of insulin granules, and attenuation of ELKS expression by small interfering RNA reduces the glucose-evoked insulin release, suggesting its role in insulin exocytosis from pancreatic β cells [15]. More recently, it has been demonstrated with CAST/ERC2 knockout mice that CAST/ERC2 deletion does not change the number of docked vesicles or other ultrastructural synapse parameters, but it causes a large increase in inhibitory, but not excitatory, neurotransmitter release [16]. In spite of the different systems employed, these accumulated observations suggest that CAST plays a pivotal role in neurotransmitter release from the active zone, however its functional linkage with voltage-dependent Ca^{2+} channels (VDCCs) still remains obscure.

In the mammalian neural system, VDCCs such as the N-, P/Q-, R-, and L-type play essential roles in neurotransmitter release from presynaptic nerve terminals [17-19]. VDCCs are characterized as

heteromultimeric protein complexes composed of the pore-forming α_1 -subunit and the auxiliary α_2/δ-, β-, and γ-subunits [20]. These VDCC complexes are known to associate with presynaptic and postsynaptic proteins including syntaxin, SNAP-25, synaptotagmin, CASK and Mint through interactions with the α_1-subunit [21-30]. Among the auxiliary subunits, the β-subunits interact with the α_1-subunit in the cytoplasm to enhance functional channel trafficking to the plasma membrane [31, 32], and to modify multiple kinetic properties [33, 34]. There are four subfamilies of β-subunits (β_1-β_4), each with splice variants, encoded by four distinct genes. Recently, several β-subunit-binding proteins have been identified and characterized [35-41]. For example, the active zone protein RIM1 has been shown to interact directly with the β-subunit, and sustain Ca^{2+} influx through inhibition of channel inactivation [40, 41]. RIM1 also associates with the α_1-subunit and anchors VDCCs to the active zones [42, 43]. In *Drosophila*, Brp is essential for clustering VDCCs [12]. Thus, we are beginning to understand the molecular relationship between the VDCC complexes and the active zone proteins.

In this study, to obtain further insight into the linkage between active zone proteins and VDCC functions, we have analyzed the physical and functional interactions between CAST and VDCCs. Biochemical studies showed that CAST interacts directly with the β-subunit of VDCC *in vitro* and *in vivo*. Moreover, coexpression of CAST with VDCCs in baby hamster kidney (BHK) cells caused a shift in the voltage dependence of activation toward the hyperpolarizing direction. Taken together, CAST regulates neurotransmitter release partly through modifying the opening of VDCCs at the presynaptic active zones.

Results

Direct interaction of CAST with the VDCC β_4-subunit

Nishimune *et al.* have recently reported that CAST or the family member, ELKS interacts with VDCC β-subunits using recombinant HEK293 cell lysates [44, 45]. To examine the interaction of the active zone protein CAST with VDCC complexes in native system, we used the immunoprecipitation assay on brain samples. First, we immunoprecipitated β_4-subunit with its antibody from the detergent extract of the mouse

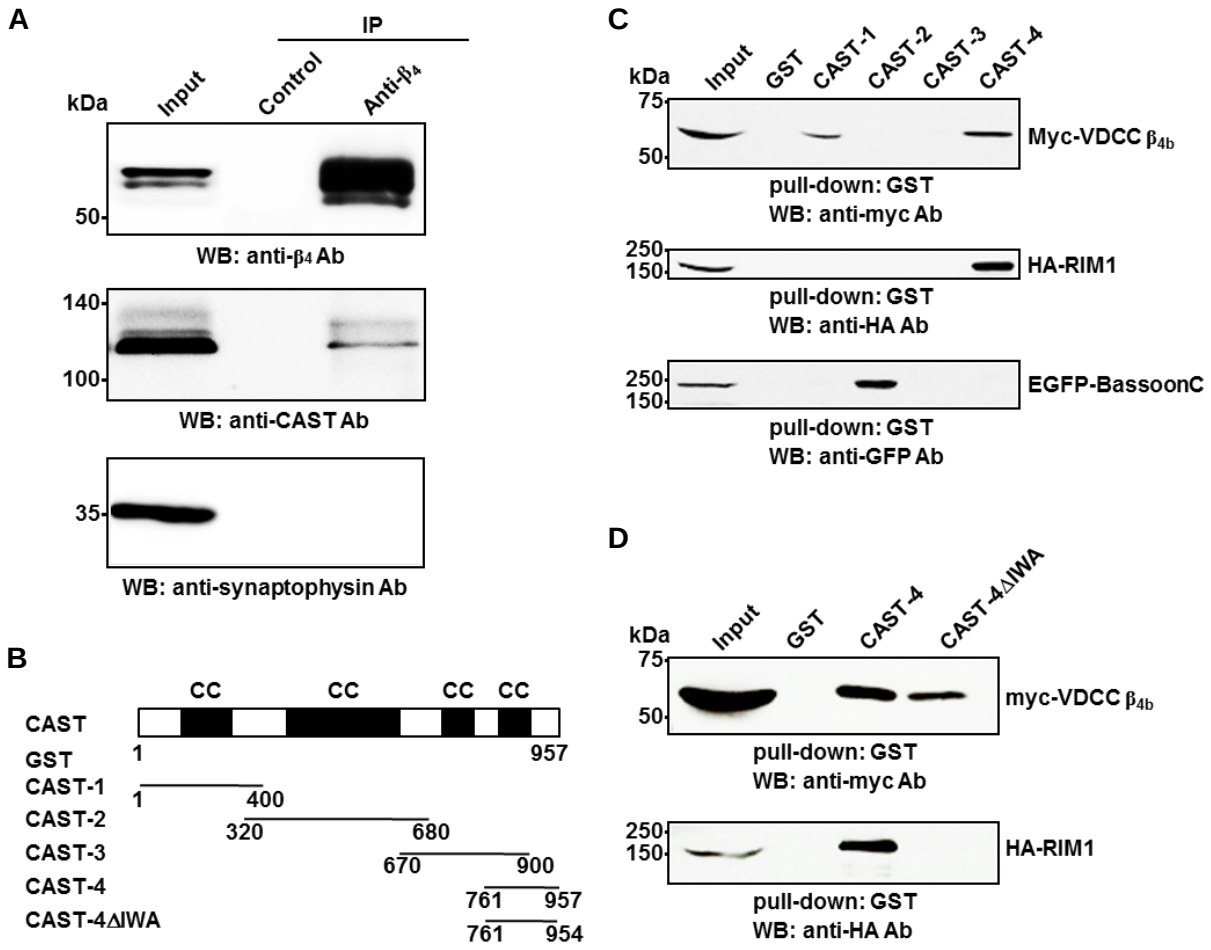

Fig. 1 Interaction of CAST and VDCC β_4-subunit. (A) Coimmunoprecipitation of CAST with VDCC β_4. The detergent extract of the mouse brain synaptosomal fraction was subjected to immunoprecipitation with the anti-β_4 antibody. The immunoprecipitate was analyzed by western blotting using antibodies against indicated proteins: anti-β_4, anti-CAST, and anti-synaptophysin. Ab, antibody; IP, immunoprecipitation; WB, western blotting. (B) GST fusion constructs of CAST. CAST-1 to -4 includes at least one coiled-coil domain (CC). And CAST-4ΔIWA lacks the C-terminal three amino acid (Ile-Trp-Ala), called IWA motif. The numbers indicate amino acid positions. (C) Direct binding of VDCC β_{4b}-subunit to CAST. The extract of HEK293 cells expressing Myc-VDCC β_{4b}, HA-RIM1, or EGFP-BassoonC was then incubated with the beads which are conjugated with various regions of CAST-1 to -4 as well as GST alone. Proteins that bound to the beads were analyzed by western blotting using the anti-Myc, anti-HA or anti-GFP antibodies. Input contains 8.0 % (for VDCC and RIM1) and 32 % (for BassoonC) of the extract was used for this assay. (D) Distinct CAST-binding regions for RIM1 and VDCC β_{4b}-subunit. The extract of HEK293 cells expressing myc-VDCC β_{4b} or HA-RIM1 was incubated with the beads immobilized with CAST-4, CAST-4ΔIWA or GST alone. HA-RIM1 only bound to the CAST-4, while Myc-VDCC β_{4b} bound both CAST-4 and CAST-4ΔIWA. Input contains 16 % (for VDCC) and 12 % (for RIM) of the extract used for this assay.

brain synaptosomal fraction. Consistent with the previous report that α_1-subunit directly binds to CAST in a heterologous expression system of HEK293 cells [44], CAST was coimmunoprecipitated with the β_4-subunit, but the synaptic vesicle protein synaptophysin was not (Fig. 1A). Moreover, when the immunoprecipitation assay was performed on the brain extract of lethargic mice, which carry a mutated form of the *VDCC β_4* gene [46], CAST was not immunoprecipitated (data not shown). Accordingly, these results suggest that CAST interacts with β_4-subunit in the intact brain.

We further examined the mode of binding between CAST and the VDCC β_4-subunit using pulldown assays with various glutathione-*S*-transferase (GST)-tagged CAST fragments (Fig. 1B). The extract of HEK293 cells expressing myc-VDCC β_{4b} was incubated with glutathione-Sepharose beads containing various GST-CAST fusion proteins. myc-VDCC β_{4b} bound to GST-CAST-1 containing the first coiled-coil (CC) domain and GST-CAST-4 containing the last CC do main and a unique C-terminal amino acid (Ile-Trp-Ala) called IWA motif, but not to the other GST fusion proteins (Fig. 1C). Under the same conditions, RIM1 and Bassoon bound to GST-CAST-4 and GST-CAST-2 respectively (Fig. 1C) [2, 10]. The IWA motif is essential for CAST to bind the PDZ domain of RIM1 [2, 3]. Thus, HA-RIM1 did not bind to GST-CAST-4ΔIWA whereas Myc-VDCC β_{4b} bound to it (Fig. 1D).

Next, we examined the ability of other β-subunits (β_{1a}, β_{2a}, and β_3) to bind to CAST. GST pulldown assays revealed that not only β_{4b}-subunit but also other β-subunits bound to GST-CAST-4 (Fig. 2A). Interestingly, GST-CAST-4 had a higher binding potency to β_{4b}-subunit, the brain-type β-subunit, compared with the skeletal muscle-type β_{1a}-subunit, the cardiac muscle type β_{2a}-subunit, and the brain-type β_3-subunit [47]. Importantly, the purified preparation of recombinant β_4-subunit (β_4 (47–475)) [40] was also pulled-down by the purified GST-CAST-4 (Fig. 2B). These results suggest that CAST forms a protein complex with VDCCs through direct interactions with VDCC β-subunits.

Complex formation of CAST with VDCC subunits in the brain

We examined the binding of CAST with VDCC subunits by pulldown assays using brain lysates. To this end, we prepared the brain fraction containing VDCC complexes [41] and incubated the extract with

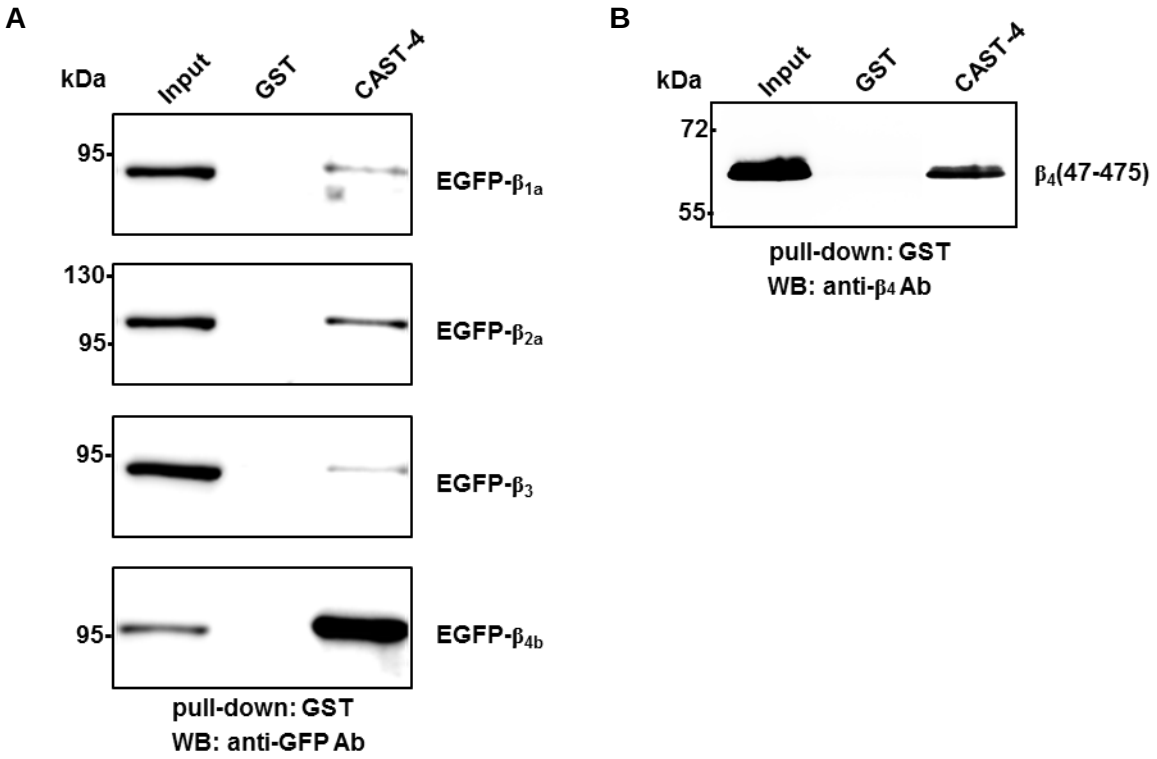

Fig. 2 Direct binding of CAST with VDCC β-subunits. (A) GST-pulldown assay of β-subunits (β_{1a}, β_{2a}, β_3, and β_{4b}) with GST-CAST-4. GST-CAST-4 bound glutathione-Sepharose beads were incubated with cell lysates obtained from EGFP-β-transfected HEK293 cells. Bound proteins were analyzed by western blotting using anti-GFP antibody. Ab, antibody; WB, western blotting. (B) *In vitro* association between the purified GST-CAST-4 and recombinant β_4-subunit (β_4(47–475)). GST-CAST-4 incubated with β_4-subunit was captured by glutathione-Sepharose beads. Captured β_4-proteins were examined by western blotting.

glutathione-Sepharose beads containing various GST-CAST proteins (Fig. 1B). Both VDCC α_1- and β_4-subunits could be detected by those subunits specific antibodies binding to GST-CAST-4 (Fig. 3). However, in contrast to the result in Fig. 1C, we did not detect binding of VDCC β_4-subunit to GST-CAST-1 in this brain lysate system (Fig. 3B).

Interaction of CAST with the VDCC α_1-subunit

In *Drosophila*, the CAST homologue Brp has been shown to interact with the C-terminal region of VDCC α_1-subunits and to regulate its clustering at the active zone [48]. In vertebrate, we found a complex formation of VDCC α_1-subunit and CAST (Fig. 3). Therefore, we examined the direct interaction between CAST and

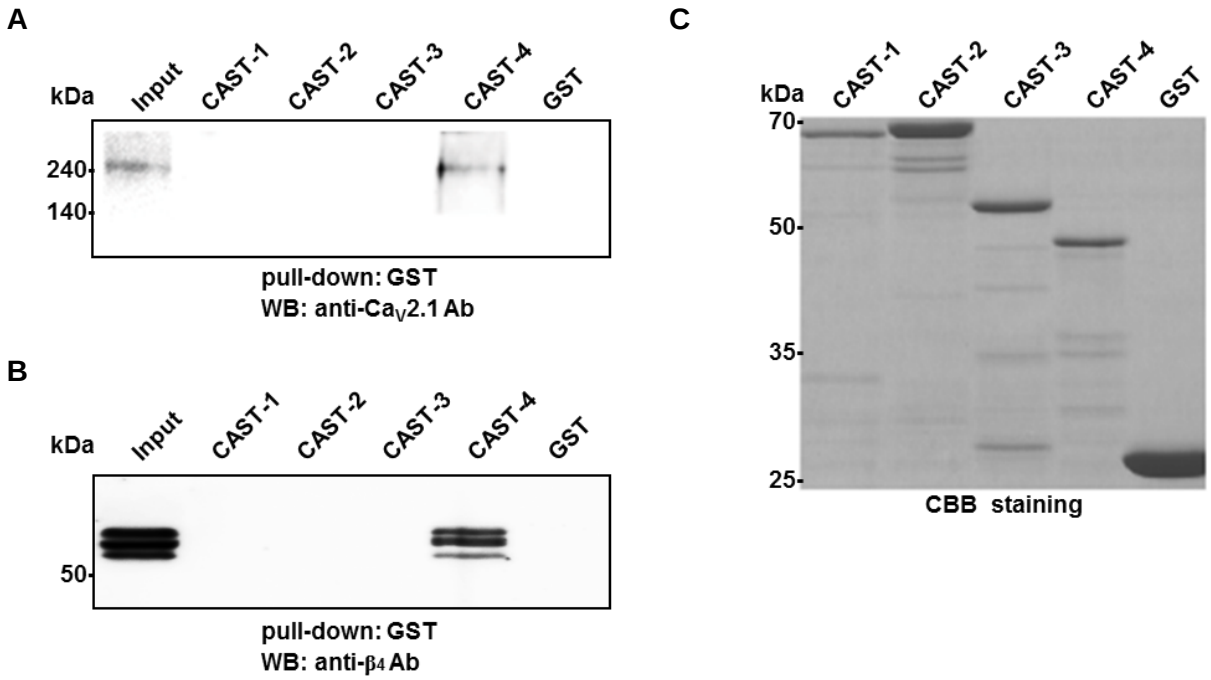

Fig. 3 Complex formation of CAST with VDCCs through the β_4-subunit. (A, B) The GST fusion proteins containing various CAST regions (Fig. 1B) as well as GST alone were immobilized on glutathione-Sepharose beads. The detergent extract of the mouse brain synaptosomal fraction was then incubated with the beads, and proteins that bound to the beads were analyzed by western blotting using the indicated antibodies. The endogenous VDCC α_1-subunit (anti-Ca$_V$2.1) and VDCC β_4-subunit were pulldowned by CAST-4. Ab, antibody; WB, western blotting. (C) Coomassie brilliant blue (CBB) staining of loaded GST fusion proteins.

VDCC α_1-subunit (Fig. 4). To this end, we prepared fragments of the N-terminal (amino acid residues 1-98), I-II linker (amino acid residues 361-488), II-III linker (amino acid residues 731-1038) and C-terminal (amino acid residues 1806-2425) regions of the VDCC α_1-subunit, Ca$_V$2.1. All these regions are located at the cytoplasmic side of the plasma membrane, and thus might bind to CAST directly. Extracts of EGFP-tagged VDCC α_1 fragments or that of VDCC β_4-subunit from HEK293 cells revealed equal expression at the protein level (Fig. 4B). Consistent with the results in Fig. 1 and Fig. 3, pulldown assay using GST-CAST-4 indicated the direct interaction of EGFP-VDCC β_4-subunit to CAST. For the α_1-subunit, not C-terminal but II-III linker of Ca$_V$2.1 interacted with GST-CAST-4 (Fig. 4A). Chen *et al.* have also reported that the C-terminal region of the VDCC α_1-subunit does not coimmunoprecipitate with CAST in a heterologous expression system of HEK cells [44]. These results indicate that interaction regions of α_1-subunit for CAST are different between

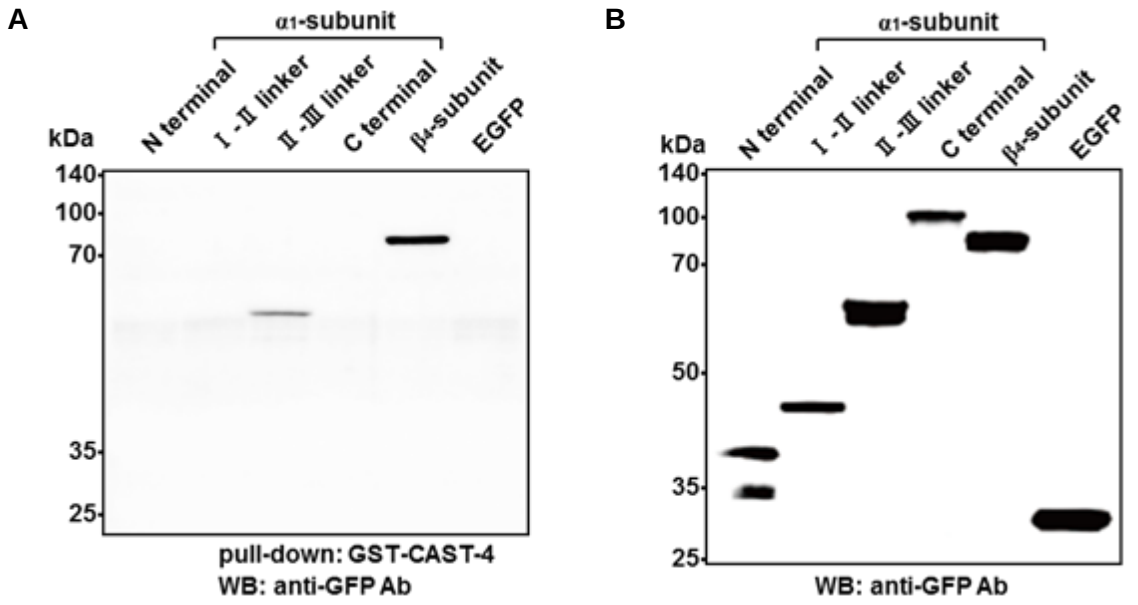

Fig. 4 Interaction of the VDCC α_1-subunit with the C-terminal region of CAST. (A) The extracts of HEK293 cells expressing the indicated EGFP-tagged fragments of the α_1-subunit, full-length β_{4b}-subunit, and control EGFP were incubated with the beads on which GST-CAST-4 was immobilized. Proteins were analyzed by western blotting using the anti-GFP antibody. Ab, antibody; WB, western blotting. (B) Expression and input of EGFP-tagged fragments of the α_1-subunit and full-length the β_{4b}-subunit were assessed by western blotting.

Drosophila and mice. In addition, the interaction of II-III linker with GST-CAST-4 was much weaker than that of β_4-subunit. Therefore, in mammalian systems, we conclude that CAST has the potency to form a complex with VDCCs mainly with β_4-subunit through its direct interaction.

Functional effects of CAST on P/Q-type VDCC currents

Biochemical and molecular biological approaches have revealed the physical and functional interactions of VDCCs with synaptic proteins such as syntaxin, SNAP-25, synaptotagmin, and RIMs [21-24, 30, 40-43]. To obtain further insight into the functional linkage between the active zone proteins and VDCCs, we elucidated the physiological significance of the direct interaction between CAST and the VDCC β-subunits. First, we examined whole-cell Ba^{2+} currents through recombinant P/Q-type VDCC expressed as α_1, α_2/δ, and β complexes containing the BI-2 variant of $Ca_V2.1$ [31] and β_{4b}-subunit in BHK cells. We focused on P/Q-type VDCC in this study, because P/Q-type VDCC is known to contribute to neurotransmitter release at presynapse

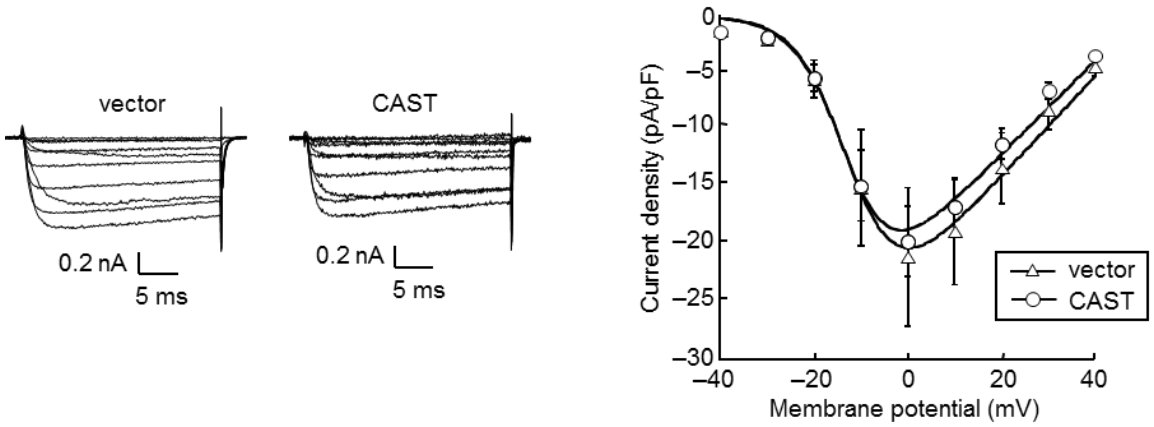

Fig. 5 Effects of CAST on the *I-V* relationships of P/Q-type Ca^{2+} channel. Voltage-dependent activation of P/Q-type Ca^{2+} channel current in BHK cells expressing α_2/δ- and β_{4b}-subunit. Representative Ba^{2+} currents evoked by 30-ms depolarizing pulses from −40 to 40 mV (*left*) with 10-mV increments from a V_h of −100 mV, and the current density-voltage (*I-V*) relationship (*right*). In the presence of CAST, the *I-V* relationship was slightly shifted to the hyperpolarization as compared to the vector alone. Data points are mean ± SEM.

[17, 18]. Fig. 5 shows Ca^{2+} channel currents and their current density-voltage (*I-V*) relationships in the BHK cells in the presence or absence of full-length CAST. Ba^{2+} currents were elicited with 30-ms depolarizing pulses from a holding potential (V_h = −100 mV) to test potentials from −40 to 40 mV with increments of 10-mV in a 3 mM Ba^{2+} solution. We found that CAST slightly shifted the *I-V* relationship in the hyperpolarizing direction by about 5 mV without affecting the current density (Fig. 5 and Table 1). These results suggest that CAST may regulate the opening of VDCCs.

Effects of CAST on activation properties of VDCC currents

To clarify this hypothesis, we next examined the effect of CAST on the activation of the P/Q-type VDCC. The activation curves were obtained by fitting the peak amplitude of tail currents with the Boltzmann equation, which showed different voltage-dependence with CAST coexpression (Fig. 6A). The voltage-dependence of activation was shifted in the hyperpolarizing direction, and the midpoints of the activation curves ($V_{0.5}$) were −10.8 ± 1.0 mV and −5.0 ± 1.3 mV in the presence and absence of CAST, respectively (Table 1). Interestingly, in the cells expressing α_1-subunit instead of β_4-subunit, the leftward shift of the voltage-dependent activation

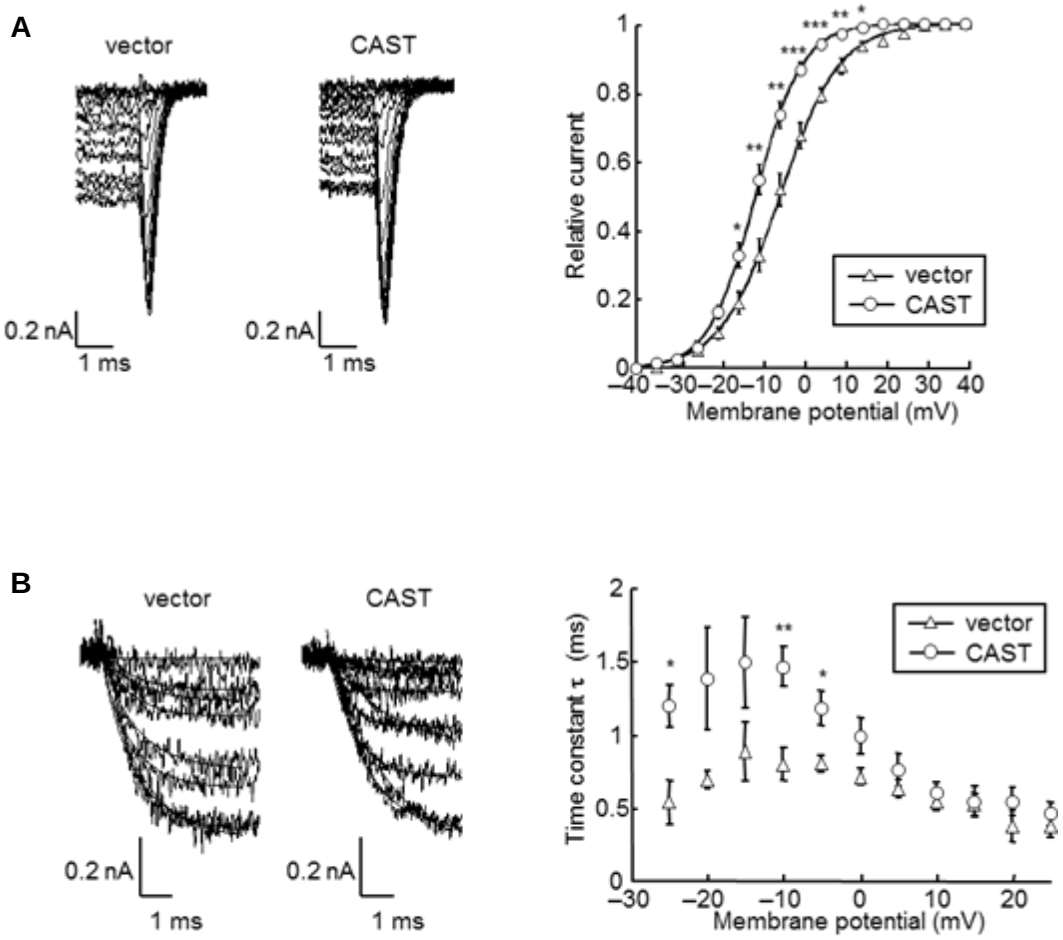

Fig. 6 Effects of CAST on the activation properties of P/Q-type Ca_{2+} channel. (A) Superimposed tail current elicited by repolarization to −60 mV after the 5-ms test pulse from −40 to 40 mV with increments of 5-mV (*left*), and normalized tail current were plotted against test-pulse potentials (*right*). The Boltzman fit to each plots represented the hyperpolarization shift of activation property of P/Q-type Ca^{2+} channel in the presence of CAST. (B) Activation kinetics of P/Q-type Ca^{2+} channel currents. *Left*, families of Ba^{2+} currents and the single exponential fit on their activation phases. Currents were evoked by 5-ms step depolarizations from −25 to 25 mV from the holding potential (V_h = −100 mV). *Right*, comparison of the activation time constant ($\tau_{activation}$). The activation time constant (τ) obtained from the single exponential fit was significantly increased in the presence of CAST at −25, −10, and −5 mV membrane potential. **P* < 0.05, ***P* < 0.01 and ****P* < 0.001. Data points are mean ± SEM.

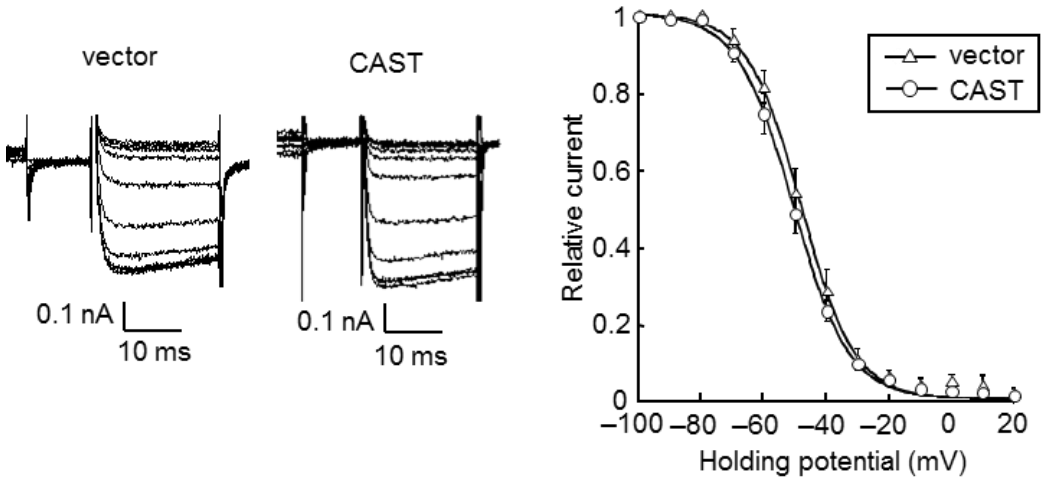

Fig. 7 Effects of CAST on the inactivation properties of P/Q-type Ca^{2+} channel. *Left,* Ba^{2+} currents were evoked by a 20-ms test pulse to 5 mV after the 10 ms repolarization to holding potential (−100 mV) following a 2-s inactivation pulse (conditional pulse) from −100 to 20 mV with increments of 10 mV. *Right,* normalized test pulse currents were plotted against conditional pulse potentials and fitted with the Boltzman equation. The inactivation curve was not significantly different with or without CAST. Data points are mean ± SEM.

Table 1 Effects of CAST on current density, activation, and inactivation of $Ca_V2.1$ channels in BHK cells expressing α_2/δ- and β_{4b}-subunits [1) 2)].

	Current density (pA / pF) [3)]	Activation parameters		Inactivation parameters	
		$V_{0.5}$ (mV)	k (mV)	$V_{0.5}$ (mV)	k (mV)
Vector	–20.6 ± 5.1 (7)	–5.0 ± 1.3 (5)	7.0 ± 0.4 (5)	–48.1 ± 2.1 (3)	–8.5 ± 0.3 (3)
CAST	–19.5 ± 3.1 (14)	–10.8 ± 1.0 (8)**	5.5 ± 0.1 (8)**	–50.6 ± 1.7 (7)	–8.5 ± 0.5 (7)

1) $^{**}P < 0.01$, versus Vector.

2) Numbers of cells analyzed are indicated in the parenthesis.

3) Ba^{2+} currents evoked by depolarizing pulse to 0 mV from a V_h (−100 mV) were divided by capacitances.

was not observed (data not shown). CAST also changed the slope factor (*k*) from 7.0 ± 0.4 mV to 5.5 ± 0.1 mV (Table 1), and modulated the activation kinetics of P/Q-type VDCCs (Fig. 6B). The time constant ($\tau_{activation}$) obtained by fitting the activation time course of inward currents with a single exponential was "bell-shaped" when plotted against different voltages (Fig. 6B). CAST decelerated the activation kinetics at membrane potentials of −25, −10 and −5 mV. Thus, in CAST-containing synapse, neurotransmission may occur at the hyperpolarizing potentials at which other synapses are not activated. Decreased activation rate of the channels may prevent Ca^{2+} overload at the hyperpolarizing potentials.

Effects of CAST on inactivation properties of VDCC currents

We examined the effect of CAST on the inactivation properties of the P/Q-type VDCC. The voltage-dependence of inactivation was determined by the use of 2-s prepulses to a series of different potentials followed by the test pulse to 5 mV. Peak current amplitudes were normalized to the peak current amplitude induced by the test pulse from a prepulse potential of −100 mV and were plotted against the prepulse potentials. CAST did not affect the voltage dependence of inactivation (Fig. 7). The estimated half-inactivation potential and the slope factor of the inactivation curves fitted by the Boltzmann equation were −50.6 ± 1.7 mV and −8.5 ± 0.5 mV in the presence of CAST, and −48.1 ± 2.1 mV and −8.5 ± 0.3 mV in the absence of CAST, respectively (Table 1).

Discussion

In the present study, we have shown that the active zone protein CAST binds the VDCC β_4-subunit directly, and forms a protein complex with VDCCs at the presynaptic active zone, modifying the opening of VDCCs. Pulldown assays and immunoprecipitation experiments have also identified their direct interaction which involves at least the C-terminal region of CAST. Therefore, our results indicate that CAST regulates neurotransmitter release by modifying the opening of VDCCs through the physical association with the VDCC β-subunit.

CAST has been shown to be localized at the active zone by immunoelectron microscopy [2, 4] and binds with a number of synaptic proteins, mainly cytoplasmic at the active zone proteins [10]. The results in our study demonstrate that CAST interacts directly with the VDCC β_4-subunit (Fig. 1) in addition to the active zone proteins Bassoon, Piccolo and RIM1 [10]. The VDCC β_4-subunit bound to the N- and C-terminal regions of CAST (GST-CAST-1 and GST-CAST-4; Fig. 1C), which are distinct from the binding regions for Bassoon, Piccolo and RIM1 [2, 10]. Intriguingly, the VDCC β_4-subunit bound to GST-CAST-4ΔIWA, to which RIM1 does not bind (Fig. 1D). These distinct CAST-binding regions for the VDCC β_4-subunit and RIM1 would be advantageous for regulating VDCC activity at the molecular level. One scenario may be that CAST recruits RIM1 at the active zone and RIM1 in turn bind to the VDCC β_4-subunit on CAST, suggesting that CAST may serve as a platform for the VDCC β_4-subunit-RIM1 interaction. Indeed, using primary rat hippocampal neuron cultures [2] and CAST/ERC2 knockout mice [16], CAST has been suggested to be involved in anchoring RIM1 to the active zone. Another possibility is that RIM1 competes with β_4-subunit for the binding to CAST. Whether CAST recruits the VDCC β_4-subunit in addition to RIM1 has not been examined, however elucidation of the involvement of CAST in anchoring the VDCC β_4-subunit to the active zone will shed new light on the molecular mechanisms responsible for direct and functional interactions between active zone proteins and VDCCs.

As mentioned above and in Fig. 1, the VDCC β_4-subunit bound to GST-CAST-4 as well as to GST-CAST-1, but the pulldown assay using the mouse brain lysate showed that the VDCC β_4-subunit bound only to GST-CAST-4 (Fig. 3B). At present, we cannot explain this difference, but we speculate that there is a protein(s) that binds the N-terminal region of CAST (CAST-1) in the brain lysate, which may interfere with the binding of the VDCC β_4-subunit to the region.

Consistent with previous observations [44], our present results demonstrate that CAST does not interact directly with the C-terminal region of VDCC α_1-subunits (Fig. 4). In this study, we have revealed that the II-III linker of α_1-subunits interacts with CAST, but the interaction appears to be weaker compared with that of the β_4-subunit. However, in *Drosophila*, Brp, the only homologue of the ELKS/CAST family, has been shown to interact directly with the C-terminal region of P/Q-type VDCC α_1-subunit homologue, Cacophony [48]. Brp

mutants and knockdown studies have shown that the clustering of Cacophony was significantly reduced at the active zones. Presently, we cannot explain the discrepancy in the binding of CAST and the VDCC α_1-subunit, but we speculate that there is a different mechanism for clustering VDCCs at the active zone of mice and flies. Indeed, the active zone proteins Bassoon and Piccolo are not conserved in invertebrates such as *C. elegans* and *Drosophila*. Recently, Chen *et al.* have also reported that Bassoon binds directly to the VDCC β_4-subunit [44]. In addition, unlike *Drosophila*, the deletion of the *C. elegans* ELKS/CAST homologue appeared to have no effect on the assembly of the active zone [49]. Thus, we suggest that the clustering of VDCCs at the active zone and its assembly are much more complicated than envisaged.

β_3- and β_4-subunits are generally known as brain-type VDCC β-subunits. However, these distributions are different in nervous systems [47, 50]. The expression of β_3-subunit is highest in the olfactory bulb and habenula. Moderate β_3-subunit signals are detected in the cortex, hippocampus, basal ganglia, nucleus interpeduncularis, superior colliculus, and cerebellum. In contrast, the expression of β_4-subunit is highest in the cerebellum, and not detected in habenula. Moderate β_4-subunit signals are found in the olfactory bulb, cortex, hippocampus, basal ganglia, and inferior colliculus. In addition, subunit compositions of VDCCs are also different in brains. Biochemical assay reveals that the most prevalent partner of $Ca_V2.2$ (N-type) is β_3-subunit, and that of $Ca_V2.1$ (P/Q-type) is β_4-subunit [47, 51, 52]. In this study, we revealed that CAST selectively interacts with β_4-subunit among β-subunits (β_1-β_4). Thus, CAST may selectively scaffold and functionally modulate P/Q-type VDCCs at β_4-containing synapses in brains.

The presynaptic VDCCs, N-type and P/Q-type Ca^{2+} channels, are subject to functional modulation by interaction with synaptic proteins that finely tune Ca^{2+} entry into nerve terminals. Most synaptic proteins affect the inactivation properties of VDCCs. Syntaxin or SNAP-25 binds to the II-III linker of the α_1-subunit to decrease channel availability with a hyperpolarizing shift in the voltage-dependence of inactivation of transiently expressed [22-24, 27] and native Ca^{2+} channels [53]. By binding to the β-subunit [40, 41] or the C-terminal of the α_1-subunit [42], RIM1 sustains Ca^{2+} influx through the inhibition of voltage-dependent inactivation of VDCCs [40, 41, 43]. In contrast, Ca^{2+}-binding protein 1 (CaBP1), which binds to the C-terminal of the α_1-subunit, modulates activation properties. CaBP1 induces a depolarizing shift in the

voltage-dependence of activation of VDCCs, thus inhibiting channel activity by antagonizing channel opening [54]. In the present study, we reveal that CAST modulates activation properties. Interestingly, CAST binds to the β-subunit but not the α_1-subunit, and shifts voltage-dependence of activation toward the hyperpolarizing direction. Thus, CAST may enhance the β-subunit action on Ca^{2+} channel properties, because the β-subunits shift the voltage dependence of activation to hyperpolarizing direction [33, 34, 47].

In summary, we show here that the direct binding of CAST and the VDCC β_4-subunit regulates the opening of the functional VDCC complex. Notably, this is the first report to show that the activation of VDCC is directly affected by an active zone protein. Further biochemical analyses focused on the potential property of CAST to anchor RIMs to the active zone [2, 16] would shed new light on our understanding of the mode of functional complex formation.

Experimental procedures

cDNAs and vector construction

Expression vectors were constructed in pGEX (Amersham Biosciences), pET23 (Novagen), pCMV-HA [55], pCI-neo (Promega), pCMV-tag3 (Stratagene) and pEGFP-C1 (Clontech) using standard molecular biological methods. Rat β_{4b} (GenBank Accession Number XM_215742) and the BI-2 variant of the rabbit $Ca_V2.1$ (GenBank Accession Number X57477) were used for expression experiments. Other constructs for CAST, RIM1 and C-terminal region of Bassoon (BassoonC) were prepared as previously described [2, 10]. RIM1 cDNA was supplied by S. Seino (Kobe University). GST fusion proteins were purified according to the manufacturer's protocol (GE Healthcare).

Antibodies

The antibodies used in this study were mouse monoclonal anti-myc (9E10; Roche), anti-HA (12C5A; Roche) and anti-synaptophysin (SY38; Chemicon), and rabbit polyclonal anti-GFP (A11122; Invitrogen), anti-β_4 [40], anti-CAST [2] and anti-$Ca_V2.1$ (Alomone Labs).

Coimmunoprecipitation and pulldown assay using mouse brain lysate

To obtain the crude synaptic membrane (CSM) fraction, subcellular fractionation was performed as previously described [29]. Whole mouse brains (8 g) were homogenized in a homogenization buffer containing 4 mM HEPES (pH 7.4), 0.32 M sucrose, 5 mM EDTA, 5 mM EGTA, and protease inhibitors. Cell debris and nuclei were removed by centrifugation at 800 × *g* for 10 min. The supernatant was centrifuged at 9,000 × *g* for 15 min to obtain the crude synaptosomal fraction in the pellet. Crude synaptosomes were resuspended in the homogenization buffer and centrifuged at 10,000 × *g* for 15 min. The washed crude synaptosomes were lysed by hypo osmotic shock in water, rapidly adjusted to 1 mM HEPES/NaOH (pH 7.4), and stirred on ice for 30 min. After centrifugation of the lysate at 25,000 × *g* for 20 min, the pellet was resuspended in 0.25 M buffered sucrose. The synaptic membranes were then further enriched through a discontinuous sucrose gradient containing 0.8/1.0/1.2 M sucrose. After centrifugation at 65,000 × *g* for 2 h, the CSM fraction was collected from the 1.0/1.2 M sucrose interface. Synaptic membrane proteins were extracted from the CSM with a solubilization buffer containing 50 mM Tris-Cl (pH 7.4), 500 mM NaCl, a mixture of protease inhibitors, and 1 % digitonin (Biosynth). After centrifugation at 147,600 × *g* for 37 min, the supernatant was diluted with a buffer containing 50 mM Tris and 0.1 % digitonin to adjust the NaCl concentration to 150 mM and incubated overnight at 4 °C. Following centrifugation at 17,400 × *g* for 15 min, the solution including neuronal VDCC complexes was obtained. For coimmunoprecipitation, the solution was incubated with ProteinA Agarose coupled to anti-β_4 antibodies [40] at 4 °C for 6 h. For the GST pulldown assay, the solution was incubated with glutathione-Sepharose beads containing the indicated GST fusion proteins at 4 °C for 1 h. After the beads were extensively washed with buffer, the bound proteins were eluted by boiling the beads in SDS sample buffer for 5 min, or by incubating the beads in SDS sample buffer containing 50 mM DTT for 30 min at room temperature. Samples were then analyzed by western blotting.

Pulldown assay using HEK293 cells

HEK293 cells transfected with cDNA plamids expressing myc-VDCC β_{4b}, HA-RIM1 or EGFP-BassoonC by

Lipofectamin® 2000 (Invitrogen) in 10 cm dishes were lysed with 1 ml of buffer containing, 20 mM Tris-Cl (pH 7.5), 150 mM NaCl, 0.5 mM EDTA, 1 mM DTT, 1 % (wt/vol) Triton X-100, 10 μg/ml leupeptin, and 10 μM APMSF at 4 °C for 1 h. Samples were centrifuged at 20,000 × *g* at 4 °C for 20 min to collect the supernatant. The HA-RIM1 and EGFP-BassoonC samples were diluted 4-fold with the buffer. These 0.5 ml supernatants were then incubated with 20 μl of glutathione-Sepharose beads containing the indicated GST fusion proteins at 4 °C for 1 h. After the beads were extensively washed with buffer, the bound proteins were eluted by boiling the beads in SDS sample buffer for 5 min. Samples were then analyzed by western blotting. EGFP fusion constructs of rat β_{1a}-, β_{2a}-, β_{3}-, β_{4b}-subunits, rabbit $Ca_V2.1$ N-terminal (amino acid residues 1-98), the I-II linker (amino acid residues 361-488), the II-III linker (amino acid residues 731-1038), and the C-terminal (amino acid residues 1806-2425) were expressed in HEK293 cells, and applied to the pulldown assay as previously described [40, 41].

In vitro binding of the purified GST-CAST-4 and recombinant β_4-protein

Recombinant β_4-proteins (β_4 (47–475)) were prepared as previously reported [40]. Purified GST-CAST-4 fusion proteins were incubated with 50 pM purified recombinant β_4-subunits for 2 h at 4 °C in phosphate-buffered saline buffer containing 0.1 % Nonidet P-40 and 50 μg/ml bovine serum albumin and then incubated with glutathione-Sepharose beads for 1 h. The beads were washed twice with the phosphate-buffered saline buffer. The proteins retained on the beads were characterized by western blotting with the anti-β_4 antibody.

Western blotting

Samples were resolved using SDS-PAGE and transferred to nitrocellulose membranes (Invitrogen) or PVDF membranes (Millipore). All membranes were blocked for 1 h with blocking solution containing 5 % skim milk (wt/vol) in TBST [20 mM Tris-Cl (pH 7.6), 140 mM NaCl, 0.1 % Tween-20 (wt/vol)], and immunoreacted with anti-myc (1:200), anti-HA (1:200), anti-EGFP (1:500), anti-β_4 (1:1000), anti-CAST (1:500), anti-$Ca_V2.1$ (1:200) and anti-synaptophysin (1:1000) antibodies. Membranes were washed and incubated for 1 h with the

HRP-linked anti-mouse or anti-rabbit secondary antibody (1:5000 for mouse, 1:2000 for rabbit) prepared in blocking solution. Membranes were then treated with ECL solution [100 mM Tris-Cl (pH 8.5), 1.25 mM Luminol, 2.2 mM *p*-coumaric acid, 0.01 % (vol/vol) H_2O_2] and exposed to imaging film (Kodak) or a LAS-4000 image analyzer (Fujifilm).

Cell culture and cDNA expression in BHK cells

The baby hamster kidney (BHK) cell line BHK6 stably expressing the α_2/δ- and β_{4b}-subunits of VDCC as previously described [56]. BHK6 cells were cultured in DMEM containing 10 % fetal bovine serum, 30 units/ml penicillin and 30 µg/ml streptomycin. Transfection of cDNA plasmids was carried out using Effecten Transfection Reagent (Qiagen). Cells were subjected to electrophysiological measurements 48 h after transfection.

Current recordings

Whole-cell patch-clamp recording was carried out at 22-25 °C with the EPC-9 (HEKA Elektronik) patch-clamp amplifier, as previously described [57]. Patch pipettes (borosilicate glass capillary, 1.5 mm outer diameter, 0.87 mm inner diameter; Hilgenberg) were pulled with the P-87 Flaming-Brown micropipette puller (Sutter Instrument Co.) and fire-polished. Pipette resistance ranged from 2 to 3.5 mega ohm when filled with the pipette solutions described below. The series resistance was electronically compensated to > 60 %, and both the leakage and the remaining capacitance were subtracted by the –P/4 method. In the experiments of activation kinetics, currents were sampled at 100 kHz after low pass filtering at 8.4 kHz (3 db), otherwise they were sampled at 20 kHz after low pass filtering at 3.0 kHz (3 db). Data were collected and analyzed using the Pulse v8.77 (HEKA Elektronik). The external solution contained (in mM): 3 $BaCl_2$, 155 tetraethylammonium chloride (TEA-Cl), 10 HEPES, and 10 glucose (pH 7.4 adjusted with TEA-OH). The pipette solution contained (in mM): 95 CsOH, 95 aspartate, 40 CsCl, 4 $MgCl_2$, 5 EGTA, 2 disodium ATP, 5 HEPES and 8 creatine phosphate (pH 7.2 adjusted with CsOH).

Voltage-dependence of activation

Tail currents were elicited by repolarization to −60 mV after a 5-ms test pulse from −40 to 40 mV with 5-mV increments. Currents were sampled at 100 kHz after low pass filtering at 8.4 kHz. The amplitude of tail currents was normalized to the tail current amplitude obtained with a test pulse of 40 mV. Mean values were plotted against test pulse potentials, and fitted to the Boltzmann equation: $n(V_m) = 1/\{1+\exp[(V_{0.5}-V_m)/k]\}$, with V_m, membrane potential, $V_{0.5}$, potential that gives a half-value of conductance, and k, slope factor.

Voltage-dependence of inactivation

The voltage-dependence of VDCC inactivation (inactivation curve) was determined by a double-pulse protocol with a 2-s inactivation pulse (conditional pulse) from −100 mV to 20 mV (10-mV increments) and a 20-ms test pulse to 5 mV following 10-ms interpulse interval at the holding potential of −100 mV. Current amplitudes elicited by the test pulses were normalized to those after the 2-s conditional pulse to –100 mV. Mean values were plotted against the potentials of the conditional pulse, and fitted to the Boltzmann equation as described above.

Statistical analyses

All data were expressed as means ± SEM. We accumulated the data for each condition from at least three independent experiments. Statistical significance was evaluated with an ANOVA followed by Tukey-Kramer test. $P < 0.05$ was considered statistically significant.

Reference

[1] Landis, D. M., Hall, A. K., Weinstein, L. A., and Reese, T. S. (1988) *Neuron*, **1**, 201-209

[2] Ohtsuka, T., Takao-Rikitsu, E., Inoue, E., Inoue, M., Takeuchi, M., Matsubara, K., Deguchi-Tawarada, M., Satoh, K., Morimoto, K., Nakanishi, H., and Takai, Y. (2002) *J. Cell Biol.*, **158**, 577-590

[3] Wang, Y., Liu, X., Biederer, T., and Südhof, T. C. (2002) *Proc. Natl. Acad. Sci. U. S. A.*, **99**, 14464-14469

[4] Deguchi-Tawarada, M., Inoue, E., Takao-Rikitsu, E., Inoue, M., Ohtsuka, T., and Takai, Y. (2004) *Genes Cells*, **9**, 15-23

[5] tom Dieck, S., Sanmartí-Vila, L., Langnaese, K., Richter, K., Kindler, S., Soyke, A., Wex, H., Smalla, K. H., Kämpf, U., Fränzer, J. T., Stumm, M., Garner, C. C., and Gundelfinger, E. D. (1998) *J. Cell Biol.*, **142**, 499-509

[6] Wang, X., Kibschull, M., Laue, M. M., Lichte, B., Petrasch-Parwez, E., and Kilimann, M. W. (1999) *J. Cell Biol.*, **147**, 151-162

[7] Fenster, S. D., Chung, W. J., Zhai, R., Cases-Langhoff, C., Voss, B., Garner, A. M., Kämpf, U., Kindler, S., Gundelfinger, E. D., and Garner, C. C. (2000) *Neuron*, **25**, 203-214

[8] Brose, N., Hofmann, K., Hata, Y., and Südhof, T. C. (1995) *J. Biol. Chem.*, **270**, 25273-25280

[9] Wang, Y., Okamoto, M., Schmitz, F., Hofmann, K., and Südhof, T. C. (1997) *Nature*, **388**, 593-598

[10] Takao-Rikitsu, E., Mochida, S., Inoue, E., Deguchi-Tawarada, M., Inoue, M., Ohtsuka, T., and Takai, Y. (2004) *J. Cell Biol.*, **164**, 301-311

[11] Hida, Y., and Ohtsuka, T. (2010) *J. Biochem.*, **148**, 131-137

[12] Kittel, R. J., Wichmann, C., Rasse, T. M., Fouquet, W., Schmidt, M., Schmid, A., Wagh, D. A., Pawlu, C., Kellner, R. R., Willig, K. I., Hell, S. W., Buchner, E., Heckmann, M., and Sigrist, S. J. (2006) *Science*, **312**, 1051-1054

[13] Wagh, D. A., Rasse, T. M., Asan, E., Hofbauer, A., Schwenkert, I., Dürrbeck, H., Buchner, S., Dabauvalle, M. C., Schmidt, M., Qin, G., Wichmann, C., Kittel, R., Sigrist, S. J., and Buchner, E. (2006) *Neuron*, **49**, 833-844

[14] Inoue, E., Deguchi-Tawarada, M., Takao-Rikitsu, E., Inoue, M., Kitajima, I., Ohtsuka, T., and Takai, Y. (2006) *Genes Cells*, **11**, 659-672

[15] Ohara-Imaizumi, M., Ohtsuka, T., Matsushima, S., Akimoto, Y., Nishiwaki, C., Nakamichi, Y., Kikuta, T., Nagai, S., Kawakami, H., Watanabe, T., and Nagamatsu, S. (2005) *Mol. Biol. Cell*, **16**, 3289-3300

[16] Kaeser, P. S., Deng, L., Chávez, A. E., Liu, X., Castillo, P. E., and Südhof, T. C. (2009) *Neuron*, **64**, 227-239

[17] Takahashi, T., and Momiyama, A. (1993) *Nature*, **366**, 156-158

[18] Wheeler, D. B., Randall, A., and Tsien, R. W. (1994) *Science*, **264**, 107-111

[19] Catterall, W. A. (1998) *Cell Calcium*, **24**, 307-323

[20] Ertel, E. A., Campbell, K. P., Harpold, M. M., Hofmann, F., Mori, Y., Perez-Reyes, E., Schwartz, A., Snutch, T. P., Tanabe, T., Birnbaumer, L., Tsien, R. W., and Catterall, W. A. (2000) *Neuron*, **25**, 533-535

[21] Sheng, Z. H., Rettig, J., Takahashi, M., and Catterall, W. A. (1994) *Neuron*, **13**, 1303-1313

[22] Bezprozvanny, I., Scheller, R. H., and Tsien, R. W. (1995) *Nature*, **378**, 623-626

[23] Wister, O., Bennett, M. K., Atlas, D. (1996) *EMBO J.*, **15**, 4100-4110

[24] Zhong, H., Yokoyama, C. T., Scheuer, T., and Catterall, W. A. (1999) *Nat. Neurosci.*, **2**, 939-941

[25] Maximov, A., Südhof, T. C., and Bezprozvanny, I. (1999) *J. Biol. Chem.*, **274**, 24453-24456

[26] Maximov, A., and Bezprozvanny, I. (2002) *J. Neurosci.*, **22**, 6939-6952

[27] Spafford, J. D., and Zamponi, G. W. (2003) *Curr. Opin. Neurobiol.*, **13**, 308-314

[28] Nishimune, H., Sanes, J. R., and Carlson, S. S. (2004) *Nature*, **432**, 580-587

[29] Kang, M. G., Chen, C. C., Wakamori, M., Hara, Y., Mori, Y., and Campbell, K. P. (2006) *Proc. Natl. Acad. Sci. U. S. A.*, **103**, 5561-5566

[30] Watanabe, H., Yamashita, T., Saitoh, N., Kiyonaka, S., Iwamatsu, A., Campbell, K. P., Mori, Y., and Takahashi, T. (2010) *J. Neurosci.*, **30**, 655-660

[31] Mori, Y., Friedrich, T., Kim, M. S., Mikami, A., Nakai, J., Ruth, P., Bosse, E., Hofmann, F., Flockerzi, V., Furuichi, T., Mikoshiba K., Imoto K., Tanabe T., and Numa S. (1991) *Nature*, **350**, 398-402

[32] Bichet, D., Cornet, V., Geib, S., Carlier, E., Volsen, S., Hoshi, T., Mori, Y., and De Waard, M. (2000) *Neuron*, **25**, 177-190

[33] Varadi, G., Lory, P., Schultz, D., Varadi, M., and Schwartz, A. (1991) *Nature*, **352**, 159-162

[34] Lacerda, A. E., Kim, H. S., Ruth, P., Perez-Reyes, E., Flockerzi, V., Hofmann, F., Birnbaumer, L., and Brown, A. M. (1991) *Nature*, **352**, 527-530

[35] Béguin, P., Nagashima, K., Gonoi, T., Shibasaki, T., Takahashi, K., Kashima, Y., Ozaki, N., Geering, K., Iwanaga, T., and Seino, S. (2001) *Nature*, **411**, 701-706

[36] Hibino, H., Pironkova, R., Onwumere, O., Rousset, M., Charnet, P., Hudspeth, A. J., and Lesage, F. (2003) *Proc. Natl. Acad. Sci. U. S. A.*, **100**, 307-312

[37] Vendel, A. C., Terry, M. D., Striegel, A. R., Iverson, N. M., Leuranguer, V., Rithner, C. D., Lyons, B. A., Pickard, G. E., Tobet, S. A., and Horne, W. A. (2006) *J. Neurosci.*, **26**, 2635-2644

[38] Gonzalez-Gutierrez, G., Miranda-Laferte, E., Neely, A., and Hidalgo, P. (2007) *J. Biol. Chem.*, **282**, 2156-2162

[39] Zhang, Y., Yamada, Y., Fan, M., Bangaru, S. D., Lin, B., and Yang, J. (2010) *J. Biol. Chem.*, **285**, 2527-2536

[40] Kiyonaka, S., Wakamori, M., Miki, T., Uriu, Y., Nonaka, M., Bito, H., Beedle, A. M., Mori, E., Hara, Y., De Waard, M., Kanagawa, M., Itakura, M., Takahashi, M., Campbell, K. P., and Mori, Y. (2007) *Nat. Neurosci.*, **10**, 691-701

[41] Uriu, Y., Kiyonaka, S., Miki, T., Yagi, M., Akiyama, S., Mori, E., Nakao, A., Beedle, A.M., Campbell, K.P., Wakamori, M., and Mori, Y. (2010) *J. Biol. Chem.*, **285**, 21750-21767

[42] Kaeser, P. S., Deng, L., Wang, Y., Dulubova, I., Liu, X., Rizo, J., and Südhof, T. C. (2011) *Cell*, **144**, 282-295

[43] Han, Y., Kaeser, P. S., Südhof, T. C., and Schneggenburger, R. (2011) *Neuron*, **69**, 304-316

[44] Chen, J., Billings, S. E., and Nishimune, H. (2011) *J. Neurosci.*, **31**, 512-525

[45] Billings, S. E., Clarke G. L., and Nishimune, H. (2012) *Neuroreport*, **23**, 49-54

[46] Burgess, D. L., Jones, J. M., Meisler, M. H., and Noebels, J. L. (1997) *Cell*, **88**, 385-392

[47] Buraei, Z., and Yang, J. (2010) *Physiol. Rev.*, **90**, 1461-1506

[48] Fouquet, W., Owald, D., Wichmann, C., Mertel, S., Depner, H., Dyba, M., Hallermann, S., Kittel, R. J., Eimer, S., and Sigrist, S. J. (2009) *J. Cell Biol.*, **186**, 129-145

[49] Deken, S. L., Vincent, R., Hadwiger, G., Liu, Q., Wang, Z. W., and Nonet, M. L. (2005) *J. Neurosci.*, **25**, 5975-5983

[50] Ludwig, A., Flockerzi, V., and Hofmann, F. (1997) *J. Neurosci.*, **17**, 1339-1349

[51] Scott, V. E. S., De Waard, M., Liu, H., Gurnett, C. A., Venzke, D. P., Lennon, V. A., and Campbell, K. P.

(1996) *J. Biol. Chem.*, **271**, 3207-3212

[52] McEnery, M. W., Vance, C. L., Begg, C. M., Lee, W.-L., Choi, Y., and Dubel, S. J. (1998) *J. Bioenerg. Biomembr.*, **30**, 409-418

[53] Stanley, E. F., Reese, T. S., and Wang, G. Z. (2003) *Eur. J. Neurosci.*, **18**, 2403-2407

[54] Lee, A., Westenbroek, R. E., Haeseleer, F., Palczewski, K., Scheuer, T., and Catterall, W. A. (2002) *Nat. Neurosci.*, **5**, 210-217

[55] Irie, M., Hata, Y., Takeuchi, M., Ichtchenko, K., Toyoda, A., Hirao, K., Takai, Y., Rosahl, T. W., and Südhof, T. C. (1997) *Science*, **277**, 1511-1515

[56] Niidome, T., Teramoto, T., Murata, Y., Tanaka, I., Seto, T., Sawada, K., Mori, Y., and Katayama, K. (1994) *Biochem. Biophys. Res. Commun.*, **203**, 1821-1827

[57] Wakamori, M., Yamazaki, K., Matsunodaira, H., Teramoto, T., Tanaka, I., Niidome, T., Sawada, K., Nishizawa, Y., Sekiguchi, N., Mori, E., Mori, Y., and Imoto, K. (1998) *J. Biol. Chem.*, **273**, 34857-34867

Chapter 2

Functional impacts of Munc18-1 on gating properties of voltage-dependent Ca^{2+} channels

Abstract

Coupling of presynaptic voltage-dependent Ca^{2+} channels (VDCCs) with the synaptic release mechanism is essential for neurotransmitter release in mammalian neurons. It has become clear that presynaptic proteins at the active zone regulate VDCCs activity and orchestrate multiple processes including neurotransmission. Munc18-1 is an active zone protein, which regulates neurotransmitter release from presynaptic nerve terminals, but the precise modality by which Munc18-1 contributes to neurotransmitter release is poorly understood. Here, we demonstrate a previously unknown molecular interaction between VDCC β_4-subunit and Munc18-1 which was identified by yeast two-hybrid screening. A β-galactosidase assay and co-immunoprecipitation revealed that Munc18-1 selectively associated with β_{1a}-, β_3- and β_{4b}-, compared to β_2-subunit. Moreover, Munc18-1 strongly associated with β_4-subunit rather than the cytoplasmic domain of $Ca_V2.1$ α_1-subunit. In the electrophysiological study we found that Munc18-1 had shifted the voltage dependence of inactivation towards more hyperpolarizing potentials of β_3- and β_4-containing P/Q-type VDCC currents, which could reduce the channel availability at neuronal resting potential. We also observed that Munc18-1 had accelerated the inactivation kinetics of β_4-containing VDCC. In NG108-15 neuroblastoma cells, the suppression of Munc18-1 expression affected the voltage-dependence of inactivation and this effect was attenuated by the suppression of syntaxin 1A. These results suggest that Munc18-1 regulates the function of VDCCs by binding to β-subunit. Our findings contribute to understanding the molecular mechanism of Munc18-1 in modulation of neurotransmitter release.

Introduction

In central synapses, the neurotransmitters are released by synaptic vesicle exocytosis at the active zone of a presynaptic nerve terminal. The active zones, which are characterized by its high-electron density under electron microscopy [1], are composed of cytomatrix and other proteins responsible for neurotransmission [2-4]. The molecular organization of the active zone proteins is essential for regulation of the neurotransmitter release triggered by membrane-depolarization induced Ca^{2+} influx via voltage-dependent Ca^{2+} channels (VDCCs). Many molecular biochemical and physiological analyses have revealed that the functionally coupling of many active zone proteins, including soluble *N*-ethylmaleimide-sensitive factor attachment protein receptor (SNARE), with VDCCs is critical for neurotransmission [4-6]. Therefore, it is greatly important to elucidate the functional significance of protein associations in understanding neurotransmission.

High-voltage-activated VDCCs including N-, P/Q, R-, and L-types play essential roles in neurotransmitter release from presynaptic nerve terminals [7-9]. VDCCs that have been characterized biochemically are complex proteins composed of four subunits, pore-forming α_1, designated as Ca_V, and auxiliary subunits α_2/δ, β, and γ [10]. Ca_V α_1-subunit is organized in four homologous domains (I-IV), with six transmembrane segments in each [11]. VDCC complexes are known to be associated with presynaptic proteins including syntaxin, SNAP-25, synaptotagmin, CASK and Mint via interactions with the α_1-subunit [5, 12-19]. On the other hand, β-subunits interact with α_1-subunit in the cytoplasm to enhance functional channel trafficking to the plasma membrane [20, 21] and to modify multiple kinetic properties [22, 23]. It has been revealed that β-subunits are also associated with other proteins [24-32]. Especially, we previously reported that Rab3 interacting molecule (RIM) family, which are scaffold proteins of active zone, directly associates with the β-subunits, inhibits VDCC inactivation and sustained the Ca^{2+} influx [28, 29]. RIM1 also interacts with the α_1-subunit, and recruits VDCCs to the active zone [33, 34]. In addition, one of active zone proteins Bassoon interacts and modulates the VDCC function [35]. Thus, molecular relationships between VDCCs and the active zone proteins have been gradually cleared.

Munc18-1, the prevailing mammalian neuronal orthologue of *C. elegans unc-18* [36], is widely distributed, especially present at the active zone [37]. Munc18-1 is essential for neurotransmitter release from presynaptic

nerve terminals [38, 39]. Munc18-1 null mutant mice show no evidence of any neurotransmission [38], and there is also a severe impairment of dense core granule exocytosis in their adrenal chromaffin cells [40]. While the interaction of Munc18-1 with syntaxin 1A with nanomolar affinity must reflect an important biological function, this is unlikely to be its only role in neurosecretion [41, 42]. Indeed, Munc18-1 has been suggested to also be involved in the docking of secretory vesicles through the interaction with syntaxin 1A [38, 39, 43, 44], supported both by peptide injection into the squid giant synapse. Current evidence suggests that Munc18-1 influences all of the steps leading to exocytosis, including vesicle recruitment, tethering, docking, priming, and membrane fusion [45].

We previously identified that RIM1 is an interacting protein with VDCC β_4-subunit by yeast two-hybrid screening. In this screening, we also identified a clone encoding Munc18-1 protein. However, physiological significance of this interaction and functional effects of Munc18-1 on VDCCs remain unclear. In this study, we have investigated the physical and functional interactions between Munc18-1 and VDCCs. Biochemical studies showed that Munc18-1 interacts directly and selectively with the VDCC β-subunits. Electrophysiological analyses revealed that Munc18-1 functionally affects the activation and inactivation properties of P/Q-type VDCC co-expressed with VDCC β_{1a}-. β_3-, and β_{4b}-subunit. Furthermore, the suppression of Munc18-1 caused a shift in the voltage-dependence of inactivation towards the hyperpolarizing potentials, and this phenomenon was attenuated by the knockdown of syntaxin 1A in NG108-15 cells. Taken together, Munc18-1 regulates VDCC function via the interaction with β-subunits.

Results

VDCC β-subunits directly interact with Munc18-1

We have previously reported that presynaptic protein RIM1α is identified as one of the VDCC β-subunit interacting proteins by performing yeast two-hybrid screening with a mouse brain complementary DNA library using full-length rat β_{4b}-subunit as a bait [28]. In this screening, we also identified a clone (no. 4-8) encoding a minor variant of mouse Munc18-1 protein (Fig. 1A). This variant contained amino acid residues

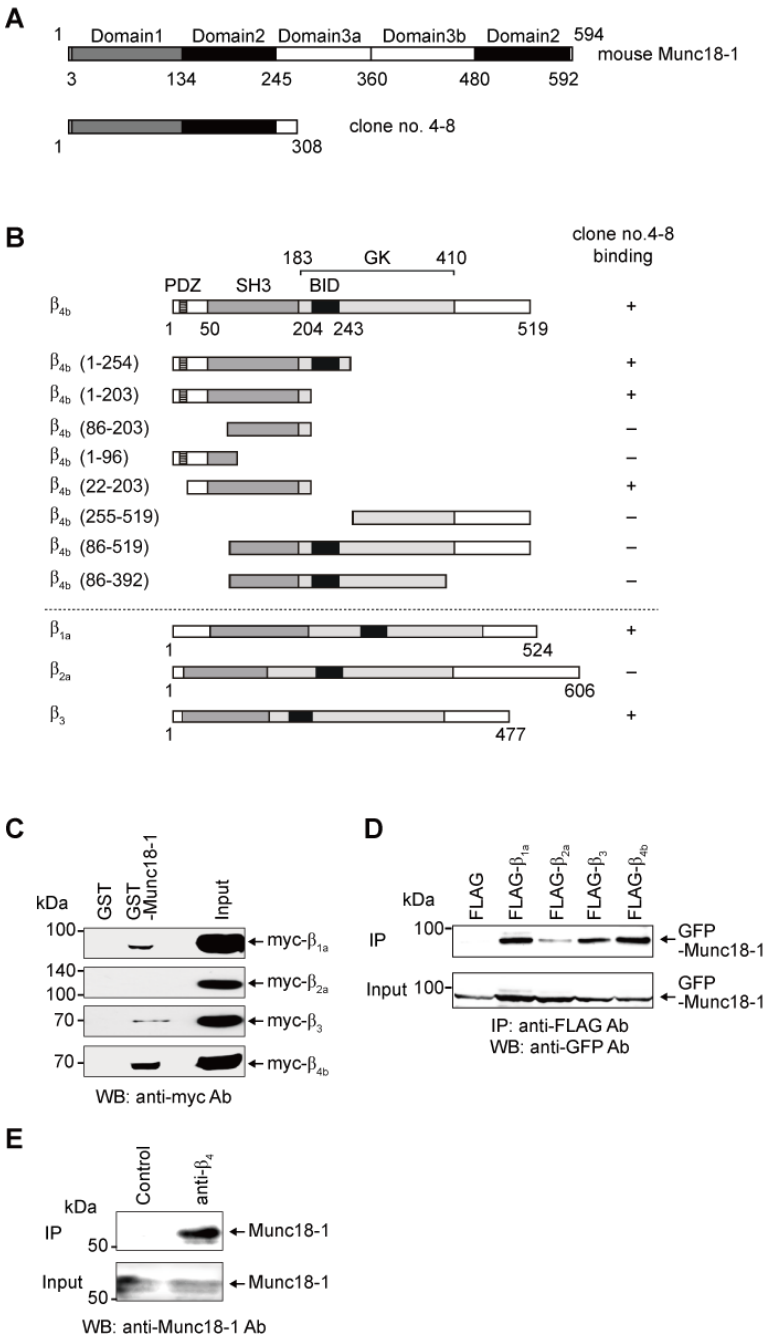

Fig. 1 Direct interaction of Munc18-1 with VDCC β-subunit. (A) Domain structure of mouse Munc18-1 (GenBank Accession Number NM_009295). The protein region encoded by clone no. 4-8 is also indicated. (B) Mapping of Munc18-1-binding sites on β_{4b} by the yeast two-hybrid assay. β-subunit constructs in bait vectors were tested with Munc18-1 (no. 4-8) in the prey vector. The interactions were scored by β-galactosidase activity and His^+ prototrophy. (C) Pulldown assay of β-subunits with GST fusion Munc18-1 constructs. GST fusion proteins immobilized on glutathione-Sepharose beads were incubated with cell lysates obtained from myc-β-transfected HEK293 cells. Bound proteins were analyzed by western blotting using an antibody for myc. Ab, antibody; WB, western blotting.

(D) Interactions of recombinant FLAG-tagged β-subunits and Munc18-1 in HEK293 cells. The interactions were evaluated by immunoprecipitation with antibody for FLAG, followed by western blotting with an antibody for GFP. IP, immunoprecipitation. (E) Co-immunoprecipitation of Munc18-1 with the β_4-subunit. Immunoprecipitation using an antibody for β_4 and subsequent western blotting for Munc18-1 was carried out on a crude synaptic membrane (CSM) from mouse brain.

1–305 of reported Munc18-1 (GenBank Accession Number NM_009295) and unique three amino acids (PLQ). To identify the interaction sites of β-subunit, we performed yeast two-hybrid assay using various β_{4b} mutants. Several β_{4b} mutants including residues 22-203, containing the Src homology 3 (SH3) domain were interacted with clone no. 4-8 of Munc18-1, hence the conserved structure of SH3 domain might be required for the interaction with Munc18-1 (Fig. 1B). Further experiments about the ability of other β-subunits to bind to Munc18-1 revealed that Munc18-1 interactes not only with β_4 but with β_{1a} and β_3-subunits in yeast two-hybrid assays. However, under same condition, we did not show the interaction between Munc18-1 and β_{2a}-subunit. To determine the interaction between a full-length Munc18-1 and β-subunits, glutathione-*S*-transferase (GST) pulldown assays were performed. Consistent with the results of yeast two-hybrid assays, GST-tagged Munc18-1 bound to β_{1a}, β_3, and β_{4b}-subunits, but not β_{2a}-subunit (Fig. 1C). Furthermore, co-immunoprecipitation experiments revealed that Munc18-1 showed higher affinity to β_{1a}, β_3, and β_{4b}-subunits compared to β_{2a}-subunit in HEK293 cells (Fig. 1D), which is consistent with the results of yeast two-hybrid assays and GST-pulldown assays. Finally, to examine the interaction of Munc18-1 with β_4-subunit in native system, we used the immunoprecipitation assay on brain samples. From the immunoprecipitation analysis of the crude synaptic membrane (CSM) fraction solubilized with 1 % digitonin-containing buffer, the Munc18-1 was co-immunoprecipitated with VDCC β_4-subunit (Fig. 1E). Accordingly, Munc18-1 physically associates with native β_4-subunit in the CSM from the mouse brain. Taken together, these results suggest that Munc18-1 directly interacts with VDCC β-subunit.

Interaction of Munc18-1 with the VDCC α_1-subunit

Chan *et al*. previously reported that Munc18-1 binds to the I-II and II-III linker of $Ca_V2.2$ α_1-subunit *in vitro* recombinant system [46]. Therefore, we examined the direct interaction between Munc18-1 and $Ca_V2.1$ α_1-subunit (Fig. 2). We used several cytoplasmic regions of the $Ca_V2.1$ α_1-subunit; the N-terminal (amino acid residues 1-98), I-II linker (amino acid residues 361-488), II-III linker (amino acid residues 731-1038) and C-terminal (amino acid residues 1806-2425) regions [31]. $Ca_V2.1$ N-terminal, the I-II linker and the II-III

linker, but not the C-terminal, also interacted with GST-Munc18-1 (Fig. 2A). The extracts of HEK293 cells expressing EGFP-tagged fragments of VDCC α_1-subunit and VDCC β_4-subunit showed equal expression at the protein level (Fig. 2B). Interestingly, the interaction of β_4-subunit with GST-Munc18-1 was much stronger than that of α_1-subunit fragments (Fig. 2A). These results suggest that Munc18-1 forms a complex with VDCC mainly via association with β_4-subunit rather than the cytoplasmic regions of α_1-subunit.

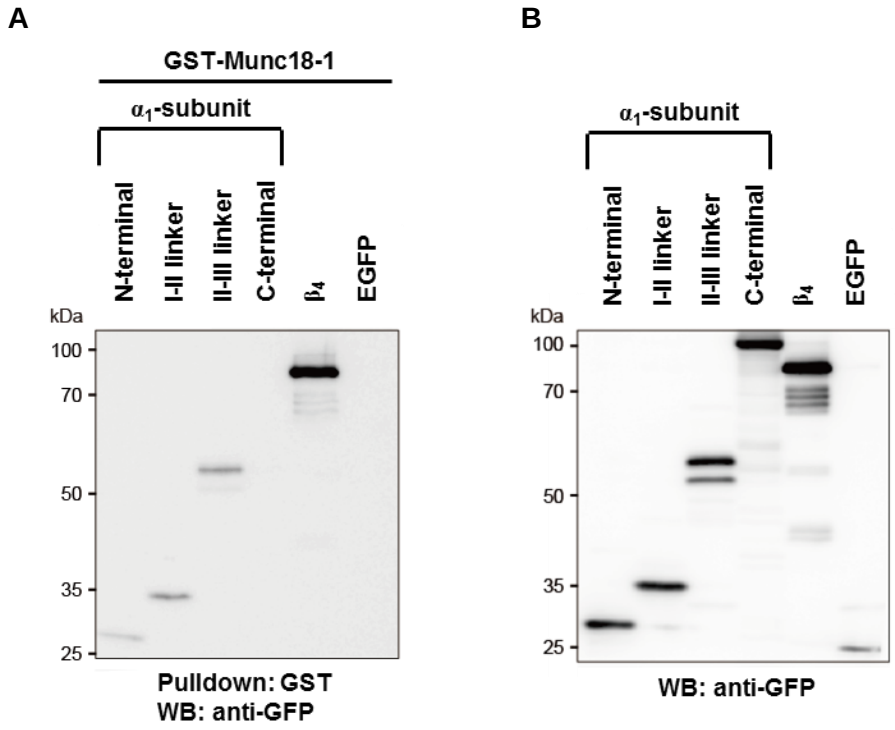

Fig. 2 Interaction of the VDCC α_1-subunit with Munc18-1. (A) GST fusion Munc18-1 immobilized on glutathione-Sepharose beads were incubated with cell lysates obtained from GFP tagged fragments of the α_1-subunit, full-length β_{4b}-subunit, and control GFP vector-transfected HEK293 cells. Bound proteins were analyzed by western blotting using an antibody for GFP. WB, western blotting. (B) Expression and input of EGFP-tagged fragments of the α_1-subunit, full-length β_{4b}-subunit were analyzed by western blotting.

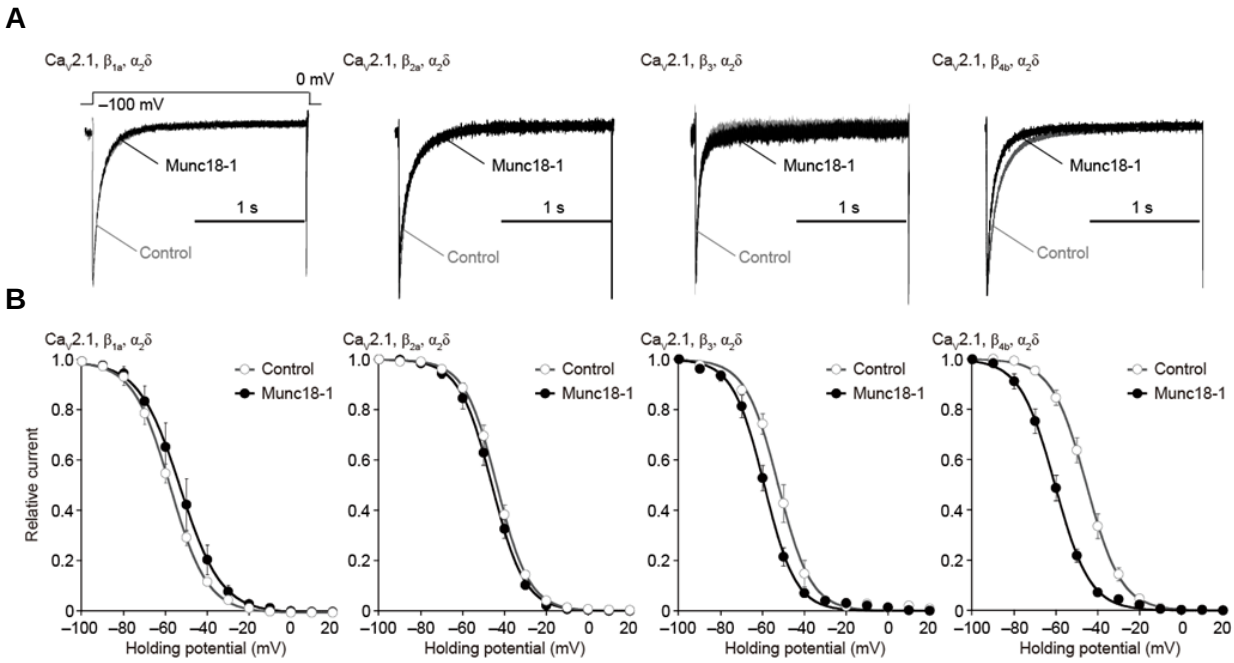

Fig. 3 Effects of Munc18-1 on the inactivation properties of recombinant P/Q-type VDCC currents. (A) Inactivation of P/Q-type VDCC currents in BHK cells expressing α_2/δ and different β-subunits. The peak amplitude before and after co-expression of Munc18-1 constructs were normalized for Ba^{2+} currents elicited by 2-s pulses to 0 mV from a holding potential (V_h) of −100 mV. (B) Inactivation curves for P/Q-type VDCC in BHK cells. Data points are mean ± SEM.

Effects of Munc18-1 on inactivation properties of P/Q-type VDCC currents

To elucidate functional significance of direct interaction between Munc18-1 and VDCC β-subunits, we examined whole-cell Ba^{2+} currents through recombinant P/Q-type VDCC expressed as a complex of the BI-2 variant of $Ca_V2.1$ α_1-subtunit and α_2/δ and various β-subunits in BHK cells [20]. Because P/Q-type VDCC is known to contribute to neurotransmitter release at presynapse [7, 8], we focused on $Ca_V2.1$ channel function in this study. The Ba^{2+} current was elicited with 2-s depolarizing pulse from a holding potential (V_h = −100 mV) to 0 mV. In β_{4b}-expressing BHK cells, inactivation kinetics was slightly accelerated by Munc18-1, whereas in other subtypes of β-subunits-expressing cells Munc18-1 did not affect inactivation kinetics (Fig. 3A). At the same condition, we examined the effect of Munc18-1 on voltage dependence of inactivation by the use of 2-s prepluses to a series of different potentials followed by test pulse to 5 mV. Munc18-1 was significantly shifted toward hyperpolarizing potentials (the half-inactivation potentials ($V_{0.5}$) ranged from

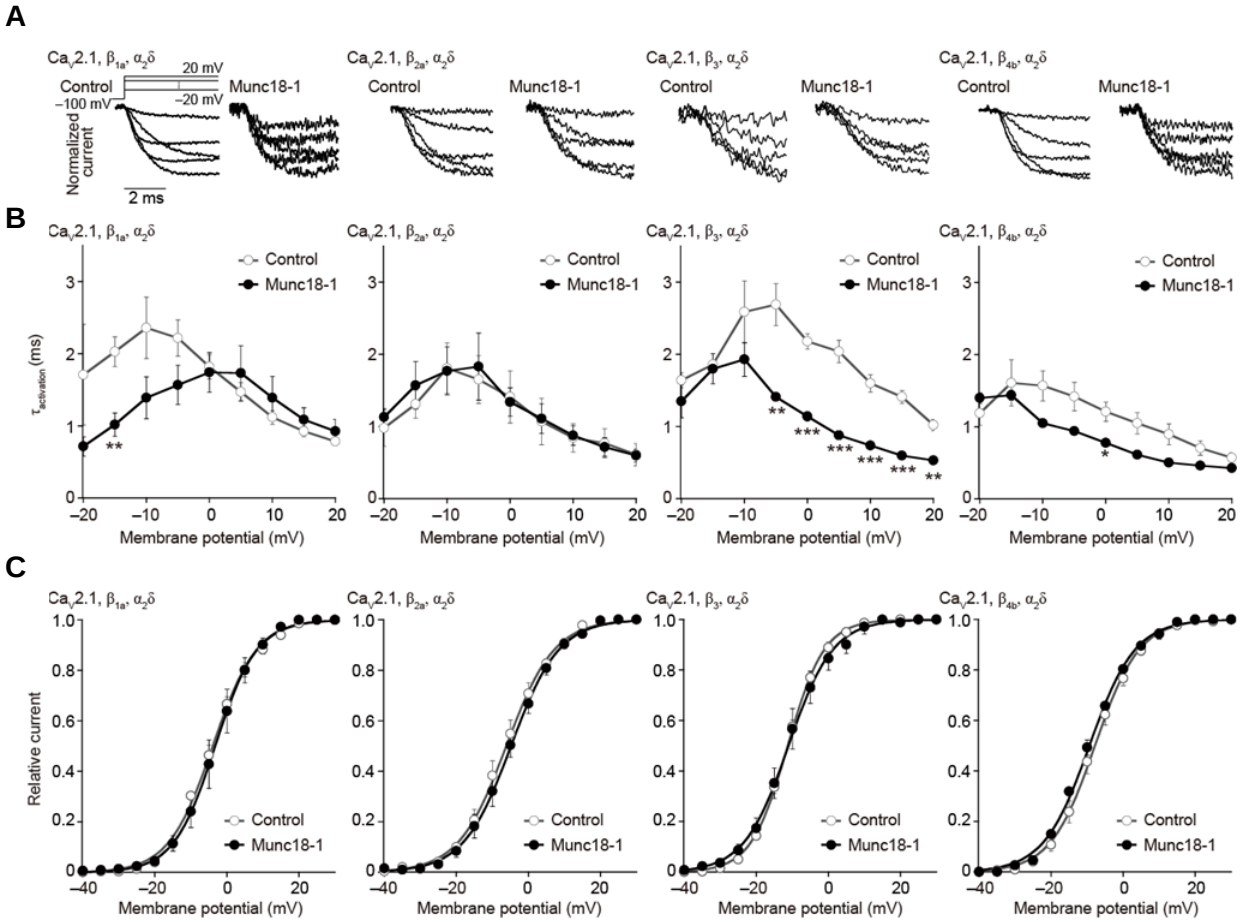

Fig. 4 Effects of Munc18-1 on the activation properties of P/Q-type VDCC currents. (A, B) Activation kinetics of P/Q-type VDCC currents in BHK cells expressing α_2/δ and different β-subunits. Families of representative Ba^{2+} currents elicited by 5-ms step depolarization from −20 to 20 mV in 10-mV increments from a V_h of −100 mV are shown in A. In B, activation time constants plotted as a function of test potential. The activation phases were well fitted by single exponential function at all potentials. $\tau_{activation}$ were obtained from currents elicited by 5-ms step depolarization from −20 to 20 mV in 5-mV increments from a V_h of −100 mV. $^{*}P < 0.05$, $^{**}P < 0.01$, $^{***}P < 0.001$ versus control. (C) Activation curves of P/Q-type VDCC in BHK cells. Tail currents elicited by repolarization to −60 mV after 5-ms test pulses from −40 to 30 mV are used to determine activation curves. Data points are mean ± SEM.

−49.9 ± 1.8 to −60.8 ± 1.7 mV) by Munc18-1 in β_{4b}-expressing cells (Fig. 3B and Table 1). VDCC containing β_3-subunit was also showed a shift of voltage dependence of inactivation toward hyperpolarizing potentials ($V_{0.5}$ ranged from −52.2 ± 2.0 to −59.4 ± 1.6 mV). However, Munc18-1 did not affect the voltage dependence of inactivation of VDCC containing β_{1a}- and β_{2a}-subunit. Thus, the promotive effect on voltage-dependent inactivation is dependent on the subtype of the β-subunit.

Effects of Munc18-1 on activation properties of P/Q-type VDCC currents

We examined the effect of Munc18-1 on the activation properties of the P/Q-type VDCC in BHK cells. Munc18-1 modulated activation kinetics of P/Q-type VDCC in β-subunit dependent manner (Fig. 4A, B). The time constant ($\tau_{activation}$) obtained by fitting the activation time course of inward currents with single exponential was "bell-shaped" when plotted against different voltages. As for P/Q-type VDCC containing β_1-subunit, Munc18-1 significantly accelerated activation kinetics at –15 mV, and activation showed the slowest speed at –10 mV and 0 mV in control and Munc18-1 expressed cells, respectively. As for β_3-subunit, Mun18-1 significantly accelerated activation kinetics at membrane potentials over –5 mV, and activation showed the slowest speed at –5 mV and –10 mV in control and Munc18-1 expressed cells, respectively. As for β_4-subunit, Munc18-1 significantly accelerated activation kinetics at 0 mV. Munc18-1 did not show any modulation in activation speeds in β_{2a}-subunit expressed cells. On the other hand, Munc18-1 failed to exert significant effects on the voltage-dependence of activation despite of the subtype of β-subunits (Fig. 4C, and Table 1).

Next, we examined the P/Q-type VDCC currents and their current density-voltage (*I-V*) relationships in BHK cells expressed various β-subunits in the presence or absence of Munc18-1 (Fig. 5). We found that Munc18-1 did not show significant effects on *I-V* relationships despite of the subtype of β-subunits (Table 1). These results suggest that Munc18-1 significantly affects P/Q-type VDCC currents in terms of activation kinetics depending on the subtype of β-subunits.

Physiological relevance of Munc18-1 effects on the inactivation properties of VDCCs

To investigate the physiological role of Munc18-1-β-subunit complexes in native systems, expression of Munc18-1 was suppressed by treatment with siRNA (Fig. 6). In NG108-15 cells, mouse neuroblastoma and rat glioma hybridoma cells, diverse VDCC types have been precisely characterized [47, 48]. We detected α_1 mRNA species (P/Q-type ($Ca_V2.1$), N-type ($Ca_V2.2$), R-type ($Ca_V2.3$), and L-type ($Ca_V1.2$, $Ca_V1.3$, $Ca_V1.4$)) and β-subunits (β_1, β_2, β_3, and β_4) in NG108-15 cells using specific primers (Fig. 6A and Table 2). Reverse

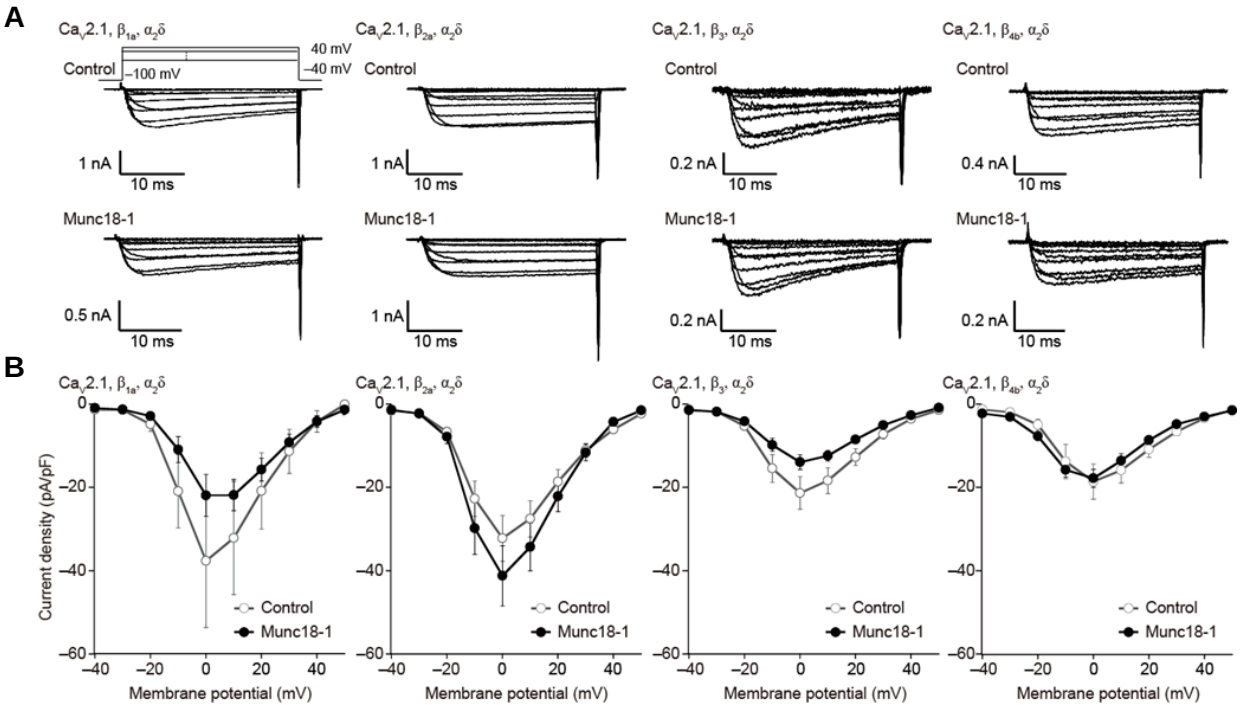

Fig. 5 Effects of Munc18-1 on the current density-voltage (*I-V*) relationships of P/Q-type VDCC. (A) Representative traces of Ba^{2+} currents on application of test pulses from −40 to 40 mV with 10-mV increments from a V_h of −100 mV. (B) *I-V* relationships of P/Q-type VDCC. Data points are mean ± SEM.

Table 1 Effects of Munc18-1 on current density, activation and inactivation properties of $Ca_V2.1$.[1) 2)]

Subunit combination		Current density[3)] (pA / pF)	Activation parameters		Inactivation parameters	
			$V_{0.5}$ (mV)	k (mV)	$V_{0.5}$ (mV)	k (mV)
$Ca_V2.1$	Vector	–37.7 ± 16 (5)	–3.5 ± 0.7 (4)	6.3 ± 0.1 (4)	–57.8 ± 1.5 (4)	–8.9 ± 0.7 (4)
+ β_{1a}	Munc18-1	–22.0 ± 5.0 (6)	–2.8 ± 1.8 (4)	6.1 ± 0.2 (4)	–52.7 ± 3.6 (6)	–8.8 ± 0.4 (6)
$Ca_V2.1$	Vector	–32.2 ± 5.5 (17)	–6.2 ± 1.3 (8)	6.1 ± 2.4 (8)	–46.3 ± 1.7 (16)	–6.9 ± 0.2 (16)
+ β_{2a}	Munc18-1	–41.1 ± 7.2 (12)	–4.9 ± 1.4 (8)	6.2 ± 0.3 (8)	–43.8 ± 1.3 (9)	–7.3 ± 0.1 (9)
$Ca_V2.1$	Vector	–21.3 ± 3.9 (16)	–5.0 ± 0.3 (8)	11.3 ± 0.6 (8)	–52.2 ± 2.0 (7)	–7.2 ± 0.5 (7)
+ β_3	Munc18-1	–13.9 ± 1.7 (9)	–5.6 ± 0.2 (6)	11.0 ± 1.8 (6)	–59.4 ± 1.6 (6)*	–7.4 ± 0.5 (6)
$Ca_V2.1$	Vector	–18.5 ± 4.2 (5)	–5.7 ± 1.5 (12)	6.7 ± 1.1 (12)	–49.9 ± 1.8 (14)	–7.5 ± 0.3 (14)
+ β_{4b}	Munc18-1	–17.7 ± 2.2 (5)	–8.6 ± 0.5 (4)	6.9 ± 0.2 (4)	–60.8 ± 1.7 (5)***	–7.9 ± 0.4 (5)

1) *P< 0.05, ***P < 0.001 versus Vector.

2) Numbers of cells analyzed are indicated in the parenthesis.

3) Ba^{2+} currents evoked by depolarizing pulse to 0 mV from a V_h of -100 mV are divied by capacitance.

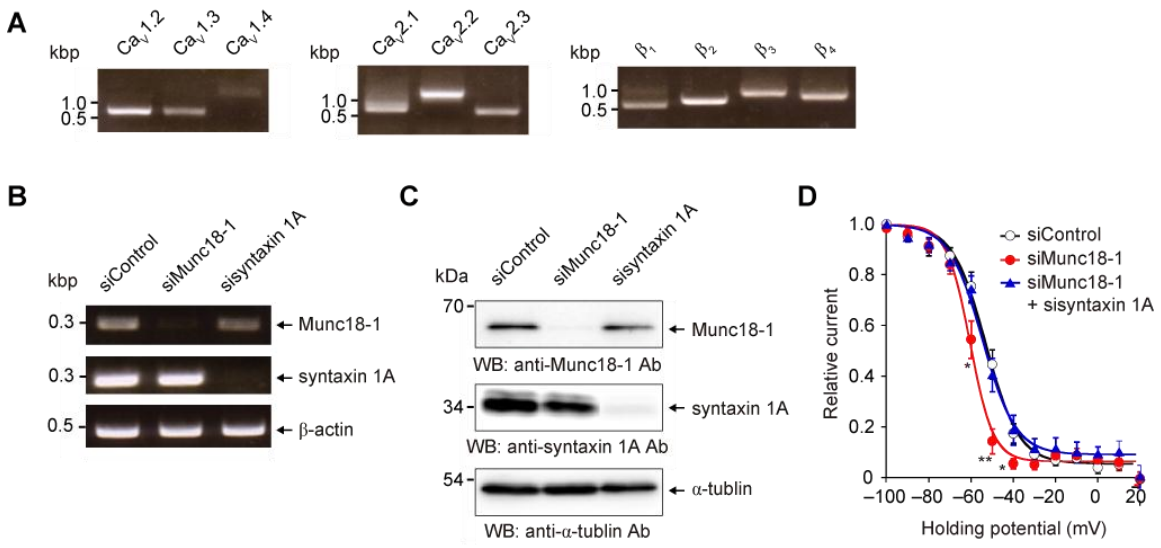

Fig. 6 Physiological relevance of Munc18-1 effects on VDCC function. (A) Molecular characterization of NG108-15 cells. RNA expression analysis of α_1- and β-subunits using RT-PCR in NG108-15 cells. (B) RT-PCR analysis of Munc18-1 and syntaxin 1A RNA expression in NG108-15 cells treated with GAPDH siRNA (siControl), Munc18-1 specific siRNA (siMunc18-1) and syntaxin 1A specific siRNA (sisyntaxin 1A). β-actin was used as loading control. (C) Western blotting analysis of Munc18-1 and syntaxin 1A protein expression in NG108-15 cells. α-tublin was used as loading control. Ab, antibody; WB, western blotting. (D) Effects of siRNA for Munc18-1 or Munc18-1 and syntaxin 1A on the inactivation curves for VDCCs in NG108-15 cells. Normalized test pulse currents were plotted against potentials of the 2-s V_h displacement and fitted to the single Boltzmann's equation. $^{*}P < 0.05$, $^{**}P < 0.01$ versus siControl. Data points are mean ± SEM.

Table 2 Antisense and sense PCR primers used in RT-PCR analysis.

Gene	Sense primers for PCR (5' to 3')	Antisense primers for PCR (5' to 3')
$Ca_v1.2$	TGGACAAGGCTATGAAGGAG	ACCTAGAGAGGCAGAGCGAAGG
$Ca_v1.3$	TTAGTGACGCCTGGAACACG	CCACATCAAGGTGTTTTATC
$Ca_v1.4$	ATGCTCTGTGCCTTCCTG	TGAGGTCCGTCCACGATG
$Ca_v2.1$	CAGCATCACAGACATCCTCG	TACTCTGCCCAGACACGCAC
$Ca_v2.2$	CGAAATGACCTCATCCATGCAG	TTCTGGAGCCTTAGCTGACTGG
$Ca_v2.3$	ATCATGAAGGCCATGGTGCC	AGCAAGCATGACTTCCTCTG
β_1	CCTATGACGTGGTGCCTTCC	CTTCCAGTAGGCTTCCAAGTAC
β_2	AGAAGACAGAGCACACTCCTCC	GGCTCAGAGGTAAAGTTGAGG
β_3	TCTCTAGCCAAGCAGAAGC	AGGCATCTGCATAGTCCTCC
β_4	TCAATGCGTCCTGTGGTGTTAGT	CAAGCGGTTCCTACTCTTGC
Munc18-1	GGTGCTACTGGATGAGGACGATG	CCACGCGGCAGAGTTTGTC
syntaxin 1A	GTCACTGTCACTGTGGACCG	CTGCGTCTTCCGGATCCTC
β-actin	TTCTACAATGAGCTGCGTGTGGC	CTCATAGCTCTTCTCCAGGGAGGA

Table 3 Effect of siRNA applications on inactivation properties of VDCC in NG108-15 cells.[1) 2)]

	Inactivation parameters		
	a	$V_{0.5}$ (mV)	*k* (mV)
siControl	0.95 ± 0.01 (6)	–53.2 ± 2.2 (6)	–7.9± 0.9 (6)
siMunc18-1	0.94 ± 0.02 (5)	–60.5 ± 1.9 (5) *	–5.3 ± 0.6 (5) *
siMunc18-1 + sisyntaxin 1A	0.91 ± 0.04 (5)	–54.7 ± 1.6 (5)	–7.8 ± 1.0 (5)

1) *P< 0.05, versus siControl.

2) Numbers of cells analyzed are indicated in the parenthesis.

transcription polymerase chanin reaction (RT-PCR) analysis showed that siRNAs for Munc18-1 and syntaxin 1A effectively suppressed the expression of target genes, whereas control siRNA (siControl) failed to exert significant effects on Munc18-1 or syntaxin 1A RNA expression (Fig. 6B). Western blotting also indicated that application of siRNAs for Munc18-1 and syntaxin 1A effectively suppressed expressions of target proteins (Fig. 6C). The voltage-dependence of VDCC inactivation in NG108-15 cells was significantly shifted toward hyperpolarizing potentials by application of siRNA for Munc18-1 (Fig. 6D and Table 3). This hyperpolarizing shift was cancelled by the knockdown of syntaxin 1A (Fig. 6D and Table 3). Thus, these results suggest that Munc18-1 and syntaxin 1A functionally competitively interact with VDCC in NG108-15 cells.

Discussion

In the present study, we have demonstrated that Munc18-1 physically associates with VDCC β-subunits. *In vitro* binding assays and co-immunoprecipitation experiments identified protein complexes formed by direct interactions of VDCC β-subunits or α_1-subunits with Munc18-1 (Fig. 1, and Fig. 2). Yeast two hybrid assay also revealed that the conserved structure of SH3 domain of β-subunit might be required for the interaction with Munc18-1. Munc18-1 physically associated with native β_4-subunit in the CSM from the mouse brain (Fig. 1*C*). Electrophysiological analyses revealed that the interactions between Munc18-1 and VDCC β-subunits reduces the availability of P/Q-type Ca^{2+} channels and accelerates their activation kinetics in

β-subunit-dependent manner (Fig. 3, and Fig. 4). In NG108-15 cells, the knockdown of Munc18-1 accelerated the inactivation of VDCC, and this effect was diminished by the suppression of syntaxin 1A expression (Fig. 6).

Previous reports have demonstrated functional impacts of syntaxin, SNAP-25 and synaptotagmin on VDCCs through their physical association with the 'synprint' region in the II-III linker of α_1-subunit [5, 13, 15]. It has also been reported that Munc18-1 associate with the synprint directly and with C terminus indirectly via Munc18-1 interacting protein (Mint) [17]. However, VDCC complex containing β_{2a}-subunit, which cannot bind to Munc18-1 (Fig. 1), did not show any modulation by Munc18-1 (Fig. 3, Fig. 4, and Fig. 5). Although there is no obvious reason why β_{2a}-subunit dose not interact with Munc18-1, it is suggested that SH3 domain of β_{2a}-subunit might be different from that of the other β-subunits in the light of the amino acid sequences and previous reported crystal structures of β_{2a}-, β_3-, and β_4-subunit [49-51]. On the other hand, Munc18-1 more strongly associates with β_4-subunit rather than α_1-subunit fragments (Fig. 2). Although Munc18-1 directly binds to the I-II and II-III linker of $Ca_V2.2$ α_1-subunit [46], these results suggest that modulation of VDCC by Munc18-1 may be dependent on β-subunit-mediated association rather than the α_1-synprint- or Mint- mediated one.

Munc18-1 has been shown to be distributed ubiquitously, but it is especially present at the active zone [37] and essential for neurotransmitter release from presynapse [38, 39]. In addition, VDCC β_3 and β_4 subunits are very abundant in the brain [52, 53]. Biochemical assay reveals that the most prevalent partner of $Ca_V2.2$ (N-type) is β_3-subunit, and that of $Ca_V2.1$ (P/Q-type) is β_4-subunit [53-55]. Both VDCCs are thought to play critical roles for neurotransmitter release [7-9]. Taken together, present studies support the idea that Munc18-1 mainly interacts with VDCC β-subunit in the nerve terminal and regulate neurotransmitter release.

The N-type and P/Q-type VDCCs at presynapse are subject to functional modulation by interaction with synaptic proteins that finely tune Ca^{2+} entry into nerve terminals. The present studies demonstrate that Munc18-1 has a functional impact on the gating of P/Q-type VDCC. It reduces the availability of P/Q-type VDCC at a neuronal resting potential near −75 mV (Fig. 3). Assuming that our findings are applicable to nerve terminals, Munc18-1 would be expected strongly to inhibit presynaptic Ca^{2+} entry. These modulations

are not appeared to be advantageous for Ca^{2+} triggered fusion, but would produce the desirable effect of reducing Ca^{2+} influx in the absence of docked synaptic vesicles. We hypothesized that Munc18-1 may allow synaptic vesicles to become docked and/or ready for fusion around VDCC without exposing fusion machinery to robust Ca^{2+} entry. We previously reported that RIM, which associates with synaptic vesicle protein Rab3, markedly inhibits voltage-dependent inactivation of VDCC via interaction with β-subunit [28, 29]. Modulation by RIM is advantageous for Ca^{2+} triggered fusion. Similar reciprocal regulation of VDCC by SNAP-25, syntaxin and synaptotagmin has been reported [15]. These three presynaptic proteins bind to synprint region in P/Q-type VDCC α_1-subunit. Inhibitory effect of SNAP-25 was reversed by syntaxin and synaptotagmin, because of competitive displacement of SNAP-25 from synprint region. Furthermore, presynaptic protein CAST/ERC2 binds to the β-subunit and shifts voltage-dependence of activation toward the hyperpolarizing direction [31]. Taken together with previous findings, we speculate that the reduction of Ca^{2+} influx by Munc18-1 might be relieved and exchanged for increase of Ca^{2+} influx by RIM and/or CAST/ERC2 following the docking of a synaptic vesicle. Reciprocal regulation of Ca^{2+} channel activity by these presynaptic proteins would ensure that Ca^{2+} entry could efficiently initiate synaptic transmission by restricting the full activity of only those presynaptic Ca^{2+} channels associated with a synaptic vesicle through SNARE-protein interactions.

Interestingly, suppression of Munc18-1 expression shifts the voltage-dependence of inactivation towards hyperpolarizing potentials in neuroblastoma-glioma hybrid NG108-15 cells, which express native VDCCs (Fig. 6). Although there are no obvious evidences that account for this discrepancy between recombinant and native system, syntaxin 1A may play essential role for VDCC inactivation [13, 14]. Munc18-1 physically associates syntaxin 1A and forms SNARE-Munc18-1 complex at presynaptic terminal [41, 42]. Thus, possible explanation for the siRNA experiments is that free syntaxin 1A is increased, and strongly affects voltage-dependence of inactivation by Munc18-1 knockdown in NG108-15 cells, which is supported by present results (Fig. 6). Consistent with these findings, it has been reported that the voltage-dependence of steady state inactivation is shifted toward hyperpolarizing potentials by Munc18-1 knockdown in an acutely isolated native chick neuron [46].

In summary, we present here that direct association between Munc18-1 and VDCCs modulates the inactivation of the functional VDCC complex. In a nerve terminal, this reversible negative shift in the voltage-dependence of inactivation would provide a molecular switch to inhibit P/Q type VDCC when associated with an immature SNARE protein complex, but to reactivate them as the synaptic core complex matures in preparation for vesicle release. Further studies using Munc18-1 knockout mice would provide new insights into the mechanism of functional coupling among the presynaptic active zone proteins.

Experimental procedures

Yeast two-hybrid screening and β-galactosidase assay

Rat β_{4b}-subunit (GenBank Accession Number XM_215742) subcloned into pGBK-T7 was used as a bait to screen a mouse brain pACT2 library (Clontech) in the yeast strain AH109 according to the manufacturer's instructions (Clontech). 1.5×10^6 transformants plated to synthetic medium lacking adenine, histidine, leucine, and tryptophan. His^+ colonies were assayed for β-galactosidase activity by a filter assay. Of the transformants, 103 were His^+, of which 21 were also $LacZ^+$. Prey clone no.4-8 encoding amino acid residues 1-305 of full length Munc18-1 (GenBank Accession Number NM_009295) and unique three amino acids was isolated. Expression plasmids pGBK-T7 carrying β_{4b} or its mutants were constructed by PCR.

cDNA cloning and construction of expression vectors

Mun18-1 (GenBank Accession Number NM_009295) was cloned from mouse brain Marathon-Ready cDNA (Clontech) using PCR, and was subcloned into pEGFP-C1 (Clontech), and pIRES2-EGFP (Clontech). Rabbit β_{1a} (GenBank Accession Number M25817), rabbit β_{2a} (GenBank Accession Number X64297), rabbit β_3 (GenBank Accession Number X64300), and rat β_{4b} (GenBank Accession Number XM_215742) were subcloned into FLAG-tagged vector pCMV-tag2 (Stratagene), or myc-tagged vector pCMV-tag3 (Stratagene). Rabbit $Ca_V2.1$ N-terminal (amino acid residues 1-98), the I-II linker (amino acid residues 361-488), the II-III linker (amino acid residues 731-1038), and the C-terminal (amino acids residues 1806-2425) were subcloned

into pEGFP-C1.

Production of GST fusion proteins

For production of GST fusion proteins for Munc18-1, cDNA for Munc18-1 construct and the GST were subcloned together into the pET23 vector (Novagen). The Rosetta strain (Novagen) of *Escherichia coli* was transformed by the expression vectors, and protein expression/purification was performed according to the manufacturer's instruction (Novagen).

GST-pulldown assay and co-immunoprecipitation in HEK293 cells

HEK293 cells were cultured in Dulbecco's modified Eagle's medium (DMEM) containing 10 % fetal bovine serum, 30 units/mL penicillin, and 30 μg/mL streptomycin. 48 h after transfection, HEK293 cells were solubilized in NP-40 buffer (150 mM NaCl, 50 mM Tris, 1 % NP-40, and protease inhibitors), and then centrifuged at 17,400 × *g* for 20 min. For pulldown assays, cell lysates were incubated with glutathione-Sepharose beads bound to purified fusion proteins, and then the beads were washed with NP-40 buffer at 4 ℃. Proteins retained on the beads were characterized by western blotting with anti-myc antibody (invitrogen). For co-immunoprecipitation, cell lysates were incubated with anti-FLAG M2 monoclonal antibody (Sigma), then immunocomplexes incubated with protein A-agarose beads (Santa Cruz), and were washed with NP-40 buffer. Immunoprecipitated proteins were characterized by western blotting with anti-GFP antibody (Clontech).

Biochemistry of native neuronal VDCC complexes

To obtain crude synaptic membrane (CSM) fraction, subcellular fractionation was performed based on a previously described method [56], with slight modification. Whole mouse brains (8 g) were homogenized in a homogenization buffer containing 4 mM HEPES, 0.32 M sucrose, 5 mM EDTA, 5 mM EGTA, and protease inhibitors (pH 7.4). Cell debris and nuclei were removed by centrifugation at 800 × *g* for 10 min. The supernatant (S1) was centrifuged at 9,000 × *g* for 15 min to obtain crude synaptosomal fraction as pellet (P2).

The supernatant was stored as S2. The crude synaptosomes were resuspended in the homogenization buffer and centrifuged at 10,000 × *g* for 15 min. The washed crude synaptosomes were lysed by hypoosmotic shock in water, rapidly adjusted to 1 mM HEPES/NaOH (pH 7.4), and stirred on ice for 30 min. After centrifugation of the lysate at 25,000 × *g* for 20 min, the pellet was resuspended in 0.25 M buffered sucrose. The synaptic membranes were then further enriched through a discontinuous sucrose gradient containing 0.8/1.0/1.2 M sucrose. After centrifugation at 65,000 × *g* for 2 h, the CSM fraction was collected from 1.0/1.2 M sucrose interface. Synaptic membrane proteins were extracted from the CSM with solubilization buffer containing 50 mM Tris, 500 mM NaCl, a mixture of protease inhibitors, and 1 % digitonin (Biosynth) (pH 7.4). After centrifugation at 40,000 × *g* for 37 min, supernatant was diluted with a buffer containing 50 mM Tris and 1 % digitonin to adjust NaCl concentration to 150 mM and incubated overnight at 4 °C. After centrifugation at 8,000 × *g* for 15 min, the supernatant was incubated with protein A-agarose coupled to anti-β_4 antibody [28]. Immunoprecipitated proteins were subjected to western blotting with anti-Munc18-1 monoclonal antibody (BD Transduction Lab).

Cell culture and cDNA expression in BHK cells

Baby hamster kidney (BHK) lines stably expressing α_2/δ and β_{2a}, β_3 or β_{4b}, and BHK6-2 line stably expressing $Ca_V2.1$, α_2/δ and β_{1a} were described previously [28, 57]. BHK cells were cultured in DMEM containing 10 % fetal bovine serum, 30 units/mL penicillin, and 30 μg/mL streptomycin. These BHK lines were co-transfected with pK4K plasmid containing cDNA for $Ca_V2.1$ α_1-subunit (for except BHK6-2) and expression plasmids carrying Munc18-1 constructs (pIRES2-EGFP-vector, pIRES2-EGFP-Munc18-1) using Effectene Transfection Reagent (Qiagen). The cells were subjected to electrophysiological measurements 48 h after transfection.

Current recordings

Whole-cell mode of the patch-clamp technique was carried out at 22-25 °C with an EPC-10 (HEKA Elektronik) patch-clamp amplifier as previously described [58]. Patch pipettes were made from borosilicate

glass capillaries (1.5 mm outer diameter, 0.87 mm inner diameter; Hilgenberg) using a model P-87 Flaming-Brown micropipette puller (Sutter Instrument Co.). The patch electrodes were fire-polished. Pipette resistance ranged from 2 to 3.5 MΩ when filled with pipette solutions described below. Series resistance was electronically compensated to > 60 %, and both the leakage and the remaining capacitance were subtracted by the –P/4 method. Currents were sampled at 100 kHz after low pass filtering at 8.4 kHz (3 db) in the experiments of activation kinetics, otherwise sampled at 20 kHz after low pass filtering at 3.0 kHz (3 db). Data were collected and analyzed using PATCHMASTER (HEKA Elektronik). The external solution contained (in mM): 3 $BaCl_2$, 155 tetraethylammonium chloride (TEA-Cl), 10 HEPES, and 10 glucose (pH 7.4 adjusted with TEA-OH) for BHK cells, and 10 $BaCl_2$, 148 TEA-Cl, 10 HEPES, 10 glucose and 0.5 μM Tetrodotoxin (pH7.4 adjusted with TEA-OH) for NG108-15 cells. The pipette solution contained (in mM): 95 CsOH, 95 aspartate, 40 CsCl, 4 $MgCl_2$, 5 EGTA, 2 disodium ATP, 5 HEPES and 8 creatine phosphate (pH 7.2 adjusted with CsOH).

Voltage-dependence of inactivation

To determine voltage-dependence of inactivation (inactivation curve) of VDCCs, Ba^{2+} currents were evoked by a 20-ms test pulse to 5 mV after 10-ms repolarization to −100 mV following 2-s holding potential (V_h) displacement from −100 mV to 20 mV with 10-mV increments. Amplitudes of currents elicited by test pulses were normalized to those after a 2-s V_h displacement to −100 mV. Mean values were plotted against potentials for 2-s V_h displacement. When the inactivation curve was monophasic, mean values were fitted to the single Boltzmann's equation: $h(V_h) = (1-a)+a/\{1+\exp[(V_{0.5}-V_h)/k]\}$, with a, rate of inactivating component, $V_{0.5}$, potential to give half-value of inactivation, and k, slope factor.

Voltage-dependence of activation

Tail currents were elicited by repolarization to −60 mV after a 5-ms test pulse from −40 to 30 mV with 5-mV increments. Currents were sampled at 100 kHz after low pass filtering at 8.4 kHz. Amplitude of tail currents were normalized to those obtained with test pulses to 30 mV. Mean values were plotted against test pulse

potentials, and fitted to Boltzmann's equation: $n(V_m) = 1/\{1+\exp[(V_{0.5}-V_m)/k]\}$, with V_m, membrane potential, $V_{0.5}$, potential to give half-value of conductance, and k , slope factor.

Cell culture and siRNA suppression of endogenous Munc18-1 in NG108-15 cells

NG108-15 neuroblastoma cells were cultured in DMEM with high concentrations of glucose and 10 % fetal bovine serum, 100 μM hypoxanthine, 1 μM aminopterin, 16 μM thymidine. To induce neuronal differentiation, 1 mM dibutyryl cyclic AMP was added to the culture medium and cells were cultured for another 7 days. The sense siRNA sequences 5'-AAGGACTTTTCCTCTAGCAAG-3' for mouse Munc18-1, and 5'-GGCGCATCCAGAGGCAGCT-3' for mouse syntaxin 1A were used. To construct siRNA oligomers, the Silencer siRNA Construction Kit (Ambion) was used. The GAPDH siRNA (siControl) was used as the control provided with the kit. Transfection of siRNAs to NG108-15 cells was carried out using Lipofectamine® 2000 (invitrogen). Suppression of RNA and protein expression was confirmed by RT-PCR analyses, and western blotting, respectively 48 h after transfection.

Statistical analysis

All data were expressed as mean ± SEM. Data were obtained under each condition from at least three independent experiments. Statistical significance was evaluated by analysis of variance followed by the Tukey-Kramer test.

Reference

[1] Landis, D. M., Hall, A. K., Weinstein, L. A., and Reese, T. S. (1988) *Neuron*, **1**, 201-209

[2] Ohtsuka, T., Takao-Rikitsu, E., Inoue, E., Inoue, M., Takeuchi, M., Matsubara, K., Deguchi-Tawarada, M., Satoh, K., Morimoto, K., Nakanishi, H., and Takai, Y. (2002) *J. Cell Biol.*, **158**, 577-590

[3] Zhai, R. G. and Bellen, H. J. (2004) *Physiology (Bethesda)*, **19**, 262-270

[4] Südhof, T. C. (2012) *Neuron*, **75**, 11-25

[5] Spafford, J. D. and Zamponi, G. W. (2003) *Curr. Opin. Neurobiol.*, **13**, 308-314

[6] Catterall, W. A. and Few, A. P. (2008) *Neuron*, **59**, 882-901

[7] Takahashi, T., and Momiyama, A. (1993) *Nature*, **366**, 156-158

[8] Wheeler, D. B., Randall, A., and Tsien, R. W. (1994) *Science*, **264**, 107-111

[9] Catterall, W. A. (1998) *Cell Calcium*, **24**, 307-323

[10] Ertel, E. A., Campbell, K. P., Harpold, M. M., Hofmann, F., Mori, Y., Perez-Reyes, E., Schwartz, A., Snutch, T. P., Tanabe, T., Birnbaumer, L., Tsien, R. W., and Catterall, W. A. (2000) *Neuron*, **25**, 533-535

[11] Catterall, W. A., Perez-Reyes, E., Snutch, T. P., and Striessnig, J. (2005) *Pharmacol. Rev.*, **57**, 411-425

[12] Sheng, Z. H., Rettig, J., Takahashi, M., and Catterall, W. A. (1994) *Neuron*, **13**, 1303-1313

[13] Bezprozvanny, I., Scheller, R. H., and Tsien, R. W. (1995) *Nature*, **378**, 623-626

[14] Wiser, O., Bennett, M. K., and Atlas, D. (1996) *EMBO J.*, **15**, 4100-4110

[15] Zhong, H., Yokoyama, C. T., Scheuer, T., and Catterall, W. A. (1999) *Nat. Neurosci.*, **2**, 939-941

[16] Maximov, A., Südhof, T. C., and Bezprozvanny, I. (1999) *J. Biol. Chem.*, **274**, 24453-24456

[17] Maximov, A. and Bezprozvanny, I. (2002) *J. Neurosci.*, **22**, 6939-6952

[18] Nishimune, H., Sanes, J. R., and Carlson, S. S. (2004) *Nature*, **432**, 580-587

[19] Watanabe, H., Yamashita, T., Saitoh, N., Kiyonaka, S., Iwamatsu, A., Campbell, K. P., Mori, Y., and Takahashi, T. (2010) *J. Neurosci.*, **30**, 655-660

[20] Mori, Y., Friedrich, T., Kim, M. S., Mikami, A., Nakai, J., Ruth, P., Bosse, E., Hofmann, F., Flockerzi, V., Furuichi, T., Mikoshiba K., Imoto K., Tanabe T., and Numa S. (1991) *Nature*, **350**, 398-402

[21] Bichet, D., Cornet, V., Geib, S., Carlier, E., Volsen, S., Hoshi, T., Mori, Y., and De Waard, M. (2000) *Neuron*, **25**, 177-190

[22] Varadi, G., Lory, P., Schultz, D., Varadi, M., and Schwartz, A. (1991) *Nature*, **352**, 159-162

[23] Lacerda, A. E., Kim, H. S., Ruth, P., Perez-Reyes, E., Flockerzi, V., Hofmann, F., Birnbaumer, L., and Brown, A. M. (1991) *Nature*, **352**, 527-530

[24] Béguin, P., Nagashima, K., Gonoi, T., Shibasaki, T., Takahashi, K., Kashima, Y., Ozaki, N., Geering, K., Iwanaga, T., and Seino, S. (2001) *Nature*, **411**, 701-706

[25] Hibino, H., Pironkova, R., Onwumere, O., Rousset, M., Charnet, P., Hudspeth, A. J., and Lesage, F. (2003) *Proc. Natl. Acad. Sci. U. S. A.*, **100**, 307-312

[26] Vendel, A. C., Terry, M. D., Striegel, A. R., Iverson, N. M., Leuranguer, V., Rithner, C. D., Lyons, B. A., Pickard, G. E., Tobet, S. A., and Horne, W. A. (2006) *J. Neurosci.*, **26**, 2635-2644

[27] Gonzalez-Gutierrez, G., Miranda-Laferte, E., Neely, A., and Hidalgo, P. (2007) *J. Biol. Chem.*, **282**, 2156-2162

[28] Kiyonaka, S., Wakamori, M., Miki, T., Uriu, Y., Nonaka, M., Bito, H., Beedle, A. M., Mori, E., Hara, Y., De Waard, M., Kanagawa, M., Itakura, M., Takahashi, M., Campbell, K. P., and Mori, Y. (2007) *Nat. Neurosci.*, **10**, 691-701

[29] Uriu, Y., Kiyonaka, S., Miki, T., Yagi, M., Akiyama, S., Mori, E., Nakao, A., Beedle, A. M., Campbell, K. P., Wakamori, M., and Mori, Y. (2010) *J. Biol. Chem.*, **285**, 21750-21657

[30] Chen, J., Billings, S. E., and Nishimune, H. (2011) *J. Neurosci.*, **31**, 512-525

[31] Kiyonaka, S., Nakajima, H., Takada, Y., Hida, Y., Yoshioka, T., Hagiwara, A., Kitajima, I., Mori, Y., and Ohtsuka, T. (2012) *J. Biochem.*, **152**, 149-159

[32] Billings, S. E., Clarke, G. L., and Nishimune, H. (2012) *Neuroreport*, **23**, 49-54

[33] Kaeser, P. S., Deng, L., Wang, Y., Dulubova, I., Liu, X., Rizo, J., and Südhof, T. C. (2011) *Cell*, **144**, 282-295

[34] Han, Y., Kaeser, P. S., Südhof, T. C., and Schneggenburger, R. (2011) *Neuron*, **69**, 304-316

[35] Nishimune, H., Numata, T., Chen, J., Aoki, Y., Wang, Y., Starr, M. P., Mori, Y., and Stanford, J. A. (2012) *PLoS One*, **7**, e38029

[36] Hata, Y., Slaughter, C. A., and Südhof, T. C. (1993) *Nature*, **366**, 347-351

[37] Okamoto, M., Matsuyama, T., and Sugita, M. (2000) *Eur. J. Neurosci.*, **12**, 3067-3072

[38] Verhage, M., Maia, A. S., Plomp, J. J., Brussaard, A. B., Heeroma, J. H., Vermeer, H., Toonen, R. F., Hammer, R. E., van den Berg, T. K., Missler, M., Geuze, H. J., and Südhof, T. C. (2000) *Science*, **287**, 864-869

[39] Weimer, R. M., Richmond, J. E., Davis, W. S., Hadwiger, G., Nonet, M. L., and Jorgensen, E. M. (2003)

Nat. Neurosci., **6**, 1023-1030

[40] Voets, T., Toonen, R. F., Brian, E. C., de Wit, H., Moser, T., Rettig, J., Südhof, T. C., Neher, E., and Verhage, M. (2001) *Neuron*, **31**, 581-591

[41] Pevsner, J., Hsu, S. C., and Scheller, R. H. (1994) *Proc. Natl. Acad. Sci. U. S. A.*, **91**, 1445-1449

[42] Misura, K. M., Scheller, R. H., and Weis, W. I. (2000) *Nature*, **404**, 355-362

[43] Dresbach, T., Burns, M. E., O'Connor, V., DeBello, W. M., Betz, H., and Augustine, G. J. (1998) *J. Neurosci.*, **18**, 2923-2932

[44] Toonen, R. F., Kochubey, O., de Wit, H., Gulyas-Kovacs, A., Konijnenburg, B., Sørensen, J. B., Klingauf, J., and Verhage, M. (2006) *EMBO J.*, **25**, 3725-3737

[45] Burgoyne, R. D., Barclay, J. W., Ciufo, L. F., Graham, M. E., Handley, M. T. W., and Morgan, A. (2009) *Ann. N. Y. Acad. Sci.*, **1152**, 76-86

[46] Chan, A. W., Khanna, R., Li, Q., and Stanley, E. F. (2007) *Channels (Austin)*, **1**, 11-20

[47] Wyatt, C. N., Page, K. M., Berrow, N. S., Brice, N. L., and Dolphin, A. C. (1998) *J. Physiol.*, **510**, 347-360

[48] Gottschalk, W., Kim, D. S., Chin, H., and Stanley, E. F. (1999) *Neuroscience*, **94**, 975-983

[49] Opatowsky, Y., Chen, C. C., Campbell, K. P., and Hirsch, J. A. (2004) *Neuron*, **42**, 387-399

[50] Van Petegem, F., Clark, K. A., Chatelain, F. C., and Minor, D. L. Jr. (2004) *Nature*, **429**, 671-675

[51] Chen, Y. H., Li, M. H., Zhang, Y., He, L. L., Yamada, Y., Fitzmaurice, A., Shen, Y., Zhang, H., Tong, L., and Yang, J. (2004) *Nature*, **429**, 675-680

[52] Ludwig, A., Flockerzi, V., and Hofmann, F. (1997) *J. Neurosci.*, **17**, 1339-1349

[53] Buraei, Z., and Yang, J. (2010) *Physiol. Rev.*, **90**, 1461-1506

[54] Scott, V. E. S., De Waard, M., Liu, H., Gurnett, C. A., Venzke, D. P., Lennon, V. A., and Campbell, K. P. (1996) *J. Biol. Chem.*, **271**, 3207-3212

[55] McEnery, M. W., Vance, C. L., Begg, C. M., Lee, W.-L., Choi, Y., and Dubel, S. J. (1998) *J. Bioenerg. Biomembr.*, **30**, 409-418

[56] Kang, M., Chen, C., Wakamori, M., Hara, Y., Mori, Y., and Campbell, K. P. (2006) *Proc. Natl. Acad. Sci.*

U. S. A., **103**, 5561-5566

[57] Niidome, T., Teramoto, T., Murata, Y., Tanaka, I., Seto, T., Sawada, K., Mori, Y., and Katayama, K. (1994) *Biochem. Biophys. Res. Commun.*, **203**, 1821-1827

[58] Wakamori, M., Yamazaki, K., Matsunodaira, H., Teramoto, T., Tanaka, I., Niidome, T., Sawada, K., Nishizawa, Y., Sekiguchi, N., Mori, E., Mori, Y., and Imoto, K. (1998) *J. Biol. Chem.*, **273**, 34857-34867

Chapter 3

Rab3 interacting molecule 3 mutations associated with autism alter regulation of voltage-dependent Ca^{2+} channels

Abstract

Autism is a neurodevelopmental psychiatric disorder characterized by impaired reciprocal social interaction, disrupted communication, and restricted and stereotyped patterns of interests. Autism is known to have a strong genetic component. Although mutations in several genes account for only a small proportion of individuals with autism, they provide insight into potential biological mechanisms that underlie autism, such as dysfunction in Ca^{2+} signaling, synaptic dysfunction, and abnormal brain connectivity. In autism patients, two mutations have been reported in the Rab3 interacting molecule 3 (RIM3) gene. We have previously demonstrated that RIM3 physically and functionally interacts with voltage-dependent Ca^{2+} channels (VDCCs) expressed in neurons via the β subunits, and increases neurotransmitter release. Here, by introducing corresponding autism-associated mutations that replace glutamic acid residue 176 with alanine (E176A) and methionine residue 259 with valine (M259V) into the C_2B domain of mouse RIM3, we demonstrate that both mutations partly cancel the suppressive RIM3 effect on voltage-dependent inactivation of Ba^{2+} currents through P/Q-type $Ca_V2.1$ recombinantly expressed in HEK293 cells. In recombinant N-type $Ca_V2.2$ VDCCs, the attenuation of the suppressive RIM3 effect on voltage-dependent inactivation is conserved for M259V but not E176A. Slowing of activation speed of P/Q-type $Ca_V2.1$ currents by RIM3 is abolished in E176A, while the physical interaction between RIM3 and β subunits is significantly attenuated in M259V. Moreover, increases by RIM3 in depolarization-induced Ca^{2+} influx and acetylcholine release are significantly attenuated by E176A in rat pheochromocytoma PC12 cells. Thus, our data raise the interesting possibility that autism phenotypes are elicited by synaptic dysfunction via altered regulation of presynaptic VDCC function and neurotransmitter release.

Introduction

Ca^{2+} is an important second messenger that regulates cellular signaling to control diverse cellular processes, ranging from ubiquitous activities (e.g., gene expression) to tissue-specific functions (e.g., neurotransmitter release and muscle contraction) [1, 2]. To control Ca^{2+} signaling, many molecules including Ca^{2+} channels and receptors tightly regulate intracellular free Ca^{2+} concentration ($[Ca^{2+}]_i$). Disruption of $[Ca^{2+}]_i$ homeostasis leads to various pathological symptoms, such as heart failure, neuronal degeneration, and psychiatric disorders.

Autism (also known as autism spectrum disorder) is a wide-spectrum neurodevelopmental psychiatric disorder, which affects about 1 in 88 children in the USA [3]. Autism is characterized by three core symptoms: impairment of reciprocal social interaction, communication deficits, and restrictive and/or repetitive behaviors. These symptoms manifest within the first few years of life, at the period of brain development that coincides with synapse formation, synapse pruning, and myelination [4]. Therefore, dysregulation of normal synaptic development and function may be involved in the molecular basis of autism, although the precise pathological mechanism of autism remains unclear.

Family histories and twin studies suggest that the etiology of autism has a strong genetic component. To date, many autism candidate genes have been identified by genome-wide linkage and association scans for susceptibility loci on human chromosomes [5]. Among the candidate genes, rare mutations have been found in genes encoding postsynaptic proteins (i.e., *NLGN3*, *NLGN4X*, and *SHANK3*), with rare copy-number variants associated with increased risk of autism [6-8]. Although variations in these genes account for only a small proportion of autistic individuals, they provide important insight into potential underlying biological mechanisms such as abnormal synaptic function.

Rab3 interacting molecules (RIMs) are multi-domain proteins expressed in secretory cells [9]. Four RIM isoforms (RIM1-4) are encoded by distinct genes in the mammalian genome. Long isoform α-RIMs, including RIM1α and RIM2α, contain an N-terminal zinc-finger domain, a central PDZ domain, and two C-terminal C2A and C_2B domains. Short isoform γ-RIMs, including RIM2γ, RIM3γ, and RIM4γ, are composed mainly of the C_2B domain, and lack the zinc-finger domain that is essential for Rab3 binding [10]. Biological

experiments have shown that α-RIMs are essential for synaptic vesicle docking and priming, and recruiting and tethering voltage-dependent Ca^{2+} channels (VDCCs) to the presynaptic active zone, thereby regulating VDCC function and short-term plasticity of neurotransmitter release [11-18]. In addition, functional coupling of RIM1α to the auxiliary β-subunit of VDCC is essential for insulin secretion in non-neuronal cells [19]. In contrast to α-RIMs, little is known about the physiological function of γ-RIMs. Studies suggest that γ-RIMs are key regulators of neurotransmitter release at the presynaptic active zone, and postsynaptic neuronal arborization [20-22].

Interestingly, genetic analysis has identified RIM3 as a candidate of causative gene for autism [23], with two mutations identified in the C_2B domain of autism patients. Specifically, these mutations replace the glutamic acid residue 177 (E177) with alanine (A), and the methionine residue 260 (M260) with valine (V). We previously demonstrated that the C_2B domain plays a critical role in binding to the β-subunit of VDCCs, thereby regulating VDCC gating [18, 20]. Here, we show that mouse RIM3 proteins carrying amino acid substitutions that correspond to mutations associated with autism (E176A and M259V) modify RIM3 interaction with VDCC β-subunits. Using electrophysiological techniques, we also show impaired functional properties of RIM3 mutants in regulating Ba^{2+} currents elicited by P/Q-type $Ca_V2.1$ and N-type $Ca_V2.2$ VDCCs. Furthermore, RIM3 mutations alter RIM3 regulation of depolarization-induced neurotransmitter release in pheochromocytoma PC12 cells. Thus, our data raises the interesting possibility that synaptic dysfunction owing to altered regulation of presynaptic VDCCs are involved in autism phenotypes.

Results

Effect of RIM3 mutations on the interaction with VDCC β-subunits

We have previously demonstrated that the C_2B domain from the RIM family proteins interacts with VDCC β-subunits [18, 20]. In autism patients, two nucleotide substitutions from A to C (nucleotide position: 92548 based on AL03189) and from A to G (nucleotide position: 95597), replacing E177 with A and M260 with V, respectively, in the C_2B domain of human RIM3 have been reported (Fig. 1A) [23]. The two residues

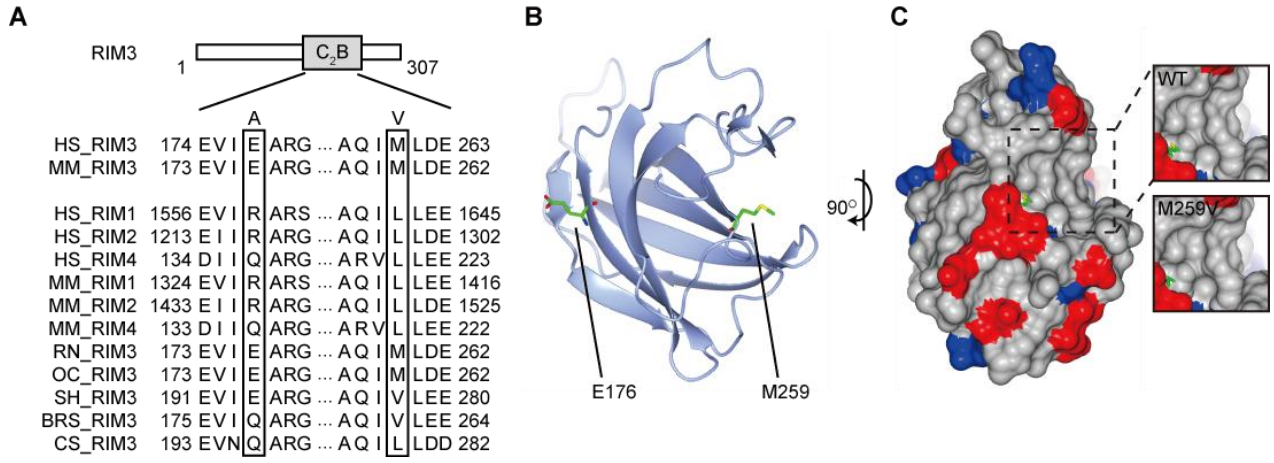

Fig. 1 Structure modeling of autism-related mutations E176A and M259V in RIM3. (A) Amino acid sequence alignment of C_2B domains. Positions of the autism substitutions (A) and (V) are indicated. Species abbreviations: HS, human (*Homo sapiens*); MM, mouse (*Mus musculus*); RN, rat (*Rattus norvegicus*); OC, rabbit (*Oryctolagus cuniculus*); SH, tasmanian devil (*Sarcophilus harrisii*); BRS, rhinoceros hornbill (*Buceros rhinoceros silvestris*); and CS, red tonguesole (*Cynoglossus semilaevis*). GenBank Accession Numbers: NM_014989 for HS_RIM1, NM_001100117 for HS_RIM2, NM_014747 for HS_RIM3, NM_001205317 for HS_RIM4, NM_053270 for MM_RIM1, NM_001256382 for MM_RIM2, NM_182929 for MM_RIM3, NM_183023 for MM_RIM4, NM_022931 for RN_RIM3, XM_008265493 for OC_RIM3, XM_003765413 for SH_RIM3, KFO86959 for BRS_RIM3, and XM_008331435 for CS_RIM3. (B) Ribbon structural model of the mouse RIM3 C_2B domain. E176 and M259 residues are represented as color-coded atoms (carbon, green; oxygen, red; nitrogen, blue; and sulfur, yellow). (C) Surface modeling of the mouse RIM3 C_2B domain colored for electrostatic potential (acidic, red; neutral, gray; and basic, blue). The view is rotated 90° to the left around a vertical axis from (B). The M259 residue is shown in the same color as (B). The presumed binding pockets of WT and M259V mutant to β-subunits are shown in boxed.

---

associated with autism are at positions E176 and M259, corresponding to human E177 and M260, respectively [23]. E176 and M259 in the C_2B domain of RIM is not conserved among other RIM isoforms or species (Fig. 1A) [24]. Protein homology modeling based on the previously reported crystal structure of RIM1 (PDB # 2Q3X) revealed that M259 is located at the end of the β-strand and surrounded by two adjacent loops (Fig. 1B) [24]. Moreover, it is predicted that M259 is a component of the C_2B domain cavity (Fig. 1C). On the other hand, molecular modeling also demonstrated that E176 is located on the opposite lateral side from this cavity (Fig. 1B). To determine if the RIM3/VDCC β-subunit interaction is modified by these mutations, we

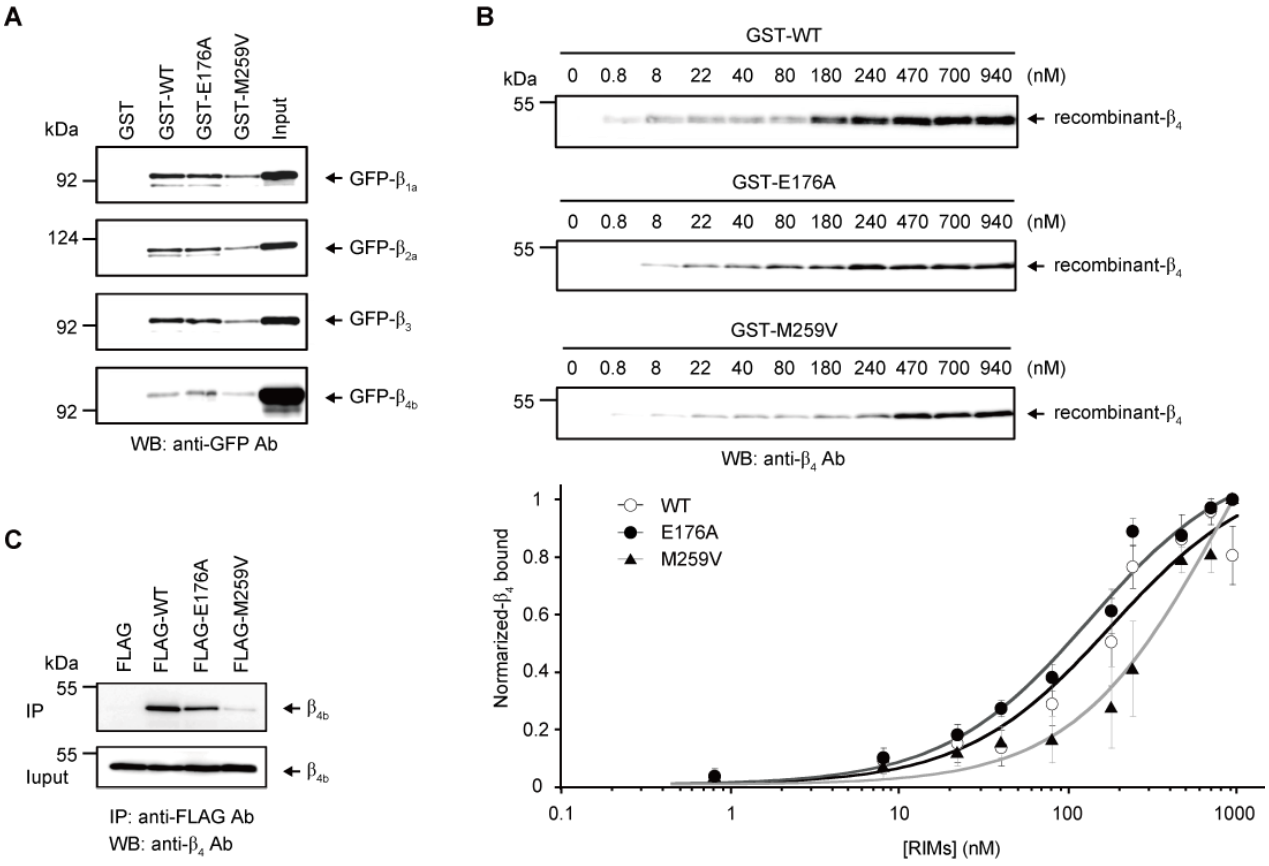

Fig. 2 Autism mutations E176A and M259V affect RIM3 interaction with VDCC β-subunits. (A) Pulldown assay between β-subunits and GST-RIM3 fusion constructs. GST fusion proteins immobilized on glutathione-Sepharose beads were incubated with cell lysates obtained from EGFP-tagged β-transfected HEK293 cells. Bound proteins were analyzed by western blotting using the anti-GFP antibody. Ab, antibody; WB, western blotting. (B) *in vitro* association between purified GST-RIM3 fusion constructs and recombinant β_4-subunit (amino-acid residues 47-475). *Upper*, GST-RIM3 proteins at various concentrations were incubated with β_4 (50 pM) and captured by glutathione-Sepharose beads. Captured β_4 proteins were examined by western blotting. *Lower*, quantitative densitometric analysis of bands shown in upper panels. Saturation curves were analyzed using the nonlinear least-squares curve-fitting method to determine the apparent dissociation constant (K_d). (C) Interaction between β_4 and RIM3 proteins in HEK293 cells. Interactions were examined by immunoprecipitation with the FLAG antibody, followed by western blotting with the anti-β_4 antibody. IP, immunoprecipitation. Data points are mean ± SEM.

constructed two mouse RIM3 mutants (E176A and M259V) and performed *in vitro* pulldown assays using glutathione-*S*-transferase (GST) fusion constructs. Cell lysates from HEK293 cells expressing EGFP-tagged constructs with different β-subunits were incubated with glutathione-Sepharose beads containing various GST-RIM3 fusion proteins. As observed for WT RIM3 (previously referred to as RIM3γ [20]), E176A bound to four β-subunit isoforms, whereas M259V suppressed the β-subunit interaction (Fig. 2A). To compare binding affinity between RIM3 mutants and the β-subunit, we performed *in vitro* binding assays and measured the dissociation constant (K_d) using purified recombinant β_4-subunit (residues 47-475) and GST-RIM3 fusion proteins. The K_d value for E176A (133 ± 18 nM) was similar to WT (178 ± 16 nM), while for the M259V mutant it was significantly higher (323 ± 48 nM) than WT and E176A RIM3 proteins ($P < 0.05$) (Fig. 2B). The K_d value for WT RIM3 was almost equal to the previous findings [20]. In addition, co-immunoprecipitation experiments between VDCC β_4-subunit and FLAG-tagged WT and mutant RIM3 proteins were performed in HEK293 cells (Fig. 2C). WT and E176A mutant more efficiently co-immunoprecipitated with VDCC β_4-subunit than the M259V mutant, consistent with our GST-pulldown assay results. Overall, these results suggest that the M259V mutation, but not E176A, diminishes the β-subunit interaction.

Functional effects of RIM3 mutations on P/Q-type and N-type VDCC currents.

We previously reported that RIM3 suppresses voltage-dependent inactivation of neuronal VDCCs via direct binding to β-subunits [20]. To determine the functional effect of the mutations on RIM3-regulated VDCC function, we examined P/Q-type VDCCs because they play an important role in presynaptic neurotransmitter release from central neurons [25]. Whole-cell Ba^{2+} currents through recombinant P/Q-type VDCCs, expressed as a complex of the BI-2 variant of $Ca_V2.1$ α_1-subunit and the α_2/δ plus β_1 subunits [26], were examined in HEK293 cells. β_1-subunit was chosen because β_4-subunit is not expressed in PC12 cells [18] used in the following experiments. Inactivation kinetics were determined using a protocol comprised of a 2-s prepulse to 0 mV from a holding potential of −100 mV. As previously reported, WT RIM3 markedly decelerated inactivation compared with vector (Fig. 3A and Table 1). Inactivation of P/Q-type VDCCs was less

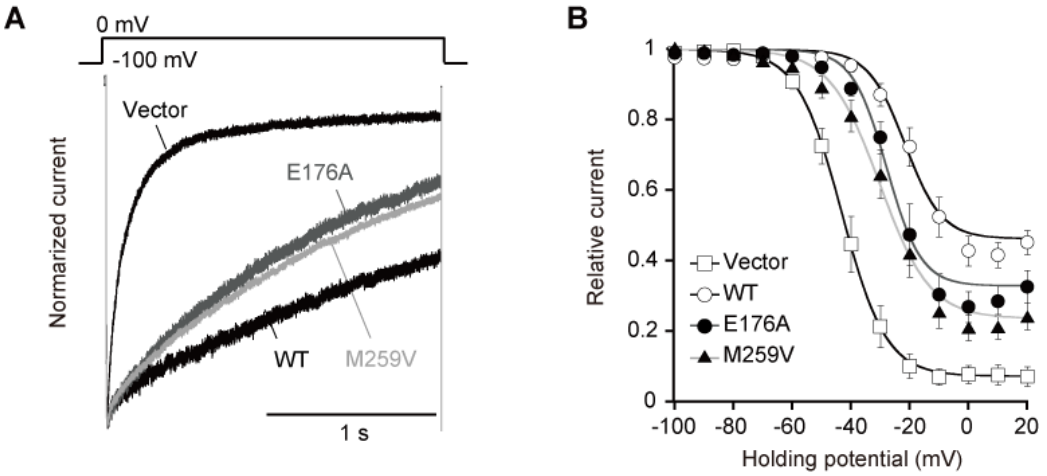

Fig. 3 Autism mutations affect RIM3 regulation of inactivation properties of $Ca_V2.1$ VDCCs. (A) Effect of WT, E176A and M259V RIM3 on inactivation kinetics of P/Q-type $Ca_V2.1$ VDCCs in HEK293 cells co-expressing α_2/δ and β_1 subunits. Peak amplitudes were normalized for Ba^{2+} currents elicited by 2-s pulses to 0 mV from a V_h of −100 mV, with or without WT, E176A, and M259V RIM3. (B) Effect of WT, E176A, and M259V on inactivation curves of P/Q-type $Ca_V2.1$ currents. Voltage dependence of inactivation determined by measuring peak current amplitudes evoked by 20-ms test pulses to 5 mV following 2-s prepulses to potentials from −100 to 20 mV in 10-mV increments from a V_h of −100 mV, were fitted using Boltzmann's equation. Data points are mean ± SEM.

extensively accelerated in E176A and M259V mutants compared with WT RIM3. Furthermore, voltage dependence of inactivation was determined using a protocol comprised of a 20-ms test pulse to 5 mV following 2-s prepulses to a series of different potentials from −100 to 20 mV. Peak current amplitudes elicited by test pulses were normalized to those elicited after a 2-s prepulse to −100 mV. Compared with WT RIM3, voltage dependence of inactivation for P/Q-type VDCCs co-expressed with E176A and M259V mutants were shifted significantly towards hyperpolarizing potentials (Fig. 3B and Table 1). Estimated half-inactivation potentials ($V_{0.5}$) were −19.7 ± 2.0 mV for WT, −25.5 ± 1.8 mV for E176A, and −28.5 ± 2.3 mV for M259V (Table 1). These results suggest that both RIM3 mutations diminish WT RIM3 effect on voltage-dependent inactivation of P/Q-type VDCCs.

Next, we examined the RIM3 mutant effect on voltage dependence of VDCC activation. The time constant ($\tau_{activation}$) obtained by fitting the activation time course of inward currents with a single exponential was "bell shaped" when plotted against different voltages. WT RIM3 significantly decelerated activation of P/Q-type

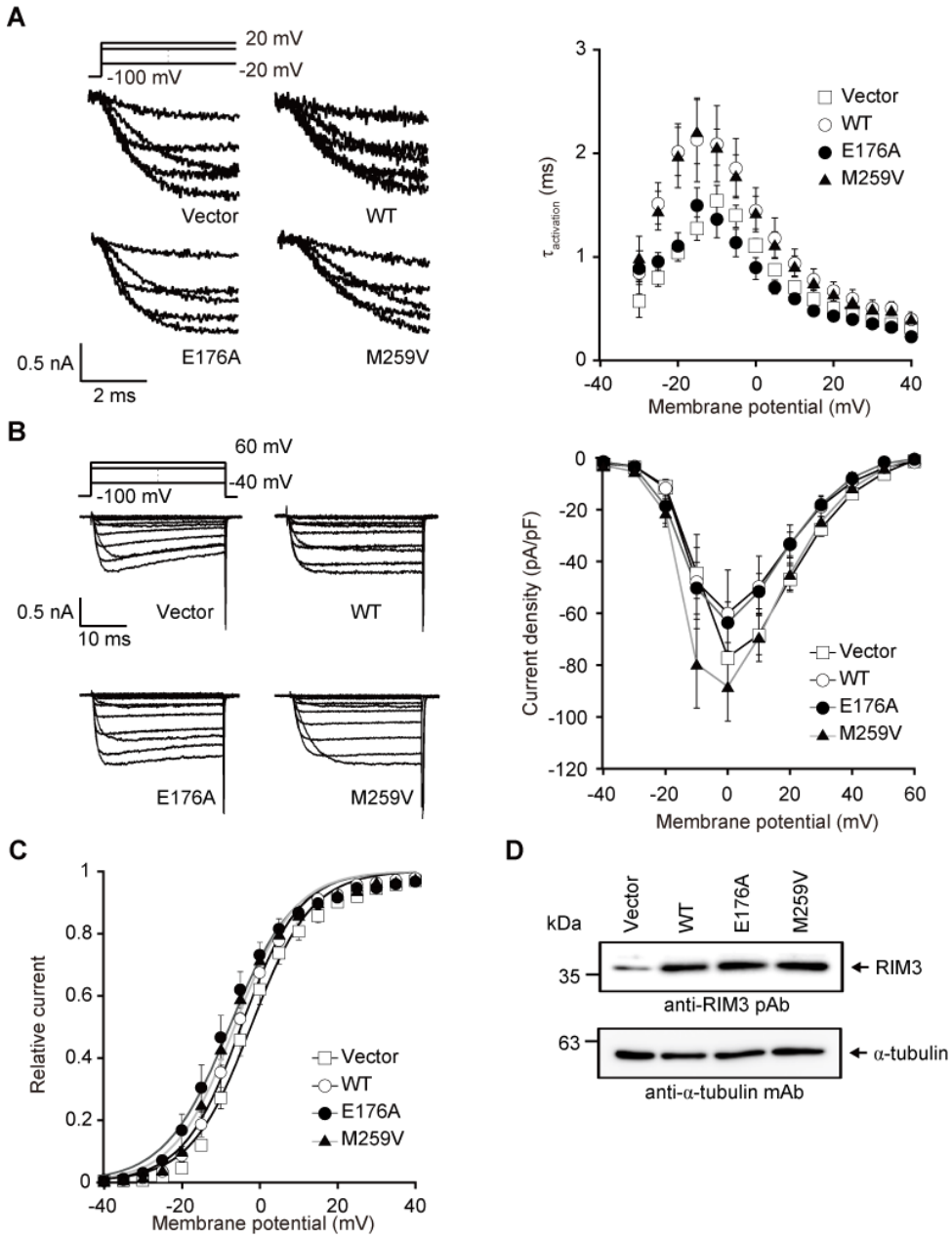

Fig. 4 Autism mutations affect RIM3 regulation of activation properties of $Ca_V2.1$ VDCCs. (A) Effect of WT, E176A, and M259V on activation kinetics of P/Q-type $Ca_V2.1$ VDCCs in HEK293 cells co-expressing α_2/δ and β_1 subunits. *Left*, representative traces for Ba^{2+} currents evoked by test pulses from −20 to 20 mV in 10-mV increments. *Right*, time constants were obtained by fitting the current activation phase elicited by a 5-ms test pulse from −30 mV to 40 mV with a single exponential function. (B) Effect of WT, E176A, and M259V on $Ca_V2.1$ current amplitudes. *Left*, representative traces in HEK293 cells co-expressing α_2/δ and β_1 subunits for Ba^{2+} currents evoked by test pulses from −40 to 60 mV in 10-mV increments. *Right*, current density-voltage relationship of $Ca_V2.1$ with V_h of −100 mV. (C) Effect of WT, E176A, and M259V on $Ca_V2.1$ current activation curves. Tail currents elicited by repolarization to −60 mV after a 5-ms test pulse from −40 to 40 mV were used to determine activation curves. (D) Protein expression analysis of WT RIM3 and the mutants using western blotting in HEK293 cells. α-tubulin was used as a loading control. Data points are mean ± SEM.

VDCCs at membrane potentials over −25 mV compared with vector (Fig. 4A), consistent with our previous finding [20]. Activation speed of P/Q-type VDCCs co-expressed with E176A significantly accelerated compared with WT at membrane potentials ≥ −25 mV (Fig. 4A). Interestingly, activation kinetics were not significantly different between M259V and WT at all tested membrane potentials (Fig. 4A and Table 2). RIM3 mutations had no effect on other functional properties such as current-voltage relationship and voltage dependence of activation of P/Q-type VDCCs at different voltages (Fig. 4B, C and Table 2). The RIM3 protein expression levels of these constructs were not different in HEK293 cells (Fig. 4D). Thus with regard to activation kinetics, E176A but not M259V impairs WT RIM3 function.

We have also evaluated effects of the mutations on RIM3-regulated N-type VDCCs function. $Ca_V2.2$ N-type VDCCs was less extensively accelerated in M259V mutant but not in E176A mutant compared with WT RIM3 (Fig. 5A and Table 3). M259V mutation also shifted $V_{0.5}$ slightly towards hyperpolarizing potentials and significantly reduced the channel availability at membrane potentials −10 mV and 0 mV in N-type VDCCs (Fig. 5B). These results suggest that M259V mutation diminishes WT RIM3 effect on voltage-dependent inactivation not only in P/Q-type but also in N-type VDCCs. As observed for P/Q-type VDCCs (Fig. 4B), both RIM3 mutants failed to exert significant effects on current-voltage relationship of N-type VDCCs (Fig. 5C).

Effect of RIM3 mutations on neurotransmitter release

It has been suggested that RIM3 is associated with regulation of neurotransmitter release [20]. Therefore, we investigated effects of the RIM3 mutants on ACh release from PC12 cells. Previously, we detected α_1-subunits mRNA (P/Q-type ($Ca_V2.1$), N-type ($Ca_V2.2$), and L-type ($Ca_V1.2$ and $Ca_V1.3$)) and β-subunits mRNA (β_1, β_2, and β_3) using PCR experiment. In addition, we identified P/Q-, N-, and L-type Ca^{2+} currents as well as high-voltage activated Ca^{2+} currents sensitive to Cd^{2+} but insensitive to the selective blockers for P/Q-, N-, and L-types in PC12 cells [18]. PC12 cells were co-transfected with RIM3 and *Chat* cDNA, encoding choline acetyltransferase, which synthesizes ACh in synaptic vesicles [27]. ACh release, triggered by Ca^{2+} influx in response to high K^+ induced membrane depolarization (extracellular K^+ concentration elevated from 5.9 to

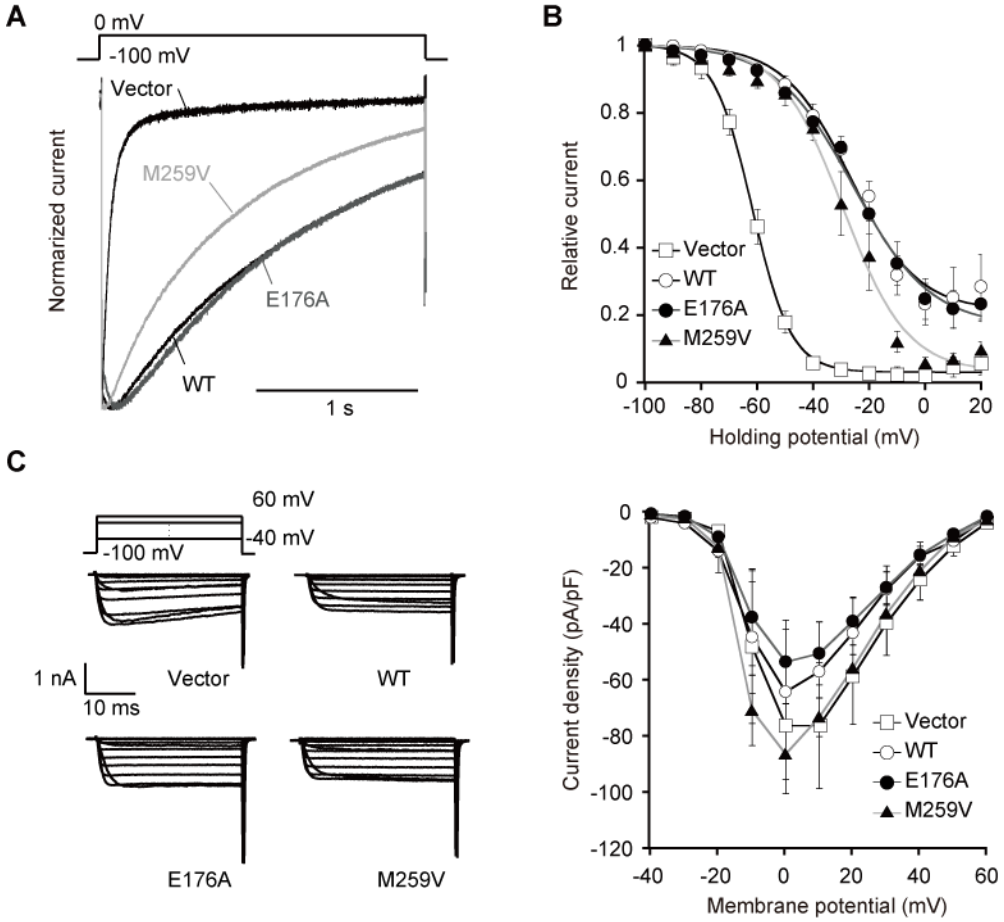

Fig. 5 Autism mutations affect RIM3 regulation of $Ca_V2.2$ VDCCs. (A) Effect of WT, E176A and M259V RIM3 on inactivation kinetics of N-type $Ca_V2.2$ VDCCs in HEK293 cells co-expressing α_2/δ and β_1 subunits. Peak amplitudes were normalized for Ba^{2+} currents elicited by 2-s pulses to 0 mV from a V_h of −100 mV, with or without WT, E176A, and M259V RIM3. (B) Effect of WT, E176A, and M259V on inactivation curves of N-type $Ca_V2.2$ currents. Voltage dependence of inactivation determined by measuring peak current amplitudes evoked by 20-ms test pulses to 5 mV following 2-s prepulses to potentials from −100 to 20 mV in 10-mV increments from a V_h of −100 mV, were fitted using Boltzmann's equation. (C) Effect of WT, E176A, and M259V on $Ca_V2.2$ current amplitudes. *Left*, representative traces in HEK293 cells co-expressing α_2/δ and β_1 subunits for Ba^{2+} currents evoked by test pulses from −40 to 60 mV in 10-mV increments. *Right*, current density-voltage relationship of $Ca_V2.2$ with V_h of −100 mV. Data points are mean ± SEM.

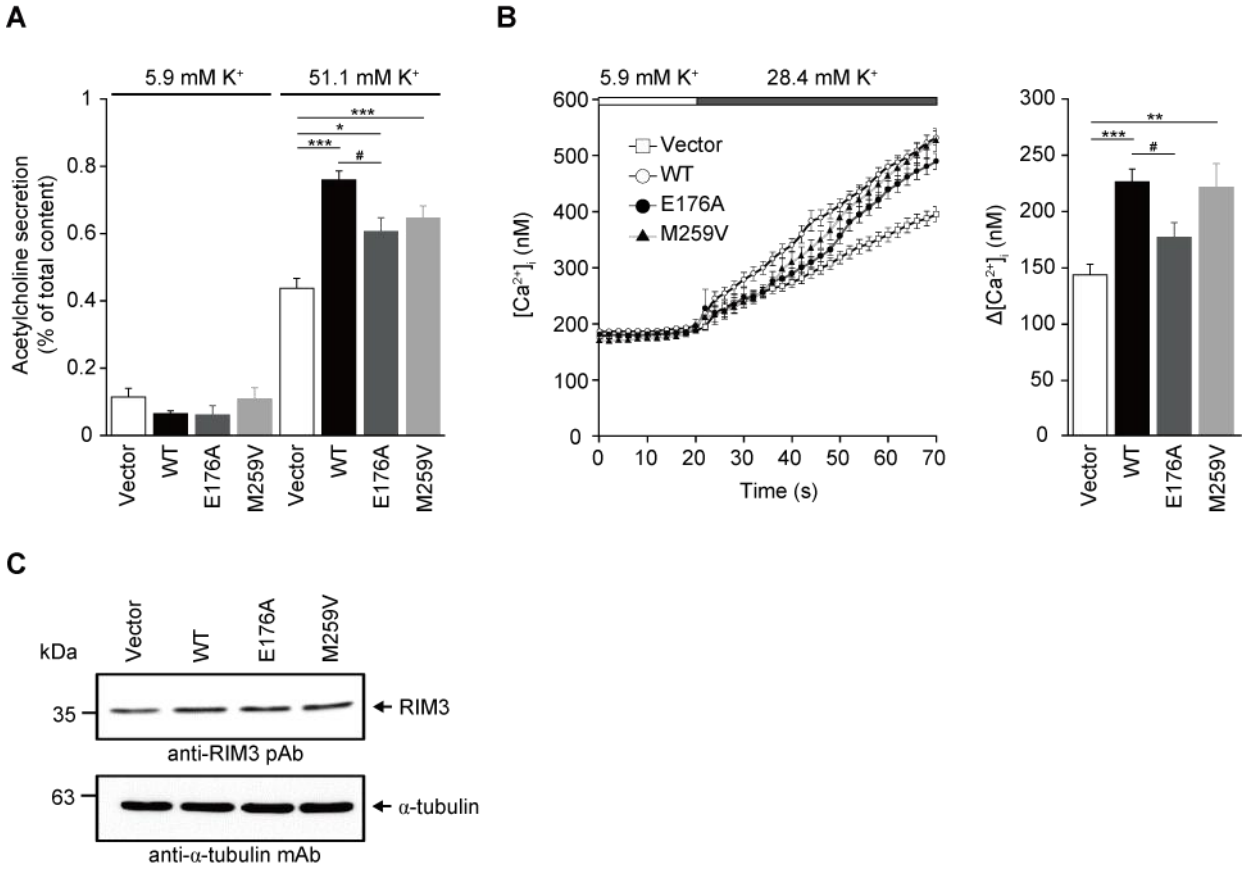

Fig. 6 Autism mutations affect RIM3 potentiation of ACh release. (A) Effect of WT, E176A and M259V RIM3 on depolarization-dependent ACh release from ChAT-cotransfected PC12 cells. Secreted ACh was determined as a percentage of cellular content for each dish. **P* < 0.05 and ****P* < 0.001 versus vector; #*P* < 0.05 versus WT. (**B**) Effect of WT, E176A, and M259V RIM3 on Ca^{2+} response to elevation of extracellular K^+ concentration from 5.9 to 28.4 mM. Average time course (*left*) and $[Ca^{2+}]_i$ increase at 30 s after treatment with 28.4 mM K^+ solution (*right*). Numbers of PC12 cells analyzed were 75, 59, 51, and 42 for transfection of vector, WT, E176A, and M259V RIM3, respectively. ***P* < 0.01 and ****P* < 0.001 versus vector; #*P* < 0.05 versus WT. (**C**) Protein expression analysis of WT RIM3 and the mutants using western blotting in PC12 cells. α-tubulin was used as a loading control. Data points are mean ± SEM.

51.1 mM for 30 s), was significantly potentiated by recombinant WT RIM3 (Fig. 6A), consistent with the previous report [20]. E176A mutation significantly attenuated this effect ($P < 0.05$), while M259V mutation induced a modest but not significant change ($P = 0.13$) (Fig. 6A). $[Ca^{2+}]_i$ elevation observed using fura-2 in 28.4 mM K^+-containing extracellular solution was effectively potentiated by RIM3 WT (Fig. 6B). We used

Table 1 Effect of RIM3 proteins on inactivation properties of P/Q-type VDCC in HEK cells expressing $Ca_V2.1$, α_2/δ and β_1[1) 2) 3)].

	Inactivation parameters			
	a	$V_{0.5}$ (mV)	*k* (mV)	*Residual current* (0mV) (relative) [4)]
Vector	0.97 ± 0.01 (7)	−42.7 ± 2.0 (7)	−6.9 ± 0.4 (7)	0.06 ± 0.02 (7)
WT	0.58 ± 0.04 (6) ***	−19.7 ± 2.0 (6) ***	−6.7 ± 0.4 (6)	0.46 ± 0.05 (6) ***
E176A	0.78 ± 0.05 (9) ***$^{\#\#}$	−25.5 ± 1.8 (9) **$^{\#}$	−5.7 ± 0.5 (9)	0.29 ± 0.04 (9) ***$^{\#}$
M259V	0.94 ± 0.03 (13) $^{\#\#\#}$	−28.5 ± 2.3 (13) **$^{\#\#}$	−7.6 ± 0.9 (13)	0.32± 0.04 (13) ***$^{\#}$

1) $^{**}P< 0.01$, $^{***}P < 0.001$ versus Vector.

2) $^{\#}P < 0.05$, $^{\#\#}P < 0.01$, $^{\#\#\#}P < 0.001$ versus WT.

3) Numbers of cells analyzed are indicated in the parenthesis.

4) Residual current was assessed after 2-s depolarization.

Table 2 Effects of RIM3 proteins on current density and activation of P/Q-type VDCC in HEK cells expressing $Ca_V2.1$, α_2/δ and β_1[1) 2) 3)].

	Current density (pA / pF)[4)]	Activation parameters			
		$V_{0.5}$ (mV)	*k* (mV)	$\tau_{activation\ (-20mV)}$ (ms)[5)]	$\tau_{activation\ (0mV)}$ (ms)[6)]
Vector	−76.9 ± 11.1 (7)	−2.2 ± 1.5 (7)	7.4 ± 0.5 (7)	1.05 ± 0.09 (7)	1.11 ± 0.06 (7)
WT	−60.1 ± 16.7 (9)	−4.7 ± 1.7 (9)	6.8 ± 0.5 (9)	1.98 ± 0.23 (6) **	1.57 ± 0.22 (6)
E176A	−63.6 ± 7.9 (11)	−7.8 ± 2.1 (11)	7.0 ± 0.5 (11)	1.11 ± 0.13 (8) $^{\#}$	0.90 ± 0.09 (8) $^{\#}$
M259V	−88.4 ± 13.4 (14)	−6.5 ± 1.3 (14)	6.9 ± 0.3 (14)	1.98 ± 0.31 (12) *	1.42 ± 0.16 (12)

1) $^{*}P< 0.05$, $^{**}P < 0.01$ versus Vector.

2) $^{\#}P < 0.05$ versus WT.

3) Numbers of cells analyzed are indicated in the parenthesis.

4) Ba^{2+} currents evoked by depolarizing pulse to 0 mV from a V_h of −100 mV are divided by capacitance.

5) Activation time constants obtained from currents elicited by 5-ms test pulse to −20 mV. The activation phases are well fitted by a single exponential function.

6) Activation time constants obtained from currents elicited by 5-ms test pulse to 0 mV.

Table 3 Effect of RIM3 proteins on inactivation properties of N-type VDCC in HEK cells expressing $Ca_V2.2$, α_2/δ and β_1[1) 2)].

	Inactivation parameters			
	a	$V_{0.5}$ (mV)	*k* (mV)	*Residual current* (0mV) (relative) [3)]
Vector	0.97 ± 0.01 (6)	−61.8 ± 0.3 (6)	−6.9 ± 0.3 (6)	0.03 ± 0.02 (6)
WT	0.79 ± 0.03 (9)	−26.7 ± 2.0 (9) ***	−12.0 ± 1.5 (9)	0.25 ± 0.05 (9) *
E176A	0.83± 0.03 (13)	−25.8 ± 1.5 (13) ***	−13.8 ± 1.1 (13)	0.22 ± 0.05 (13) *
M259V	0.97 ± 0.03 (7)	−29.3 ± 1.6 (7) ***	−11.4 ± 1.3 (7)	0.12 ± 0.03 (7) *

1) *P< 0.05, ***P < 0.001 versus Vector.

2) Numbers of cells analyzed are indicated in the parenthesis.

3) Residual current was assessed after 2-s depolarization.

Table 4 Primer sequences used for overlap extension PCR in producing mutants.

Gene	Mutants	Mutation primer sequences (5' to 3')	External primer sequences (5' to 3')
RIM3	E176A	for: GAAGTGATTGCAGCTCGGGGCCTGACC	
		rev: GGCCCCGAGCTGCAATCACTTCCACCTCCAG	for: ATGTTTAACGGGGAGCCTG
	M259V	for: CAGATCGTGCTGGACGAGCTGGACCTGAGTGC	rev: TTAAGAGCACGAGGGGCTGG
		rev: GTCCAGCACGATCTGGGCCATACCCATGAAG	

for: forward primer, rev: reverse primer

28.4 mM K^+ stimulation because robust $[Ca^{2+}]_i$ elevation was obtained with 51.1 mM K^+ stimulation in control vector-transfected cells, resulting in a minimal effect of RIM3 WT on $[Ca^{2+}]_i$ elevation with 51.1 mM K^+ stimulation (data not shown). E176A mutation significantly reduced the RIM3 promotive effect at 30 s after depolarization (P < 0.05), while M259V mutation reduced $[Ca^{2+}]_i$ elevation immediately after 28.4 mM K^+ stimulation but not 30 s after depolarization (Fig. 6B). The RIM3 protein levels of these constructs were not different in PC12 cells (Fig. 6C). Of the two mutations tested, E176A significantly impaired RIM3-mediated enhancement of ACh release in PC12 cells.

Discussion

Several candidate proteins with functional changes that lead to abnormalities in synaptic function have been implicated in the pathogenesis of autism by genetic studies [5, 28]. Here, we demonstrate that the two mutations, E176A and M259V, corresponding to human mutations in autism patients and identified in the C_2B domain of RIM3, diminish RIM3 function. Our *in vitro* binding assay and electrophysiological experiments reveal that E176A mutation alters WT RIM3 regulation of P/Q-type VDCC functions but not N-type VDCC functions. M259V mutation alters RIM3 regulation of both P/Q-type and N-type VDCC inactivation properties. The physical interaction of RIM3 with VDCC β-subunits is unaffected by E176A mutation but is diminished by M259V mutation. In addition, E176A mutation reduces RIM3-mediated augmentation of depolarization-induced ACh release in PC12 cells.

VDCC complexes are well known to be associated with presynaptic proteins including syntaxin, SNAP-25, and synaptotagmin via interactions with the Ca_V α_1-subunit [29-32]. It has been revealed that β-subunits directly associate with presynaptic proteins including RIMs [18, 20, 33-35]. RIM proteins are widely distributed in the brain, and abundantly localized at the pre- and post-synapse. Although long α-RIM isoforms (RIM1 and RIM2) have been shown to play an essential role in synaptic vesicle recruitment, modulating VDCC function, and regulating presynaptic neurotransmitter release, physiological significance of the short γ-RIM isoforms (RIM2γ, RIM3γ, and RIM4γ) is still elusive [9, 18]. We have previously shown a functional role of γ-RIMs in modulating presynaptic Ca^{2+} influx via direct binding to VDCC β-subunits, suggesting that γ-RIMs regulate vesicle exocytosis at presynaptic terminals [20]. The C-terminal C_2B domain, which is highly conserved among RIM family members, interacts with VDCC β-subunits [18, 20, 24]. In this study, pulldown and co-immunoprecipitation assays revealed that the M259V mutant interacts more weakly with β-subunits than WT RIM3 (Fig. 2A, 2C). M259 is predicted as a component of C_2B domain cavity (Fig. 1C), suggesting that replacement of M259 with V in this cavity may affect interaction with β-subunits. Conversely, our binding experiments did not identify a distinguishable alteration in the interaction between RIM3 and VDCC β-subunits by E176A mutation (Fig. 2A, 2C). In addition, K_d binding values for WT or E176A mutant RIM3 to the β_4-subunit show comparable binding affinities (Fig. 2B). Interestingly, protein homology modeling

revealed that E176 is located on the opposite side from the C_2B domain cavity (Fig. 1B). Therefore, it is possible that E176 is not located at an essential position in terms of interaction with β-subunits and other presynaptic proteins, such as α-liprin, SNAP-25, and synaptotagmin-1 [12, 24, 36].

E176A mutation attenuated RIM3-mediated suppression of kinetics and voltage dependence of inactivation (Fig. 3A, 3B), yet failed to show any alteration in interaction with β-subunits. E176A also caused abolition of deceleration in activation kinetics (Fig. 4A). In addition, E176A mutant failed to show any effects on N-type VDCCs inactivation properties (Fig. 5A, 5B). Interestingly, RIM1 and RIM2, which have positively charged arginine residues at the position corresponding to E176 (Fig. 1A), show no effect on activation kinetics of P/Q-type VDCCs, in contrast to RIM3 [20]. These findings suggest that negatively charged E176 may play a key role in modulating VDCC gating properties through interaction with $Ca_V2.1$ α_1-subunits. With regard to the M259V mutant, RIM3-mediated suppressive effects of inactivation speed and voltage dependence of P/Q-type VDCCs were attenuated (Fig. 3A, 3B). Also, M259V mutant attenuated the RIM3 effect on voltage dependence of inactivation of other neuronal VDCC, N-type $Ca_V2.2$ (Fig. 5A, 5B). These attenuations may be caused by alteration of the interaction between mutant RIM3 and the β-subunit. However, taking into consideration the fact that M259V mutant slows activation kinetics, like WT, it is possible that the M259V mutant maintains weak association with the β-subunit and attenuates inactivation properties via allosteric modification of electrostatic interactions with other residues, such as E176.

Neurotransmitter release is mediated by depolarization-induced Ca^{2+} influx via presynaptic VDCCs, including N- and P/Q-type Ca^{2+} channels. In PC12 cells, WT RIM3 expression enhanced membrane depolarization-dependent ACh release (Fig. 6A). This enhancement is thought to be due to, at least in part, sustained Ca^{2+} influx by suppression of voltage-dependent inactivation of VDCCs [18, 20]. Indeed, WT RIM3 in PC12 cells stimulated global $[Ca^{2+}]_i$ elevation with moderate depolarization elicited by 28.4 mM K^+ (Fig. 6B). Consistent with our electrophysiological recording results, E176A mutant significantly attenuated ACh release and $[Ca^{2+}]_i$ elevation compared with WT RIM3. WT and E176A mutant, which show comparable K_d values for the β-subunit interaction (Fig. 2B), may compete out and extrude endogenous RIM proteins from the binding site on the β-subunits, resulting in the observed functional effects of E176A mutant on ACh

release and $[Ca^{2+}]_i$ elevation in PC12 cells. However, M259V mutant did not significantly attenuate ACh release and $[Ca^{2+}]_i$ elevation. This is presumably because M259V mutant interacts weakly with VDCC β-subunits, resulting in intact interaction of endogenous RIM proteins with β-subunits (as compared with the control vector group) and additive association of M259V mutant proteins with β-subunits free from endogenous RIM in PC12 cells.

Several groups have proposed that cortical networks in autism may be characterized by an imbalance between excitatory glutamatergic and inhibitory GABAergic neurotransmission [37, 38]. We and others have previously demonstrated that presynaptic VDCCs (including P/Q-type) are associated with glutamate release in cultured cerebellar neurons [18, 20, 39]. In addition, N- and P/Q-type VDCCs regulate GABA release in hippocampal neurons and cerebellar Purkinje cells [40, 41]. These findings suggest that functional changes in neurotransmitter release induced by RIM3 mutation at the presynapse may underlie certain forms of autism. Previous findings demonstrate that transient increase in $[Ca^{2+}]_i$ regulates neuronal differentiation in neuron or PC12 cells [42, 43]. It is interesting to note that RIM3 is important for neurite development and axonal outgrowth. Furthermore, RIM3 plays an important role in synapse formation and synaptic transmission at the post-synapse [21]. Thus, our findings may suggest that human RIM3 mutations affect $[Ca^{2+}]_i$ regulation and neuronal differentiation and synapse formation/maturation in autism patients. Shank3 is associated with autism and also plays a role in synapse formation and dendritic spine maturation, and coordinately regulates presynaptic and postsynaptic functions that promote increased formation of excitatory synapses [44, 45]. Therefore, as for Shank3, RIM3 may coordinate pre-/post-signaling.

The molecular mechanisms that underlie autism remain largely unknown, but several recent lines of evidence suggest that some autistic phenotypes result from abnormalities in Ca^{2+} signaling [46]. Increases in intracellular Ca^{2+} levels and signaling activation are important for regulating processes such as neuronal survival, differentiation, and synaptogenesis [47-49]. Impairment in these developmental cellular processes may give rise to some of the neuroanatomical abnormalities identified in autism patients [50]. Furthermore, many autism-associated mutations in genes that encode Ca^{2+}-regulatory molecules lead to dysfunction in Ca^{2+} signaling [51-54], suggesting that autism may result from disruption of Ca^{2+}-dependent processes. These

previous reports are consistent with our findings on RIM3 mutants and their impact on Ca^{2+} influx pathways.

In conclusion, we have demonstrated that the mouse RIM3 mutants, E176A and M259V, which are equivalent to human autism mutations, alter RIM3 function in regulating VDCC currents and neurotransmitter release in PC12 cells. Previous studies have revealed changes in RIM3 expression levels in schizophrenia [55, 56]. In addition, several studies have suggested that functional mutations in genes encoding VDCCs can lead to autism, and SNAP-25 single nucleotide polymorphisms are associated with autism [51-53, 57]. These reports further suggest that synaptic dysfunction through RIM3 functional abnormalities in Ca^{2+} regulation may be relevant for the pathogenesis underlying neurodevelopmental disorders such as autism.

Experimental procedures

cDNA cloning and construction of expression vectors

RIM3γ (GenBank Accession Number NM_182929) was cloned from mouse brain Marathon-Ready cDNA (Clontech) using polymerase chain reaction (PCR), and subcloned into FLAG-tagged vector pCMV-tag2 (Stratagene), pIRES2-EGFP (Clontech) and pCI-neo (Promega). Mouse $Ca_V2.2$ (GenBank Accession Number NM_001042528) was cloned from mouse brain Marathon-Ready cDNA using PCR, and subcloned into pCI-neo. Rabbit β_{1a} (GenBank Accession Number M25817), rabbit β_{2a} (GenBank Accession Number X64297), rabbit β_3 (GenBank Accession Number X64300), and rat β_{4b} (GenBank Accession Number XM_215742) were subcloned into pEGFP-C1 (Clontech) and pCI-neo. To introduce point mutations into mouse RIM3γ, overlapping extension PCR was used for site-directed mutagenesis. The two residues associated with autism are at positions E176 and M259, corresponding to human E177 and M260, respectively [23]. Amino acids in these positions were changed to A (E176A) and V (M259V). The primers used for these mutants are summarized in Table 4.

Structure modeling

To build a three-dimensional structural model of the RIM3 C_2B domain, SWISS-MODEL Workspace, a

Web-based integrated service dedicated to protein structure homology modeling [58-60], was used. The C_2B domain of rat RIM1 (PDB # 2Q3X) was selected as the template for modeling [24]. The amino acid sequence of mouse RIM3 was submitted to SWISS-MODEL Automatic Modeling Mode. Structures were visualized using CCP4mg software version 2.9.0 [61].

Production of GST fusion proteins and recombinant β_4-subunit proteins

For production of GST fusion proteins for wild-type (WT) and mutant RIM3, cDNAs for each RIM construct and GST were subcloned into the pET23 vector (Novagen). The Rosetta strain (Novagen) of *Escherichia coli* were transformed with expression vectors, and protein expression/purification performed according to the manufacturer's instruction (Novagen). Recombinant β_4-subunit proteins [β_4 (47-475)] were prepared as previously reported [18].

GST-pulldown assay and co-immunoprecipitation in HEK293 cells

HEK293 cells were cultured in Dulbecco's modified Eagle's medium (DMEM) containing 10 % fetal bovine serum, 30 units/mL penicillin, and 30 μg/mL streptomycin. 48 h after transfection, HEK293 cells were solubilized using Nonidet P-40 (NP-40) buffer (150 mM NaCl, 50 mM Tris, 1 % NP-40, and protease inhibitors), and then centrifuged at 17,400 × *g* for 20 min. For GST pulldown assays, cell lysates were incubated with glutathione-Sepharose beads bound to purified fusion proteins, and then the beads were washed with NP-40 buffer at 4 °C. Proteins retained on the beads were characterized by western blotting with anti-GFP antibody (Clontech). For co-immunoprecipitation, cell lysates were incubated with anti-FLAG M2 monoclonal antibody (Sigma), then immunocomplexes incubated with protein A-agarose beads (Santa Cruz), and washed with NP-40 buffer. Immunoprecipitated proteins were characterized by western blotting with an anti-β_4 antibody [18].

in vitro binding of purified RIM3-GST fusion proteins and recombinant β_4 protein

RIM3-GST fusion proteins (WT and mutant) at various concentrations were incubated with 50 pM purified

recombinant β_4-subunit for 3 h at 4 °C in phosphate-buffered saline (PBS) containing 0.1 % NP-40 and 50 μg/mL bovine serum albumin, and then incubated with glutathione-Sepharose beads for 1 h. Beads were centrifuged and washed twice with PBS. Proteins retained on the beads were characterized by western blotting with the anti-β_4 antibody, and detected by enhanced chemiluminescence (Pierce). Protein signal densities were calculated using the NIH image (National Institute of Health). Protein signal densities obtained at a linear relationship with applied amount of proteins were normalized to densities obtained from maximal binding. Three independent experiments were performed.

Cell culture and cDNA expression in HEK293 cells

A HEK293 cell line stably expressing rabbit $Ca_V2.1$, α_2/δ, and β_{1a} subunits has been described previously [62, 63]. For the recording of $Ca_V2.2$ currents, we used HEK 293 cells transiently expressing mouse $Ca_V2.2$, rabbit α_2/δ, and human β_{1a} (GenBank Accession Number NM_000723). HEK293 cells were cultured in DMEM containing 10 % fetal bovine serum, 30 units/mL penicillin, and 30 μg/mL streptomycin. Transfection of cDNA plasmids was performed using SuperFect Transfection Reagent (Qiagen). Cells were subjected to the analysis of protein expression and electrophysiological measurements 48 h after transfection. Anti-RIM3 polyclonal antibody [20] and anti-α-tubulin monoclonal antibody (Sigma) were used in the protein expression analysis.

Current recordings

Whole-cell mode of the patch-clamp technique was performed at 22-25 °C with an EPC-10 (HEKA Elektronik) patch-clamp amplifier, as previously described [64]. Patch pipette resistance ranged from 2 to 3.5 MΩ when filled with pipette solutions (described below). Series resistance was electronically compensated to >60 %, and both leakage and remaining capacitance were subtracted using the –P/4 method. For activation kinetics, currents were sampled at 100 kHz after low-pass filtering at 8.4 kHz (3 db), otherwise currents were sampled at 20 kHz after low-pass filtering at 3.0 kHz (3 db). Data were collected and analyzed using PATCHMASTER (HEKA Elektronik). The external solution contained (in mM): 3 $BaCl_2$, 155

tetraethylammonium chloride (TEA-Cl), 10 HEPES, and 10 glucose (pH 7.4 adjusted with TEA-OH) for P/Q-type VDCCs recording, and 5 $BaCl_2$, 148 TEA-Cl, 10 HEPES, and 10 glucose (pH 7.4 adjusted with TEA-OH) for N-type VDCCs recording. The pipette solution contained (in mM): 95 CsOH, 95 aspartate, 40 CsCl, 4 $MgCl_2$, 5 EGTA, 2 disodium ATP, 5 HEPES, and 8 creatine phosphate (pH 7.2 adjusted with CsOH).

Voltage-dependence of inactivation

To determine voltage dependence of inactivation (inactivation curve) of VDCCs, Ba^{2+} currents were evoked by a 20-ms test pulse to 5 mV after 10-ms repolarization to −100 mV following 2-s holding potential (V_h) displacement from −100 to 20 mV with 10-mV increments. Current amplitudes elicited by test pulses were normalized to those after a 2-s V_h displacement to −100 mV. Mean values were plotted against potentials for 2-s V_h displacement. Mean values were fitted to the single Boltzmann's equation: $h(V_h) = (1-a)+a/\{1+\exp[(V_{0.5}-V_h)/k]\}$, with a, rate of inactivating component, $V_{0.5}$, potential for half-value of inactivation, and k, slope factor.

Voltage-dependence of activation

Tail currents were elicited by repolarization to −60 mV after a 5-ms test pulse from −40 to 40 mV with 5-mV increments. Currents were sampled at 100 kHz after low-pass filtering at 8.4 kHz. Tail current amplitudes were normalized to those obtained with test pulses to 30 mV. Mean values were plotted against test pulse potentials, and fitted to Boltzmann's equation: $n(V_m) = 1/\{1+\exp[(V_{0.5}-V_m)/k]\}$, with V_m, membrane potential, $V_{0.5}$, potential for half-value of conductance, and k, slope factor.

PC12 cell culture and release assay

PC12 cells were cultured as described previously [27]. Acetylcholine (ACh) secretion experiments were performed as previously reported [18]. Briefly, PC12 cells were plated in poly-D-lysine-coated 35-mm dishes (BD Bioscience) with 5×10^5 cells per dish. Cells were co-transfected with 5 μg of each RIM3 plasmid and 1 μg of pEFmChAT encoding mouse choline acetyltransferase (ChAT) cDNA using Lipofectamine® 2000

(Invitrogen). 72 h after transfection, PC12 cells were washed with 5.9 mM K^+ solution containing (in mM): 0.01 eserine, 140 NaCl, 4.7 KCl, 1.2 KH_2PO_4, 2.5 $CaCl_2$, 1.2 $MgSO_4$, 11 glucose, and 15 HEPES (pH 7.4 adjusted with NaOH), and incubated for 30 s with 5.9 mM K^+ solution at 37 °C. To measure K^+-stimulated ACh release, cells were then incubated for 30 s with a 51.1 mM K^+ solution containing (in mM): 0.01 eserine, 94.8 NaCl, 49.9 KCl, 1.2 KH_2PO_4, 2.5 $CaCl_2$, 1.2 $MgSO_4$, 11 glucose, and 15 HEPES (pH 7.4 adjusted with NaOH). The supernatant after stimulation of 51.1 mM K^+ solution was used to measure secreted ACh. The supernatant from cells solubilized in NP-40 buffer and centrifuged at 17,400 × *g* for 20 min at 4 °C was used to measure cellular ACh that was not secreted. ACh was measured by HPLC with electrochemical detection (HTEC-500; EiCOM) as follows. ACh was separated on a styrene polymer reversed-phase column and subsequently catalyzed in a postcolumn enzyme reactor containing immobilized acetylcholinesterase (AChE) and choline oxidase (ChO). ACh was hydrolyzed by AChE to acetate and choline, and choline was oxidized by ChO to produce hydrogen peroxide and betaine. The amount of hydrogen peroxide corresponding to ACh was electrochemically detected by a platinum working electrode (EiCOM). The signal from the detector was recorded using a data acquisition system and analyzed using PowerChrom software (EiCOM). RIM3 proteins expression level was analyzed by western blotting.

Fluorescent $[Ca^{2+}]_i$ measurement

PC12 cells were co-transfected with 3 μg of each RIM3 plasmid and 0.6 μg of pEGFP-C1 using Lipofectamine® 2000. 48 h after transfection, PC12 cells were plated onto poly-L-lysine-coated glass coverslips. 72 h after transfection, cells on coverslips were loaded with fura-2 by incubation in DMEM containing 10 μM fura-2/AM (Dojindo Laboratories), 0.04 % Pluronic F-127 (Biotium), 5 % fetal bovine serum, and 5 % horse serum at 37 °C for 40 min, and washed with 5.9 mM K^+ solution. Coverslips were then placed in a perfusion chamber mounted to the microscope stage. Fluorescence cell images were recorded and analyzed using a video image analysis system (AQUACOSMOS; Hamamatsu Photonics). Fura-2 fluorescence at an emission wavelength of 510 nm was observed at 37 ± 1 °C by exciting fura-2 alternately at 340 and 380 nm. Measurements were taken in 5.9 mM K^+ solution and 28.4 mM K^+ solution containing (in mM): 117.5

NaCl, 27.2 KCl, 1.2 KH_2PO_4, 2.5 $CaCl_2$, 1.2 $MgSO_4$, 11 glucose, and 15 HEPES (pH 7.4 adjusted with NaOH). Images of 340:380 nm ratios were obtained on a pixel-by-pixel basis and converted to Ca^{2+} concentrations by *in vivo* calibration using 40 μM ionomycin [65].

Statistical analysis

All data were expressed as mean ± SEM. Data were obtained under each condition from at least three independent experiments. Statistical significance was evaluated by analysis of variance followed by the Tukey-Kramer test.

Reference

[1] Miller, R. J. (1988) *Trends Neuorsci.*, **11**, 415-419

[2] Berridge, M J., Lipp, P., and Bootman, M. D. (2000) *Nat. Rev. Mol. Cell Biol.*, **1**, 11-21

[3] Autism and Developmental Disabilities Monitoring Network Surveillance Year 2008 Principal Investigators (2012) *MMWR. Surveill. Summ.*, **61**, 1-19

[4] Johnson, M. H. (2001) *Nat. Rev. Neurosci.*, **2**, 475-483

[5] Abrahams, B. S., and Geschwind, D. H. (2008) *Nat. Rev. Genet.*, **9**, 341-355

[6] Jamain, S., Quach, H., Betancur, C., Råstam, M., Colineaux, C., Gillberg, I. C., Soderstrom, H., Giros, B., Leboyer, M., Gillberg, C., Bourgeron, T.; Paris Autism Research International Sibpair Study (2003) *Nat. Genet.*, **34**, 27-29

[7] Durand, C. M., Betancur, C., Boeckers, T. M., Bockmann, J., Chaste, P., Fauchereau, F., Nygren, G., Rastam, M., Gillberg, I. C., Anckarsäter, H., Sponheim, E., Goubran-Botros, H., Delorme, R., Chabane, N., Mouren-Simeoni, M. C., de Mas, P., Bieth, E., Rogé, B., Héron, D., Burglen, L., Gillberg, C., Leboyer, M., and Bourgeron, T. (2007) *Nat. Genet.*, **39**, 25-27

[8] Malhotra, D., and Sebat, J. (2012) *Cell*, **148**, 1223-1241

[9] Südhof, T. C. (2012) *Neuron*, **75**, 11-25

[10] Wang, Y., and Südhof, T. C. (2003) *Genomics*, **81**, 126-137

[11] Koushika, S. P., Richmond, J. E., Hadwiger, G., Weimer, R. M., Jorgensen, E. M., and Nonet, M. L. (2001) *Nat. Neurosci.*, **4**, 997-1005

[12] Schoch, S., Castillo, P. E., Jo, T., Mukherjee, K., Geppert, M., Wang, Y., Schmitz, F., Malenka, R. C., and Südhof, T. C. (2002) *Nature*, **415**, 321–326

[13] Gracheva, E. O., Hadwiger, G., Nonet, M. L., and Richmond, J. E. (2008) *Neurosci. Lett.*, **444**, 137-142

[14] Kaeser, P. S., Deng, L., Wang, Y., Dulubova, I., Liu, X., Rizo, J., and Südhof, T. C. (2011) *Cell*, **144**, 282-295

[15] Deng, L., Kaeser, P. S., Xu, W., and Südhof, T. C. (2011) *Neuron*, **69**, 317-331

[16] Han, Y., Kaeser, P. S., Südhof, T. C., and Schneggenburger, R. (2011) *Neuron*, **69**, 304–316

[17] Castillo, P. E., Schoch, S., Schmitz, F., Südhof, T. C., and Malenka, R. C. (2002) *Nature*, **415**, 327-330

[18] Kiyonaka, S., Wakamori, M., Miki, T., Uriu, Y., Nonaka, M., Bito, H., Beedle, A. M., Mori, E., Hara, Y., De Waard, M., Kanagawa, M., Itakura, M., Takahashi, M., Campbell, K. P., and Mori, Y. (2007) *Nat. Neurosci.*, **10**, 691-701

[19] Gandini, M. A., Sandoval, A., González-Ramírez, R., Mori, Y., De Waard, M., and Felix, R. (2011) *J. Biol. Chem.*, **286**, 15757-15765

[20] Uriu, Y., Kiyonaka, S., Miki, T., Yagi, M., Akiyama, S., Mori, E., Nakao, A., Beedle, A.M., Campbell, K.P., Wakamori, M., and Mori, Y. (2010) *J. Biol. Chem.*, **285**, 21750-21767

[21] Alvarez-Baron, E., Michel, K., Mittelstaedt, T., Opitz, T., Schmitz, F., Beck, H., Dietrich, D., Becker, A. J., and Schoch, S. (2013) *J. Neurosci.*, **33**, 824-839

[22] Liang, F., Zhang, B., Tang, J., Guo, J., Li, W., Ling, E. A., Chu, H., Wu, Y., Chan, Y. G., Cao, Q. (2007) *J. Comp. Neurol.*, **503**, 501-510

[23] Kumar, R. A., Sudi, J., Babatz, T. D., Brune, C. W., Oswald, D., Yen, M., Nowak, N. J., Cook, E. H., Christian, S. L., and Dobyns, W. B. (2010) *J. Med. Genet.*, **47**, 81-90

[24] Guan, R., Dai, H., Tomchick, D. R., Dulubova, I., Machius, M., Südhof, T. C., and Rizo, J. (2007) *Biochemistry*, **46**, 8988-8998

[25] Tsien, R. W., Ellinor, P. T., and Horne, W. A. (1991) *Trends Pharmacol. Sci.*, **12**, 349-354

[26] Mori, Y., Friedrich, T., Kim, M. S., Mikami, A., Nakai, J., Ruth, P., Bosse, E., Hofmann, F., Flockerzi, V., Furuichi, T., Mikoshiba K., Imoto K., Tanabe T., and Numa S. (1991) *Nature*, **350**, 398-402

[27] Itakura, M., Misawa, H., Sekiguchi, M., Takahashi, S., and Takahashi, M. (1999) *Biochem. Biophys. Res. Commun.*, **265**, 691-696

[28] Zoghbi, H. Y. (2003) *Science*, **302**, 826-830

[29] Sheng, Z. H., Rettig, J. Takahashi, M., and Catterall, W. A. (1994) *Neuron*, **13**, 1303-1313

[30] Bezprozvanny, I., Scheller, R. H., and Tsien, R. W. (1995) *Nature*, **378**, 623-626

[31] Wiser, O., Bennett, M. K., and Atlas, D. (1996) *EMBO J.*, **15**, 4100-4110

[32] Zhong, H., Yokoyama, C. T., Scheuer, T., and Catterall, W. A. (1999) *Nat. Neurosci.*, **2**, 939-941

[33] Chen, J., Billings, S. E., and Nishimune, H. (2011) *J. Neurosci.*, **31**, 512-525

[34] Billings, S. E., Clarke, G. L., and Nishimune, H. (2012) *Neuroreport*, **23**, 49-54

[35] Kiyonaka, S., Nakajima, H., Takada, Y., Hida, Y., Yoshioka, T., Hagiwara, A., Kitajima, I., Mori, Y., and Ohtsuka, T. (2012) *J. Biochem.*, **152**, 149-159

[36] Coppola, T., Magnin-Luthi, S., Perret-Menoud, V., Gattesco, S., Schiavo, G., and Regazzi, R. (2001) *J. Biol. Chem.*, **276**, 32756-32762

[37] Hussman, J. P. (2001) *J. Autism Dev. Disord.*, **31**, 247-248

[38] Rubenstein, J. L., and Merzenich, M. M. (2003) *Genes Brain Behav.*, **2**, 255-267

[39] Meir, A., Ginsburg, S., Butkevich, A., Kachalsky, S. G., Kaiserman, I., Ahdut, R., Demirgoren, S., and Rahamimoff, R. (1999) *Physiol. Rev.*, **79**, 1019-1088

[40] Poncer, J. C., McKinney, R. A., Gähwiler, B. H., and Thompson, S. M. (1997) *Neuron*, **18**, 463-472

[41] Stephens, G. J., Morris, N. P., Fyffe, R. E., and Robertson, B. (2001) *Eur. J. Neurosci.*, **13**, 1902-1912

[42] Gu, X., and Spitzer, N. C. (1995) *Nature*, **375**, 784-787

[43] Solem, M., McMahon, T., and Messing, R. O. (1995) *J. Neurosci.*, **15**, 5966-5975

[44] Boeckers, T. M., Bockmann, J., Kreutz, M. R., and Gundelfinger, E. D. (2002) *J. Neurochem.*, **81**, 903-910

[45] Arons, M. H., Thynne, C. J., Grabrucker, A. M., Li, D., Schoen, M., Cheyne, J. E., Boeckers, T. M., Montgomery, J. M., and Garner, C. C. (2012) *J. Neurosci.*, **32**, 14966-14978

[46] Krey, J. F., and Dolmetsch, R. E. (2007) *Curr. Opin. Neurobiol.*, **17**, 112-119

[47] Aamodt, S. M., and Constantine-Paton, M. (1999) *Adv. Neurol.*, **79**, 133-144

[48] Cline, H. T. (2001) *Curr. Opin. Neurobiol.*, **11**, 118-126

[49] Spitzer, N. C., Root, C. M., and Borodinsky, L. N. (2004) *Trends Neurosci.*, **27**, 415-421

[50] DiCicco-Bloom, E., Lord, C., Zwaigenbaum, L., Courchesne, E., Dager, S. R., Schmitz, C., Schultz, R. T., Crawley, J., and Young, L. J. (2006) *J. Neurosci.*, **26**, 6897-6906

[51] Splawski, I., Timothy, K. W., Sharpe, L. M., Decher, N., Kumar, P., Bloise, R., Napolitano, C., Schwartz, P. J., Joseph, R. M., Condouris, K., Tager-Flusberg, H., Priori, S. G., Sanguinetti, M. C., and Keating, M. T. (2004) *Cell*, **119**, 19-31

[52] Splawski, I., Yoo, D. S., Stotz, S. C., Cherry, A., Clapham, D. E., and Keating, M. T. (2006) *J. Biol. Chem.*, **281**, 22085-22091

[53] Hemara-Wahanui, A., Berjukow, S., Hope, C. I., Dearden, P. K., Wu, S. B., Wilson-Wheeler, J., Sharp, D. M., Lundon-Treweek, P., Clover, G. M., Hoda, J. C., Striessnig, J., Marksteiner, R., Hering, S., and Maw, M. A. (2005) *Proc. Natl. Acad. Sci. U. S. A.*, **102**, 7553-7558

[54] Laumonnier, F., Roger, S., Guérin, P., Molinari, F., M'rad, R., Cahard, D., Belhadj, A., Halayem, M., Persico, A. M., Elia, M., Romano, V., Holbert, S., Andres, C., Chaabouni, H., Colleaux, L., Constant, J., Le Guennec, J. Y., and Briault, S. (2006) *Am. J. Psychiatry*, **163**, 1622-1629

[55] Weidenhofer, J., Bowden, N. A., Scott, R. J., and Tooney, P. A. (2006) *Mol. Cell. Neurosci.*, **31**, 243-250

[56] Weidenhofer, J., Scott, R. J., and Tooney, P. A. (2009) *J. Psychiatr. Res.*, **43**, 282-290

[57] Guerini, F. R., Bolognesi, E., Chiappedi, M., Manca, S., Ghezzo, A., Agliardi, C., Sotgiu, S., Usai, S., Matteoli, M., and Clerici, M. (2011) *Pharmacol. Res.*, **64**, 283-288

[58] Guex, N., and Peitsch, M. C. (1997) *Electrophoresis*, **18**, 2714-2723

[59] Arnold, K., Bordoli, L., Kopp, J., and Schwede, T.(2006) *Bioinformatics*, **22**, 195-201

[60] Bordoli, L., Kiefer, F., Arnold, K., Benkert, P., Battey, J., and Schwede, T. (2009) *Nat. Protoc.*, **4**, 1-13

[61] McNicholas, S., Potterton, E., Wilson, K. S., and Noble, M. E. (2011) *Acta Crystallogr. D Biol. Crystallogr.*, **67**, 386-394

[62] Niidome, T., Teramoto, T., Murata, Y., Tanaka, I., Seto, T., Sawada, K., Mori, Y., and Katayama, K. (1994) *Biochem. Biophys. Res. Commun.*, **203**, 1821-1827

[63] Kang, M. G., Chen, C. C., Wakamori, M., Hara, Y., Mori, Y., and Campbell, K. P. (2006) *Proc. Natl. Acad. Sci. U. S. A.*, **103**, 5561-5566

[64] Wakamori, M., Yamazaki, K., Matsunodaira, H., Teramoto, T., Tanaka, I., Niidome, T., Sawada, K., Nishizawa, Y., Sekiguchi, N., Mori, E., Mori, Y., and Imoto, K. (1998) *J. Biol. Chem.*, **273**, 34857-34867

[65] Nishida, M., Nagao, T., and Kurose, H. (1999) *Biochem. Biophys. Res. Commun.*, **262**, 350-354

Chapter 4

Tankyrase contributes to the risk of spinocerebellar ataxia type 6 by binding of the C-terminal of voltage-dependent Ca^{2+} channels

Abstract

Spinocerebellar ataxia type 6 (SCA6), which is an autosomal dominantly inherited neurodegenerative disorder, is known to be caused by the expansion of polyglutamine in the carboxy (C-) terminal region of the voltage-dependent Ca^{2+} channel $Ca_V2.1$ α_1-subunit. However, as well as many other polyglutamine diseases, the precise pathogenic mechanism is unclear. We show that novel interacting molecule with calcium channels might be involved with SCA6 pathogenesis. We identified tankyrase, a part of poly ADP-ribose polymerase family associated with the telomere elongation, that was strongly associated with the C-terminus of $Ca_V2.1$ in proportion to the length of polyglutamine. In the electrophysiological analysis, we found that tankyrase reduces the current density of $Ca_V2.1$ channels, has shifted the voltage-dependency of inactivation toward more hyperpolarized potentials, and accelerates inactivation kinetics of polyglutamine containing $Ca_V2.1$ currents. Moreover, an auxiliary subunit β_4-subunit is translocated into nucleus in a polyglutamine length-dependent manner. These results suggest that tankyrase-association with the polyglutamine region of $Ca_V2.1$ induces the reduction of calcium availability at neuronal resting potential by interfering calcium channel assembly; the resulting low calcium concentration may disrupt the cellular function and induce cell death. Therefore, regulation of tankyrase activity may be a new therapeutic target of SCA6.

Introduction

Spinocerebellar ataxia type 6 (SCA6) is an autosomal dominantly inherited neurodegenerative disorder, which is characterized by gaze-evoked nystagmus, dysarthria, progressive imbalance, and severe limb incoordination [1, 2]. Alternatively, late-onset cerebellar ataxia, moderate cerebellar atrophy and selective loss of Purkinje cells may occur in some SCA6 patients [2-4]. The disease usually progresses slowly and does not shorten lifespan, but most patients become wheelchair bound by their late 60s. The prevalence of SCA6 varies by geographic area, being highest in Japan and moderate in Europe. SCA6 is known to be caused by the expansion of a CAG trinucleotide repeat in the exon coding for the carboxy (C-) terminal region of the voltage-dependent Ca^{2+} channel (VDCC) $Ca_V2.1$ α_1-subunit [1]. Because the CAG repeat encodes a polyglutamine tract, SCA6 is classified as one of the group of polyglutamine (polyQ) diseases including Huntington's disease, dentatorubral pallidoluysian atrophy, and other types of spinocerebellar ataxia [5]. In contrast to other polyQ diseases, SCA6 arises from a relatively small expansion, which is ranged from 21 to 33 repeats, compared with other polyQ diseases in which 35-300 repeats cause disease [6-8]. This raises a possibility that SCA6 is caused by a mechanism different from that underlying the other polyQ disease in common.

P/Q-type $Ca_V2.1$ α_1-subunit gene (*CACNA1A*) was first identified primary structure and functional expression in 1991 [9]. The channel is classified into high voltage-activated Ca^{2+} channels and is predominantly expressed in cerebellum, olfactory bulb, cerebral cortex, hippocampus, inferior colliculus and auditory brain stem [10]. P/Q-type $Ca_V2.1$ channel is functionally expressed as a complex composed of four subunits, pore-forming $Ca_V2.1$ α_1-subunit and three auxiliary subunits α_2/δ, β, and γ [11]. $Ca_V2.1$ channel complex is known to be associated with many cytosolic proteins including syntaxin, SNAP-25, synaptotagmin, CASK and Mint through physical association with the 'synprint' region in the domain II-III intracellular loop of $Ca_V2.1$ α_1-subunit [12-20]. On the other hand, the intracellular C-terminus of the $Ca_V2.1$ α_1-subunit has been implicated in a number of protein-protein interactions that play a prominent role in modulating Ca^{2+} channel activity [21]. For example, calcium calmodulin readily binds to an EF hand motif in the C-terminus of $Ca_V2.1$, and inhibits channel currents and alters synaptic efficacy [22, 23]. Gα-protein mediated channel

inhibition is occurred through the interaction with the C-terminus [24]. Furthermore, β_4 auxiliary subunit, which is thought to mainly bind to the domain I-II region, binds to the C-terminus of $Ca_V2.1$ and alters channel kinetics [25]. Thus, it is suggested that the C-terminus of $Ca_V2.1$ α_1-subunit is an important region for functional channel modulation by other factors.

To date, numerous studies have attempted to determine how the polyQ expansion affects the properties and molecular assembly of P/Q-type $Ca_V2.1$ channel, and ultimately how a small expansion in the C-terminus may lead to cell death [26-36]. Although these results appear highly variable and depend on experimental conditions, all of these studies provide insight into the various aspects of SCA6 pathology [37]. In this study, we hypothesize that there is unknown interacting protein with the C-terminus of $Ca_V2.1$ α_1-subunit, and the disruption of relationships among these proteins may lead to functionally channel modulation and SCA6 pathogenesis. To examine the hypothesis, we performed yeast two-hybrid screening using C-terminus of $Ca_V2.1$ as a bait to identify the interacting protein. Here we demonstrate a novel molecular interaction of the $Ca_V2.1$ C-terminus with tankyrase, which is a part of poly ADP-ribose polymerase (PARP) family [38-41]. The tankyrase-C-terminus interaction is modified by the length of polyQ tracts in the C-terminus of $Ca_V2.1$.

Results

C-terminus of $Ca_V2.1$ directly interacts with tankyrase-2

To identify the C-terminus of $Ca_V2.1$ α_1-subunit-interacting proteins, we performed yeast two-hybrid screening with a human brain complementary DNA library using the C-terminus fragment human $Ca_V2.1$ subunit (GenBank Accession Number NM_023035) as a bait. Screening identified a clone encoding the N-terminal region (amino acid residues 89-380) of the human tankyrase-2 protein [38-41], a part of Ankyrin repeat domain (Fig. 1A). Subsequent two-hybrid assays using $Ca_V2.1$ α_1-subunit mutants showed that amino acid residues 2266-2510, containing polyQ11 domains, were required for the interaction of $Ca_V2.1$ with tankyrase-2 (Fig. 1B). Interestingly, $Ca_V2.1$ variant without polyQ11 domain could not interact with tankyrase-2 (Fig. 1B, 1C). *In vitro* pulldown assays using glutathione-*S*-transferase (GST) fusion constructs of

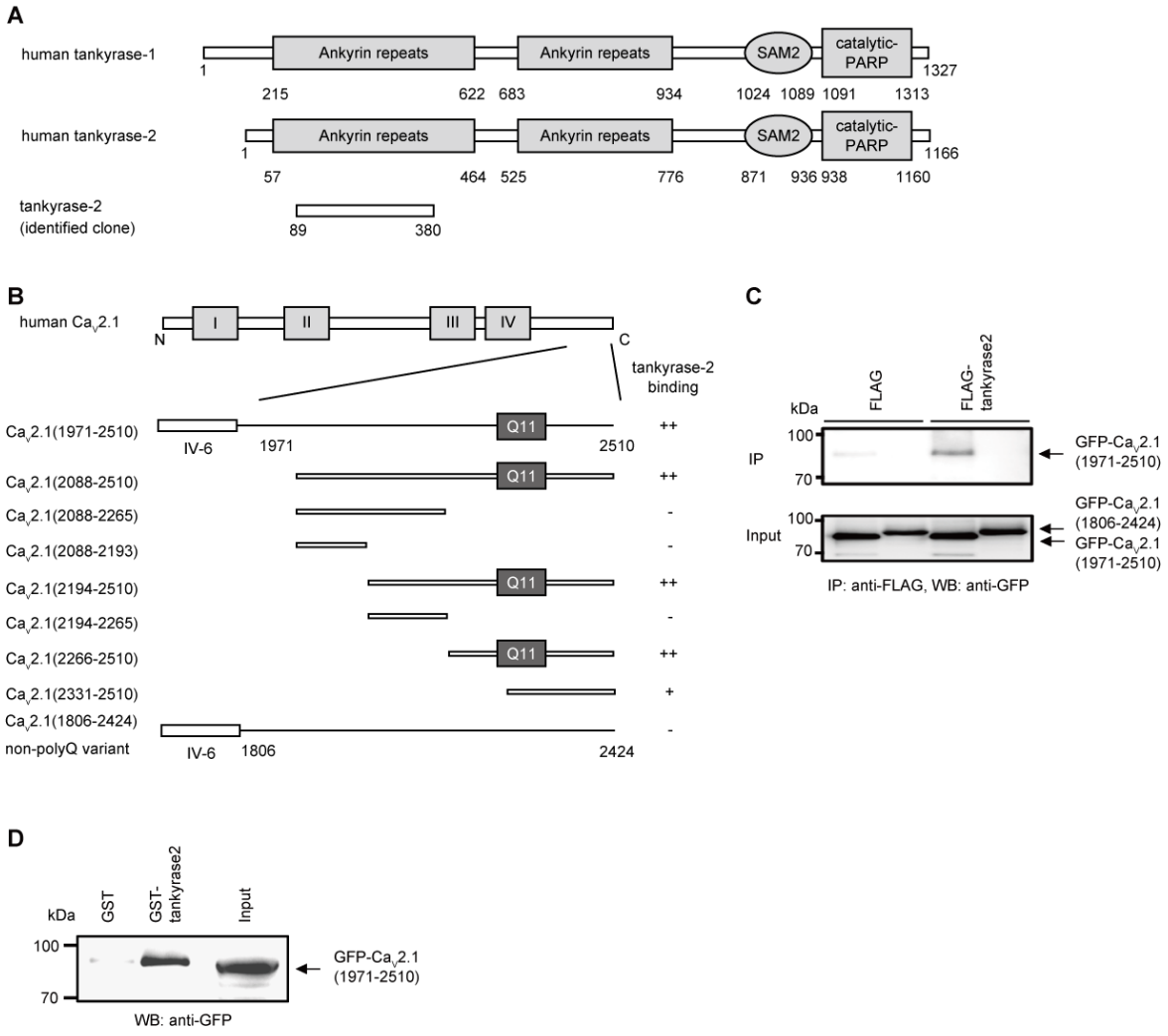

Fig. 1 Direct intraction of tankyrase-2 with the C-terminus of $Ca_V2.1$ subunit. (A) Domain structure of tankyrase-1 and tankyrase-2. Sterile alpha motif (SAM) 2 domain and catalytically active poly-ADP ribose polymerase (PARP) domain are located at the C-terminus of tankyrase. The protein region encoded by identified clone is also indicated. (B) Mapping of tankyrase-2 binding sites on the C-terminus of $Ca_V2.1$ subunit by the yeast two-hybrid assay. $Ca_V2.1$ subunit constructs in bait vectors were tested with tankyrase-2 in the prey vector. The interactions were scored by β-galactosidase activity and His^+ prototrophy. (C) Interaction of recombinant C-terminus of $Ca_V2.1$ and tankyrase-2 in HEK293 cells. The interaction was evaluated by immunoprecipitation with antibody for FLAG, followed by western blotting with antibody for GFP. $Ca_V2.1$ (1971-2510) or $Ca_V2.1$ (1806-2424) is a variant with or without polyQ domain, respectively. IP, immunoprecipitation; WB, western blotting. (D) Pulldown assay of C-terminus of $Ca_V2.1$ with GST fusion tankyrase-2. GST fusion proteins immobilized on glutathione-Sepharose beads were incubated with cell lysates obtained from GFP-$Ca_V2.1$ (1971-2510)-transfected HEK293 cells. Bound proteins were analyzed by western blotting using antibody for GFP.

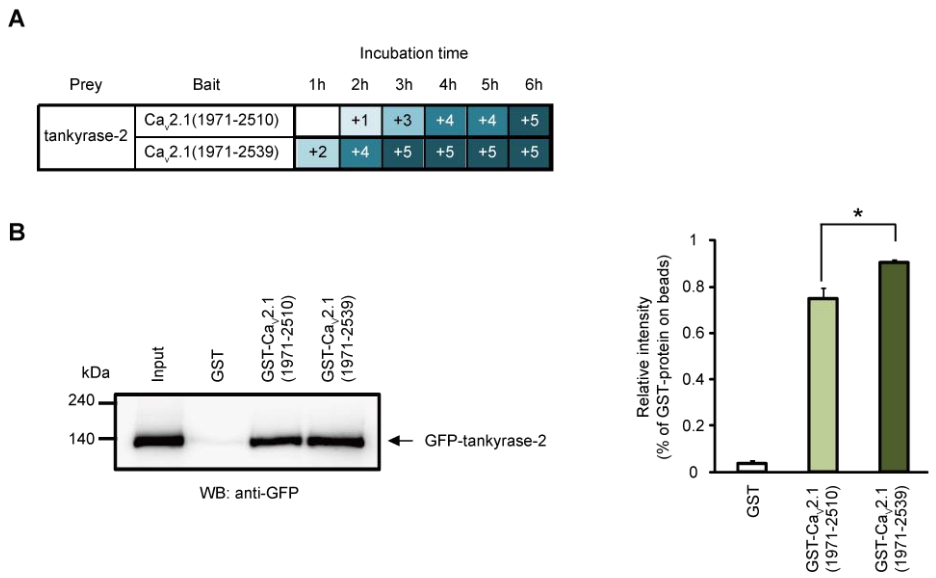

Fig. 2 The interaction between C-terminus of $Ca_V2.1$ and tankyrase-2 is augmented by elongated-polyQ. (A) Interaction of tankyrase-2 and C-terminus of $Ca_V2.1$ with different polyQ length by yeast two-hybrid assay. Two constructs in bait vectors were tested with tankyrase-2 in the prey vector. The interactions were scored by β-galactosidase activity. The blue color phenotype was scored (+5: very strong, +4: strong, +3: intermediate, +2: weak, +1: very weak, blank: no binding). (B) Pulldown assay of tankyrase-2 with GST fusion C-terminus proteins of $Ca_V2.1$. *Left*, representative images of western blotting. GST fusion proteins immobilized on glutathione-Sepharose beads were incubated with cell lysates obtained from GFP-tankyrase-2-transfected HEK293 cells. Bound proteins were analysed using antibody for GFP. WB, western blotting. *Right*, Quantitative analysis of western blotting. Relative intensities were quantified using NIH software and normalized by GST-fusion protein on beads. $^*P < 0.05$. Data points are mean ± SEM.

---

tankyrase-2 also identified the interaction of tankyrase-2 with the C-terminus of $Ca_V2.1$ (Fig. 1D). These results suggest that a direct protein-protein interaction occurs between tankyrase-2 and polyQ domain of $Ca_V2.1$ C-terminus.

The interaction between C-terminus of $Ca_V2.1$ and tankyrase-2 is augmented by elongated-polyQ

An intermediated polyQ length, ranging from 21 to 40 repeats, is identified in SCA6 patients, compared to the number of repeat (4-20) in healthy control [6-8]. Thus we next examined the effects of polyQ elongation on the interaction between tankyrase-2 and the C-terminus of $Ca_V2.1$. We constructed the C-terminus containing 40 CAG repeats ($Ca_V2.1$ (1971-2539)) by the synthetic oligonucleotides. Yeast two-hybrid assays

demonstrated that $Ca_V2.1$ (1971-2539) bound to tankyrase more strongly than $Ca_V2.1$ (1971-2510) (Fig. 2A). Similarly, *in vitro* pulldown assays revealed that the interaction of tankyrase-2 with the C-terminus was slightly augmented by the elongation of polyQ in mammalian system (Fig. 2B). Therefore, polyQ length may affect the physical association between tankyrase-2 and $Ca_V2.1$ subunit.

Tankyrase-2 reduces current densities of P/Q-type $Ca_V2.1$

To elucidate the functional significance of direct tankyrase-2-$Ca_V2.1$ coupling, we characterized whole-cell Ba^{2+} currents through recombinant P/Q-type VDCCs expressed as α_1,·α_2/δ, and·β_4 complexes containing the BI-1 variant with CAG (12 or 40) of $Ca_V2.1$ in BHK cells [9, 27]. In following experiments, we used $Ca_V2.1$

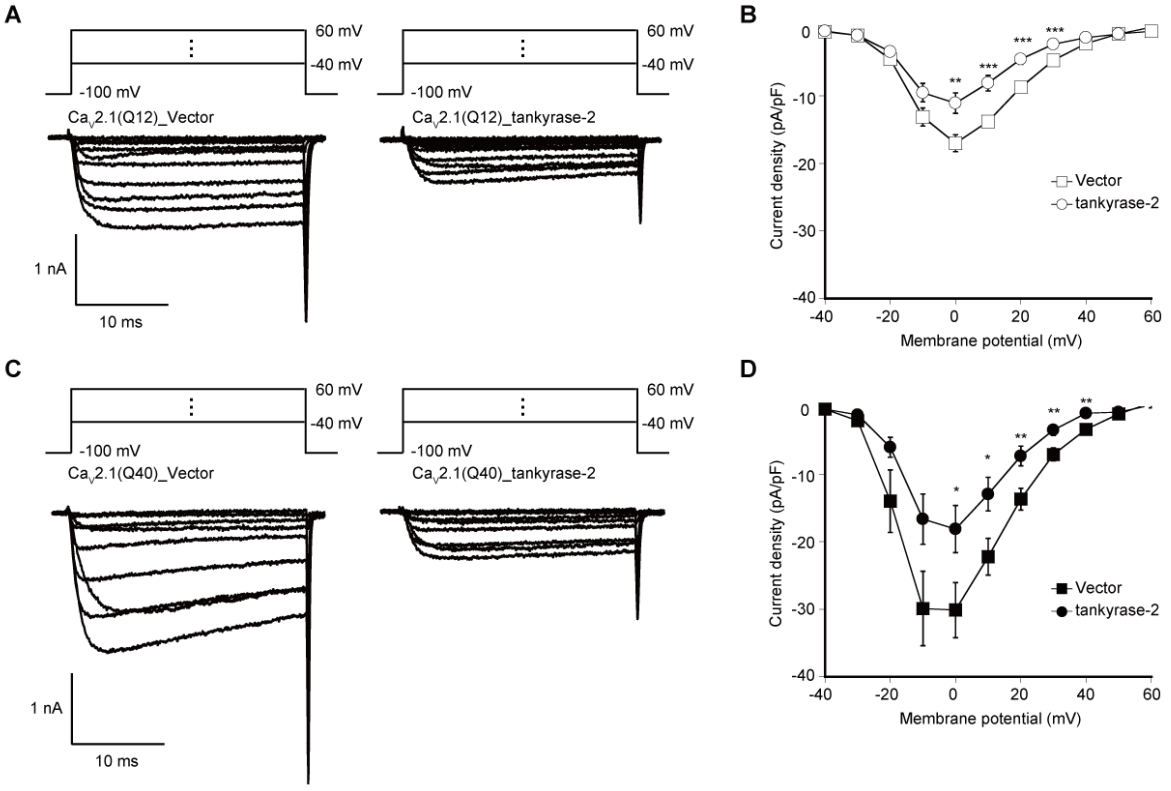

Fig. 3 Effects of tankyrase-2 on the current density-voltage (*I-V*) relationships of P/Q-type $Ca_V2.1$ with Q12 or Q40. (A, C) Representative traces of Ba^{2+} currents with or without tankyrase-2 on application of test pulses from −40 to 60 mV with 10-mV increments from a V_h of −100 mV. $Ca_V2.1$ with Q12 (A) or Q40 (C) was expressed in BHK cells. (B, D) *I-V* relationships of P/Q-type $Ca_V2.1$ with Q12 (B) or Q40 (D). $^{*}P < 0.05$, $^{**}P < 0.01$, $^{***}P < 0.001$ compared with Vector control. Data points are mean ± SEM.

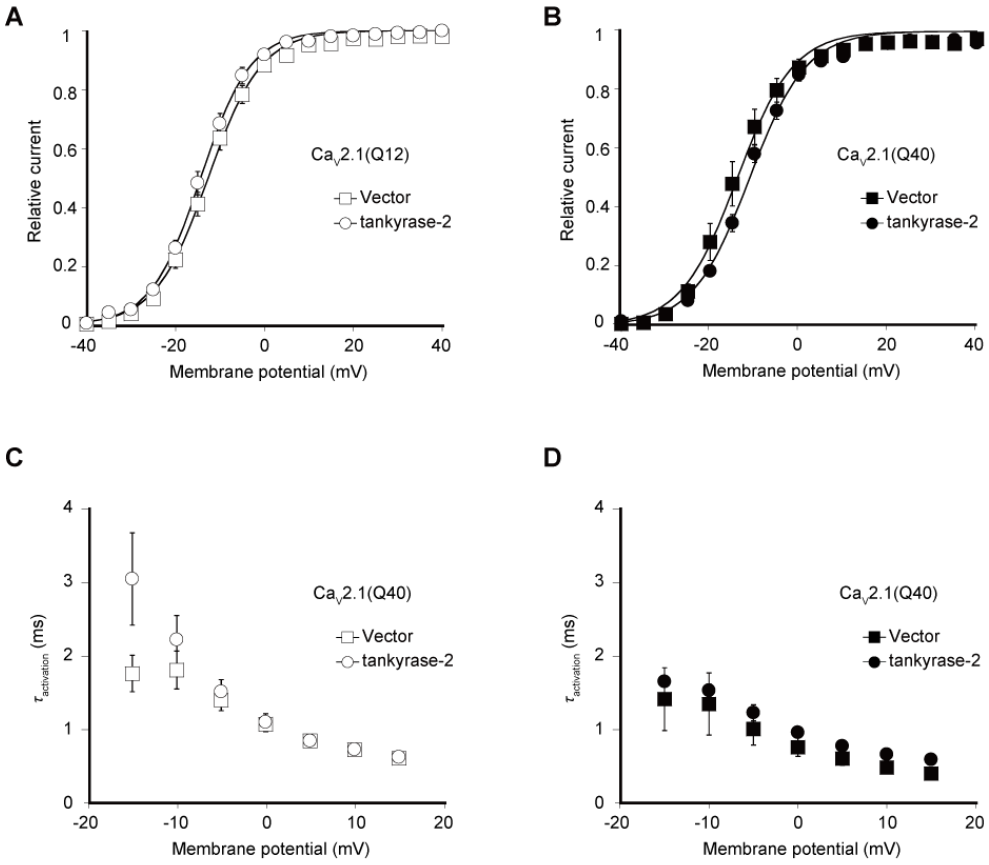

Fig. 4 Effects of tankyrase-2 on the activation properties of P/Q-type Ca$_V$2.1 currents. (A, C) Activation curves of P/Q-type Ca$_V$2.1 with Q12 (A) or Q40 (C) in BHK cells. Tail currents elicited by repolarization to −60 mV after 5-ms test pulses from −40 to 40 mV are used to determine activation curves. (B, D) Activation time constants plotted as a function of test potential. The activation phases were well fitted by single exponential function at all potentials. $\tau_{activation}$ were obtained from currents elicited by 5-ms step depolarization from −15 to 15 mV in 5-mV increments from a V_h of −100 mV. Ca$_V$2.1 with Q12 (B) or Q40 (D) was expressed in BHK cells. Data points are mean ± SEM.

---

with polyQ12 construct as a control. Fig. 3 shows Ca$_V$2.1 with polyQ12 (Fig. 3A, 3B) or polyQ40 (Fig. 3C, 3D) currents and their current density-voltage (*I-V*) relationships in BHK cells in the presence or absence of full-length tankyrase-2. Ba^{2+} currents were elicited with 30-ms depolarizing pulses from a holding potential (V_h = −100 mV) to test potentials from −40 to 40 mV with increments of 10 mV. We found that tankyrase-2 reduced current densities from −17.0 ± 1.3 mV to −11.1 ± 1.5 mV, or −30.1 ± 4.1 mV to −18.1 ± 3.5 mV in polyQ12 or polyQ40 expressing BHK cells, respectively (Fig. 3B, 3D and Table 1). These results suggest that tankyrase-2 reduces the number of available Ca^{2+} channels independent of polyQ length.

On the other hand, tankyrase-2 failed to exert significant effects on the voltage-dependent activation. The estimated half-activation potentials in polyQ12 or polyQ40 expressing cells were −12.5 ± 1.0 mV or −10.5 ± 0.7 mV in the absence of tankyrase-2, and −14.1 ± 0.8 mV or −10.3 ± 1.6 mV in the presence of tankyrase-2, respectively (Fig. 4A, 4B and Table 1). Furthermore, tankyrase-2 expression did not modulate activation kinetics of VDCC despite of the length of polyQ (Fig. 4C, 4D). Thus, tankyrase-2 might not be involved in the regulation of activation properties.

Tankyrase-2 modulates inactivation properties of P/Q-type $Ca_V2.1$

We next examined the effects of tankyrase-2 on voltage-dependent inactivation of VDCC in $Ca_V2.1$ with polyQ12 or polyQ40 expressing BHK cells. The voltage-dependence of inactivation was determined by the use of 2-s prepulses to a series of different potentials followed by the test pulse to 5-mV. Peak current amplitudes were normalized to the peak current amplitude induced by the test pulse from a prepulse potential of −100 mV and were plotted against the prepulse potentials. In polyQ12 expressing cells, the voltage-dependent inactivation was shifted in the hyperpolarizing direction, and the midpoints of the inactivation curves ($V_{0.5}$) fitted by the Boltzmann equation were −50.0 ± 1.7 mV and −65.3 ± 2.6 mV in the absence and presence of tankyrase-2, respectively (Fig. 5A, 5B and Table 2). Similarly, tankyrase-2 also shifted the voltage-dependence of inactivation toward hyperpolarizing potentials from −52.9 ± 3.7 mV to −63.3 ± 1.8 mV in polyQ40 expressing cells (Fig. 5C, 5D and Table 2). These results suggest that tankyrase-2 tend to inactivate the channel at neuronal resting potentials (about −75 mV), and reduces the availability of P/Q-type channels.

The C-terminus of $Ca_V2.1$ is partly subjected to functional modulation on the inactivation speed by VDCC β_4-subunit [25]. Therefore, we analyzed the decay phase of Ba^{2+} currents evoked by 2 s prepulses. The decay phase was well fitted by two exponential functions with a non-inactivating component (Fig. 6A, 6D). Interestingly, tankyrase-2 significantly accelerated not slow but fast inactivation time constant (τ_{slow} and τ_{fast}, respectively) compared with control at test potentials between −20 mV and 30 mV in polyQ12 expressing BHK cells (Fig. 6B, 6C). There were no difference in the ratio of the three components, fast, slow, and

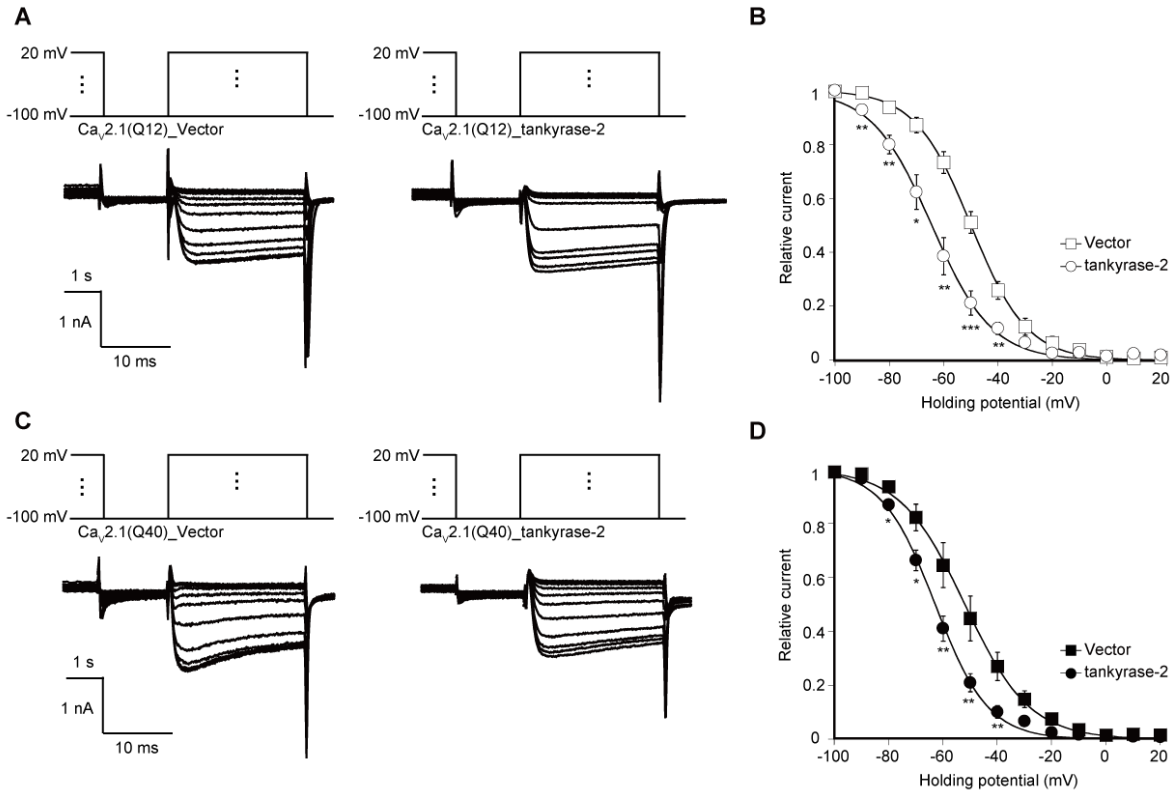

Fig. 5 Effects of tankyrase-2 on the inactivation curves of P/Q-type $Ca_V2.1$ currents with Q12 or Q40. (A, C) Representative traces of Ba^{2+} currents with or without tankyrase-2. $Ca_V2.1$ with Q12 (A) or Q40 (C) was expressed in BHK cells. (B, D) The voltage dependence of inactivation, determined by measuring the amplitude of the peak currents evoked by 20-ms test pulses to 5 mV following 2-s prepulses to potentials from −100 to 20 mV with increments of 10-mV from a V_h of −100 mV, was fitted with the Boltzmann's equation. $Ca_V2.1$ with Q12 (B) or Q40 (D) was expressed in BHK cells. $^{*}P < 0.05$, $^{**}P < 0.01$, $^{***}P < 0.001$ compared with Vector control. Data points are mean ± SEM.

non-inactivating components at test potentials (data not shown). On the other hand, in polyQ40 expressing cells, tankyrase-2 did not affect both τ_{slow} and τ_{fast} at test potentials between −20 mV and 30 mV (Fig. 6E, 6F). These data indicate that tankyrase-2 modulates the inactivation kinetics dependent on the length of polyQ at the C-terminus of $Ca_V2.1$.

VDCC β_4-subunit is translocated to nucleus by the elongation of polyQ tracts

Walker *et al*. have previously demonstrated that the C-terminus deletion mutant of β_4 cannot interact with C-terminus of $Ca_V2.1$ α_1-subunit, and results in slowing inactivation kinetics of VDCC [25] Thus, we

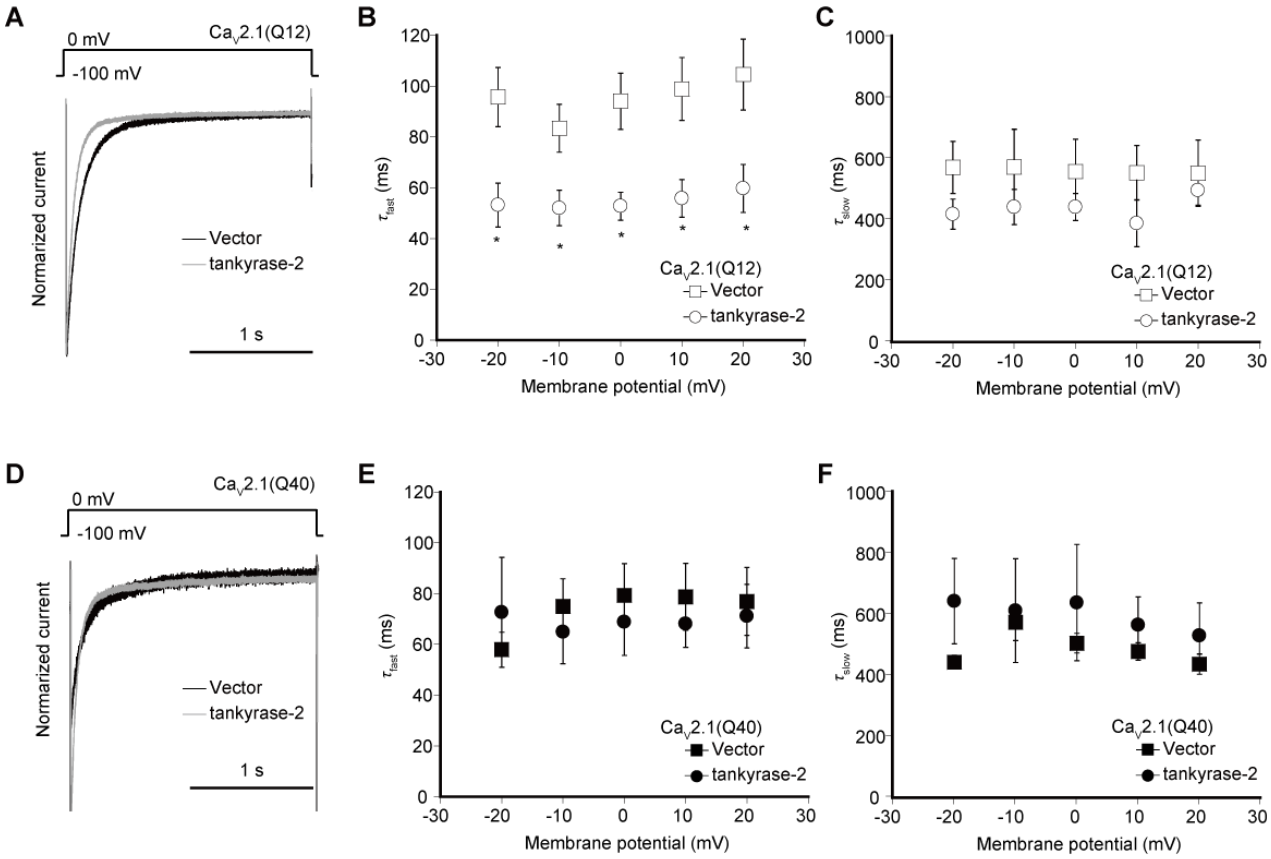

Fig. 6 Effects of tankyrase-2 on the inactivation kinetics of P/Q-type $Ca_V2.1$ channel with Q12 or Q40. (A, D) The peak amplitudes were normalized for Ba^{2+} currents elicited by 2-s pulses to 0 mV from a holding potential (V_h) of −100 mV before and after expression of tankyrase-2. $Ca_V2.1$ with Q12 (A) or Q40 (D) was expressed in BHK cells. (B, C) Voltage dependence of the two inactivation time constants, τ_{fast} (B) and τ_{slow} (C) in polyQ12-expressing cells. The mean inactivation time constants were plotted as a function of test potential from −20 mV to 30 mV. $^*P < 0.05$ compared with Vector control. (E, F) Voltage dependence of the two inactivation time constants, τ_{fast} (E) and τ_{slow} (F) in polyQ40-expressing cells. The mean inactivation time constants were plotted as a function of test potential from −20 mV to 30 mV. Data points are mean ± SEM.

---

hypothesized that overexpression of tankyrase may interfere the β_4-subunit-C-teminus of $Ca_V2.1$ interaction, and modify the β_4 subcellular localization. We then examined the effect of tankyrase on the β_4 subcellular localization in $Ca_V2.1$ with distinct length of polyQ expressing HEK293 cells. pK4K-BI-1-CAG (12 or 40), pEGFP-tankyrase-2 and pCI-β_4 were transfected into HEK293 cells. In polyQ12 expressing cells, tankyrase and β_4 highly expressed at the cytoplasm beside nucleus, the ratio of the fluorescence intensity at the cytoplasm, to that in a whole-cell—F_{cyto}/F_{total}—was 0.59 ± 0.02 (Fig. 7A, 7B). Interestingly, in polyQ40

Table 1 Effects of tankyrase-2 proteins on current density and activation of P/Q-type VDCC in BHK cells expressing $Ca_V2.1$ (Q12 or Q40), α_2/δ and β_4[1) 2) 3)].

		Current density (pA / pF)[4)]	Activation parameters	
			$V_{0.5}$ (mV)	k (mV)
Q12	Vector	–17.0 ± 1.3 (20)	–12.5 ± 1.0 (15)	5.7 ± 0.3 (15)
	tankyrase-2	–11.1 ± 1.5 (27) **	–14.1 ± 0.8 (17)	5.4 ± 0.3 (17)
Q40	Vector	–30.1 ± 4.1 (14)	–10.5 ± 0.7 (11)	6.1 ± 0.4 (11)
	tankyrase-2	–18.1 ± 3.5 (16) #	–10.3 ± 1.6 (9)	6.0 ± 0.6 (9)

1) $^{**}P < 0.01$ versus Q12_Vector.

2) $^{\#}P < 0.05$ versus Q40_Vector.

3) Numbers of cells analyzed are indicated in the parenthesis.

4) Ba^{2+} currents evoked by depolarizing pulse to 0 mV from a V_h of −100 mV are divided by capacitance.

Table 2 Effects of tankyrase-2 proteins on inactivation properties of P/Q-type VDCC in BHK cells expressing $Ca_V2.1$ (Q12 or Q40), α_2/δ and β_4[1) 2) 3)].

		Inactivation parameters		
		a	$V_{0.5}$ (mV)	k (mV)
Q12	Vector	1.00 ± 0.00 (6)	–50.0 ± 1.7 (6)	–10.0 ± 1.1 (6)
	tankyrase-2	0.97 ± 0.01 (9) **	–65.3 ± 2.6 (9) ***	–8.9 ± 0.7 (9)
Q40	Vector	0.98 ± 0.01 (8)	–52.9 ± 3.7 (8)	–9.3 ± 0.3 (8)
	tankyrase-2	0.98 ± 0.01 (7)	–63.3 ± 1.8 (7) ##	–8.9 ± 0.7 (7)

1) $^{**}P< 0.01$, $^{***}P < 0.001$ versus Q12_Vector.

2) $^{\#\#}P < 0.01$ versus Q40_Vector

3) Numbers of cells analyzed are indicated in the parenthesis.

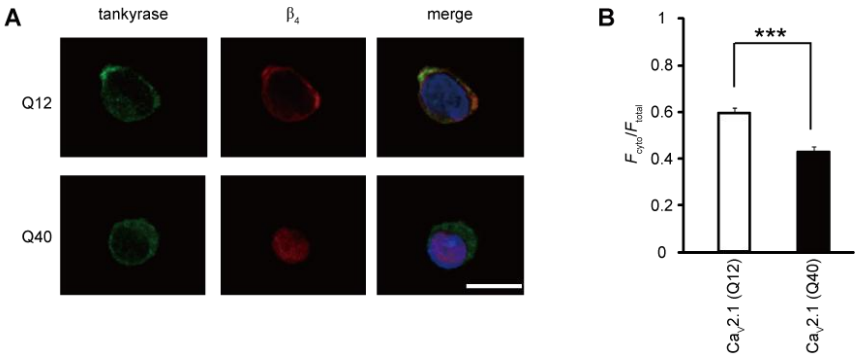

Fig. 7 Nuclear translocation of β_4-subunit in HEK293 cells expressing $Ca_V2.1$ Q12 or Q40. (A) Confocal imaging of HEK293 cells expressing EGFP-tankyrase-2 and recombinant β_4 with $Ca_V2.1$ Q12 or Q40.β_4 was immunostained by the antibody for β_4 [49]. Nuclei were stained with Hoechst 33342. Scale bar, 10 μm. (B) Subcellular localization of β_4 in a whole-cell. F_{cyto} and F_{total} mean the fluorescence intensity at the cytoplasm besides nucleus, and that in a whole-cell, respectively. ***$P < 0.001$. Data points are mean ± SEM.

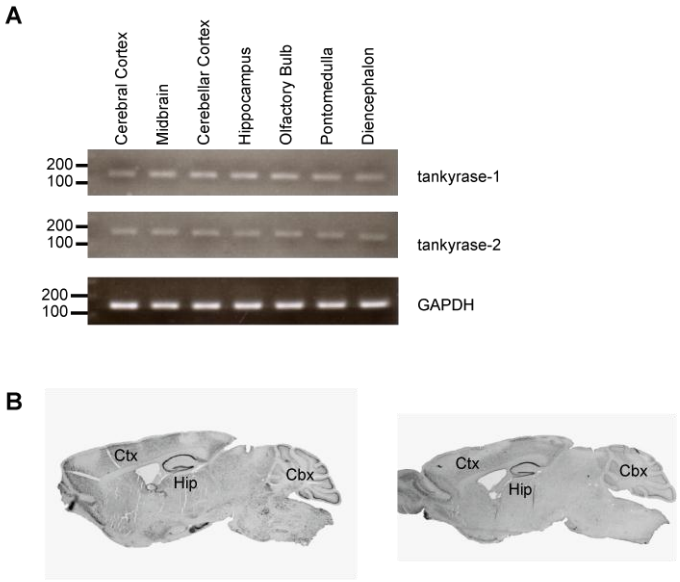

Fig. 8 Distribution of tankyrase in the brain. (A) RT-PCR analyses of the distribution of tankyrase RNAs in the brain. GAPDH is a loading control. (B) *in situ* hybridization photomicrographs show expression of tankyrase-1 (*left*) and tankyrase-2 (*right*) in the brain.

Table 3 Antisense and sense PCR primers used in RT-PCR analysis.

Gene	Orientation	Pair of primers for PCR (5' to 3')
tankyrase-1	Sense	TGCCTCTCTGATCTCACCAG
	Antisense	CAACTTCTCCTTCCTTCCTTTC
tankyrase-2	Sense	GCCAACCATCCGAAATACAG
	Antisense	GACTTTCTGCCATCACTTGC

expressing cells, the subcellular localization of tankyrase was not changed, whereas β_4 was dramatically translocated to the nucleus (Fig. 7A). The F_{cyto}/F_{total} ratio was statically reduced (0.43 ± 0.04) compared with that in polyQ12 expressing cells (Fig. 7B). These findings suggest that tankyrase binds to the C-terminus of $Ca_V2.1$ replacing with β_4 in the polyQ length-dependent manner, leading to the changes of VDCC function.

Discussion

In this work we have identified the novel interaction between tankyrase and C-terminus of $Ca_V2.1$, and functional modulation of tankyrase on electrophysiological properties of VDCC. Tankyrases are PARP family members that are comprised of ankyrin repeat domain, oligomerization domain called as SAM, and catalytic PARP domain (Fig. 1A). To date, it has been reported that ankyrin repeat domain often function in interaction with other proteins [42]. In addition, several molecules, such as polyglutamine binding protein 1, also interact with polyQ region of each protein [43]. Yeast two-hybrid assay and GST-pulldown assay have revealed that tankyrase binds to polyQ-elongated $Ca_V2.1$ α_1-subunit more strongly compared to the C-terminus of $Ca_V2.1$ with normal polyQ length. Therefore, our data indicate that the interaction of tankyrase with C-terminus is altered, hence the molecular assembly around VDCC might be changed in SCA6 patients.

Tankyrase 1 and 2 are broadly expressed in mice brain at mRNA levels (Fig. 8). Tankyrases bind to the telomeric protein TRF1, a negative regulator of telomere length maintenance [38], which is involved in telomere elongation and cell survivals [44-46]. Moreover, it has been reported that tankyrase poly ADP-ribosylated Axin, which is a negative regulator of Wnt/β-catenin signals, and destabilized Axin-β-catenin

complex [47]. However, few studies have been investigated for the function of tankyrase in a brain, except for a recent study about the remyelination from oligodendrocyte precursor cells [48]. We firstly demonstrate that tankyrase interacts with the C-terminus of $Ca_V2.1$ α_1-subunit, alters the microenvironment around VDCC complex, and functionally modulates VDCC properties. The fact that the interaction of tankyrase-2 with the C-terminus of $Ca_V2.1$ is augmented by the elongation of polyQ suggests that tankyrase affects the complex formation surrounding Ca^{2+} channels in SCA6 patients.

To date, several studies have showed that the polyQ expansion affects the electrophysiological function of P/Q-type $Ca_V2.1$ channel. Matsuyama *et al.* have reported that expansion of 30 or 40 polyQ in the C-terminus causes a significant shift in the voltage-dependence of inactivation in the hyperpolarizing direction [27]. Similar phenomenon has been observed in HEK293 cells system from another group [29]. On the other hand, other groups have demonstrated that polyQ expansion shifts the voltage-dependence of activation toward hyperpolarizing potentials in rabbit/human chimeric $Ca_V2.1$ carrying an SCA6 mutation expressed in *Xenopus* oocytes, or increases current density in human $Ca_V2.1$ with an expanded polyQ stretch expressed HEK293 cells [28, 30]. Main reason of these inconsistent results might be due to the differences in recombinant expression system. In either case, our data strongly support an idea that the dysfunction of VDCC has occurred in SCA6. In present study, tankyrase shifted the voltage-dependence of inactivation toward hyperpolarizing potentials in $Ca_V2.1$ with both polyQ length expressed BHK cells, despite the fact that the interaction between tankyrase and C-terminus of $Ca_V2.1$ is augmented by elongated polyQ length (Fig. 5). These results indicate that tankyrase may decrease the number of available channels at resting potentials. Although the reason for these differences between the molecular interaction and functional modulation is not completely understood, these effects might not be irrelevant. Furthermore, tankyrase reduced the current density of VDCC, thus it has been suggested that tankyrase suppresses the expression of Ca^{2+} channels at plasma membrane and inhibits the signal transduction after Ca^{2+} influx. This reduction of current density might be implicated in the fact that C-terminal fragment of $Ca_V2.1$ is translocated to the nucleus [37].

In consist with previous findings that VDCC β_4-subunit binds to the C-terminus of $Ca_V2.1$ and accelerates inactivation kinetics of VDCC [25], we have showed that tankyrase also accelerates VDCC inactivation in

polyQ12 expressed cells (Fig. 6). In addition, we have demonstrated that tankyrase facilitates the nuclear translocation of β_4 in a polyQ length dependent manner (Fig. 7). These results indicate that the acceleration of VDCC inactivation by tankyrase results from altering β_4-subunit localization at subcellular level. β_4 is present in the nucleus, and an atypical short splice variant of β_4 (β_{4c}) interacts with a nuclear protein, heterochromatin protein 1 gamma [49-51]. Recently, it has been reported that β_4 accumulates in the nucleus and regulates gene expression under membrane depolarization [52]. Thus, VDCC β_4-subunit might be movable and modulate several cellular responses. Taken together with our data that molecular interaction between tankyrase and C-terminus of $Ca_V2.1$ is dependent of the length of polyQ, it might be involved with the pathogenesis of SCA6 that tankyrase and β_4 may competitively associate with the C-terminus and regulate the Ca^{2+} channel function.

In conclusion, we demonstrate here that the direct interaction of tankyrase with polyQ containing C-terminus of $Ca_V2.1$, and modulate the channel function and the surrounding environment around Ca^{2+} channel, thus tankyrase might contribute the cause of SCA6. To uncover the role of tankyrase in disease condition, further *in vivo* experiments are required.

Experimental procedures

Yeast two-hybrid screening and β-galactosidase assay

The C-terminus (encoding 1971-2510 amino acid residue) of human $Ca_V2.1$ α_1-subunit (GenBank Accession Number AF_004884) subcloned from human brain Marathon-Ready cDNA (Clontech) into pGBK-T7 was used as a bait to screen a human brain pACT2 library (Clontech) in the yeast strain AH109 according to the manufacturer's instructions (Clontech). 2.5×10^6 transformants plated to synthetic medium lacking adenine, histidine, leucine, and tryptophan. His^+ colonies were assayed for β-galactosidase activity by a filter assay. Of the transformants, 56 were His^+, of which 6 were also $LacZ^+$. Prey clone encoding amino acid residues 89-380 of full length tankyrase-2 (GenBank Accession Number NM_025235) was isolated. Expression plasmids pGBK-T7 carrying $Ca_V2.1$ α_1- or its mutants were constructed by polymerase chain reaction (PCR).

cDNA cloning and construction of expression vectors

Tankyrase-1 (GenBank Accession Number NM_003747) and tankyrase-2 were cloned from human brain Marathon-Ready cDNA (Clontech) using PCR, and was subcloned into pEGFP-C1 (Clontech), the FLAG-tagged vector pCMV-tag2 (Stratagene), and the pIRES2-EGFP (Clontech). Human $Ca_V2.1$ C-terminus (amino acid residues 1971-2510) was subcloned into the pEGFP-C1. β_4-subunit (GenBank Accession Number XM_215742) was subcloned into pCI-neo (Clontech).

Construction of CAG-elongated $Ca_V2.1$

To construct CAG-elongated $Ca_V2.1$, the *Apa*I (7186)–*Msc*I (7230) fragment of human $Ca_V2.1$ (GenBank Accession Number AF_004884) containing 11 CAG repeats was replaced by the synthetic oligonucleotides containing CAG (40); the SCA6 sequence contains forty CAG repeats. For electrophysiological experiments, we used pK4K-BI-1-CAG (12) and CAG (40) described previously [27].

Production of GST fusion proteins

For production of GST fusion proteins for tankyrase-2 and the C-terminus of $Ca_V2.1$, cDNA for tankyrase-2 or C-terminal constructs, and the GST were subcloned together into the pET23 vector (Novagen). The Rosetta strain (Novagen) of *Escherichia coli* was transformed by the expression vectors, and protein expression/purification was performed according to the manufacturer's instruction (Novagen).

GST-pulldown assay and co-immunoprecipitation in HEK293 cells

HEK293 cells were cultured in Dulbecco's modified Eagle's medium (DMEM) containing 10 % fetal bovine serum, 30 units/ml penicillin, and 30 μg/ml streptomycin. 48 h after transfection, HEK293 cells were solubilized in Nonidet P-40 (NP-40) buffer (150 mM NaCl, 50 mM Tris, 1 % NP-40, and protease inhibitors), and then centrifuged at 17,400 × *g* for 20 min. For pulldown assay, the cell lysate was incubated with glutathione-Sepharose beads bound with purified fusion proteins at 4 °C, and then the beads were washed with

NP-40 buffer. The proteins retained on the beads were characterized by western blotting with anti-myc antibody (invitrogen). For co-immunoprecipitation, the cell lysate was incubated with anti-FLAG M2 monoclonal antibody (Sigma), and then the immunocomplexes were incubated with protein A-agarose beads (Santa Cruz), and the beads were washed with NP-40 buffer. Immunoprecipitated proteins were characterized by western blotting with anti-GFP antibody (Clontech).

Cell culture and cDNA expression in BHK cells

Baby hamster kidney (BHK) lines stably expressing α_2/δ and β_{4b} was described previously [53]. BHK cells were cultured in DMEM containing 10 % fetal bovine serum, 30 units/ml penicillin, and 30 μg/ml streptomycin. This BHK line was co-transfected with pK4K-BI-1-CAG (12 or 40) subunit and expression plasmids carrying tankyrase-2 constructs (pIRES2-EGFP-vector, pIRES2-EGFP-tankyrase-2) using Effectene Transfection Reagent (Qigagen). The cells were subjected to electrophysiological measurements 48 h after transfection.

Current recordings

Whole-cell mode of the patch-clamp technique was carried out at 22-25 °C with EPC-10 (HEKA Elektronik) patch-clamp amplifier as previously described [54]. Patch pipettes were made from borosilicate glass capillaries (1.5 mm outer diameter, 0.87 mm inner diameter; Hilgenberg) using a model P-87 Flaming-Brown micropipette puller (Sutter Instrument Co.). The patch electrodes were fire-polished. Pipette resistance ranged from 2 to 3.5 megohm when filled with the pipette solutions described below. The series resistance was electronically compensated to > 60 %, and both the leakage and the remaining capacitance were subtracted by –P/4 method. Currents were sampled at 100 kHz after low pass filtering at 8.4 kHz (3 db) in the experiments of activation kinetics, otherwise sampled at 20 kHz after low pass filtering at 3.0 kHz (3 db). Data were collected and analyzed using the PATCHMASTER (HEKA Elektronik). The external solution contained (in mM): 3 $BaCl_2$, 155 tetraethylammonium chloride (TEA-Cl), 10 HEPES, and 10 glucose (pH 7.4 adjusted with TEA-OH). The pipette solution contained (in mM): 95 CsOH, 95 aspartate, 40 CsCl, 4 $MgCl_2$, 5 EGTA, 2

disodium ATP, 5 HEPES and 8 creatine phosphate (pH 7.2 adjusted with CsOH).

Voltage-dependence of inactivation

To determine the voltage-dependence of inactivation (inactivation curve) of VDCCs, Ba^{2+} currents were evoked by 20-ms test pulse to 5 mV after the 10-ms repolarization to –100 mV following 2-s holding potential (V_h) displacement from −100 mV to 20 mV with 10-mV increments. Amplitudes of currents elicited by the test pulses were normalized to those elicited by the test pulse after a 2-s V_h displacement to −100 mV. The mean values were plotted against potentials of the 2-s V_h displacement. When the inactivation curve was monophasic, the mean values were fitted to the single Boltzmann's equation: $h(V_h) = (1–a)+a/\{1+\exp[(V_{0.5}–V_h)/k]\}$, with a, rate of inactivating component, $V_{0.5}$, potential to give a half-value of inactivation, and k, slope factor.

Voltage dependence of activation

Tail currents were elicited by repolarization to −60 mV after 5-ms test pulse from −40 to 40 mV with 5-mV increments. Currents were sampled at 100 kHz after low pass filtering at 8.4 kHz. Amplitude of tail currents were normalized to the tail current amplitude obtained with a test pulse to 30 mV. The mean values were plotted against test pulse potentials, and fitted to the Boltzmann's equation: $n(V_m) = 1/\{1+\exp[(V_{0.5}–V_m)/k]\}$, with V_m, membrane potential, $V_{0.5}$, potential to give a half-value of conductance, and k, slope factor.

Confocal imaging and immunocytochemistry

At 48 h after transfection, HEK293 cells were plated onto poly-L-lysine coated glass coverslips. Fluorescence images were acquired with a confocal laser-scanning microscope (Olympus FV500) using the 405-nm line of an laser diode for excitation and a 430-nm to 460-nm 5 band-pass filter for emission (Hoechst 33342), the 488-nm line of an argon laser for excitation and a 505-nm to 525-nm band-pass filter for emission (EGFP), or the 543-nm line of a HeNe laser for excitation and a 560-nm long pass filter for emission (Cy3). The specimens were viewed at high magnification using plan oil objectives (x60, 1.40 numerical aperture (NA),

Olympus). For immunocytochemistry, HEK293 cells were fixed in 0.1 M phosphate-buffer (PB, pH7.4) containing 4 % paraformaldehyde for 20 min at room temperature thoroughly washed with PB. Fixed cells were permeabilized with 5 % bovine serum albumin (BSA)/0.3 % Triton X-100/PB for 30 min at room temperature, and then incubated overnight with primary β_4 antibody [55] diluted in the blocking buffer (1 % BSA/PB) at 4 °C. The next day, cells were washed three times with PB and then were incubated with Cy3-conjugated secondary antibody at a 1:1000 dilution and Hoechst 33342 (1 μg/ml, Dojindo) in blocking buffer for 90 min at room temperature. Hoechst 33342 was used to stain nuclei.

RNA preparation, reverse transcription PCR (RT-PCR), and in situ hybridization histochemistry

Total RNA was prepared from various brain regions of 2-month-old C57BL/6 mice with ISOGEN total RNA isolation reagent (Nippon Gene) according to the manufacturer's instructions. RT-PCR analysis was performed using the LA-PCR kit (TaKaRa), according to the manufacturer's instructions. Primer sequences are indicated in Table 3. For histological staining of the central nervous system (CNS), adult mice (C57BL/6, body weight 20-25 g) were deeply anesthetized with an overdose of Nembutal and then transcardially perfused by 0.9 % NaCl, followed by 3 % paraformaldehyde in 0.1 M PB. The brains of the animals were dissected. Cryoprotection of the tissue blocks in 30 % sucrose for 24 h at 4 °C was followed by histological sectioning on a cryostat (Leica). For details about in situ hybridization histochemistry, see Kagawa *et al.* [56]. Briefly, *in vitro* transcribed DIG-labeled cRNA probe was generated against template tankyrase-1 or tankyrase-2 cDNA fragment corresponding to cording sequence of mouse tankyrase-1 or tankyrase-2 using DIG High Prime kit (Roche Applied Science). The probe (0.3 μg/ml) was hybridized overnight to mouse CNS histological 35-μm-thick sections at 50 °C. Positive signals were detected by alkaline phosphatase-conjugated antidigoxigenin antibody and the nitro blue tetrazolium/5-bromo-4-chloro-3'-indolyl phosphate reaction.

Statistical analysis

All data are expressed as means ± SEM. We accumulated the data under each condition from at least three independent experiments. Statistical significance was evaluated with an ANOVA followed by Tukey-Kramer

test. $P < 0.05$ was considered statistically significant.

Reference

[1] Zhuchenko, O., Bailey, J., Bonnen, P., Ashizawa, T., Stockton, D. W., Amos, C., Dobyns, W. B., Subramony, S. H., Zoghbi, H. Y., and Lee, C. C. (1997) *Nat. Genet.*, **15**, 62-69

[2] Gomez, C. M., Thompson, R. M., Gammack, J. T., Perlman, S. L., Dobyns, W. B., Truwit, C. L., Zee, D. S., Clark, H. B., and Anderson, J. H. (1997) *Ann. Neurol.*, **42**, 933-950

[3] Murata, Y., Kawakami, H., Yamaguchi, S., Nishimura, M., Kohriyama, T., Ishizaki, F., Matsuyama, Z., Mimori, Y., and Nakamura, S. (1998) *Arch. Neurol.*, **55**, 1348-1352

[4] Ishikawa, K., Watanabe, M., Yoshizawa, K., Fujita, T., Iwamoto, H., Yoshizawa, T., Harada, K., Nakamagoe, K., Komatsuzaki, Y., Satoh, A., Doi, M., Ogata, T., Kanazawa, I., Shoji, S., and Mizusawa, H. (1999) *J. Neurol. Neurosurg. Psychiatry*, **67**, 86-89

[5] Gusella, J. F., and MacDonald, M. E. (2000) *Nat. Rev. Neurosci.*, **1**, 109-115

[6] Zoghbi, H. Y., and Orr, H. T. (2000) *Annu. Rev. Neurosci.*, **23**, 217-247

[7] Mariotti, C., Gellera, C., Grisoli, M., Mineri, R., Castucci, A., and Di Donato, S. (2001) *Neurology*, **57**, 1502-1504

[8] Gatchel, J. R., and Zoghbi, H. Y. (2005) *Nat. Rev. Genet.*, **6**, 743-755

[9] Mori, Y., Friedrich, T., Kim, M. S., Mikami, A., Nakai, J., Ruth, P., Bosse, E., Hofmann, F., Flockerzi, V., Furuichi, T., Mikoshiba K., Imoto K., Tanabe T., and Numa S. (1991) *Nature*, **350**, 398-402

[10] Fletcher, C. F., Lutz, C. M., O'Sullivan, T. N., Shaughnessy, J. D. Jr., Hawkes, R., Frankel, W. N., Copeland, N. G., and Jenkins, N. A. (1996) *Cell*, **87**, 607-617

[11] Ertel, E. A., Campbell, K. P., Harpold, M. M., Hofmann, F., Mori, Y., Perez-Reyes, E., Schwartz, A., Snutch, T. P., Tanabe, T., Birnbaumer, L., Tsien, R. W., and Catterall, W. A. (2000) *Neuron*, **25**, 533-535

[12] Sheng, Z. H., Rettig, J., Takahashi, M., and Catterall, W. A. (1994) *Neuron*, **13**, 1303-1313

[13] Bezprozvanny, I., Scheller, R. H., and Tsien, R. W. (1995) *Nature*, **378**, 623-626

[14] Wiser, O., Bennett, M. K., and Atlas, D. (1996) *EMBO J.*, **15**, 4100-4110

[15] Zhong, H., Yokoyama, C. T., Scheuer, T., and Catterall, W. A. (1999) *Nat. Neurosci.*, **2**, 939-941

[16] Maximov, A., Südhof, T. C., and Bezprozvanny, I. (1999) *J. Biol. Chem.*, **274**, 24453-24456

[17] Maximov, A. and Bezprozvanny, I. (2002) *J. Neurosci.*, **22**, 6939-6952

[18] Spafford, J. D. and Zamponi, G. W. (2003) *Curr. Opin. Neurobiol.*, **13**, 308-314

[19] Nishimune, H., Sanes, J. R., and Carlson, S. S. (2004) *Nature*, **432**, 580-587

[20] Watanabe, H., Yamashita, T., Saitoh, N., Kiyonaka, S., Iwamatsu, A., Campbell, K. P., Mori, Y., and Takahashi, T. (2010) *J. Neurosci.*, **30**, 655-660

[21] Catterall, W. A., and Few, A. P. (2008) *Neuron*, **59**, 882-901

[22] Lee, A., Wong, S. T., Gallagher, D., Li, B., Storm, D. R., Scheuer, T., and Catterall, W. A. (1999) *Nature*, **399**, 155-159

[23] DeMaria, C. D., Soong, T. W., Alseikhan, B. A., Alvania, R. S., and Yue, D. T. (2001) *Nature*, **411**, 484-489

[24] Furukawa, T., Nukada, T., Mori, Y., Wakamori, M., Fujita, Y., Ishida, H., Fukuda, K., Kato, S., and Yoshii, M. (1998) *J. Biol. Chem.*, **273**, 17585-17594

[25] Walker, D., Bichet, D., Campbell, K. P., and De Waard, M. (1998) *J. Biol. Chem.*, **273**, 2361-2367

[26] Ishikawa, K., Fujigasaki, H., Saegusa, H., Ohwada, K., Fujita, T., Iwamoto, H., Komatsuzaki, Y., Toru, S., Toriyama, H., Watanabe, M., Ohkoshi, N., Shoji, S., Kanazawa, I., Tanabe, T., and Mizusawa, H. (1999) *Hum. Mol. Genet.*, **8**, 1185-1193

[27] Matsuyama, Z., Wakamori, M., Mori, Y., Kawakami, H., Nakamura, S., and Imoto, K. (1999) *J. Neurosci.*, **19**, RC14

[28] Restituito, S., Thompson, R. M., Eliet, J., Raike, R. S., Riedl, M., Charnet, P., and Gomez, C. M. (2000) *J. Neurosci.*, **20**, 6394-6403

[29] Toru, S., Murakoshi, T., Ishikawa, K., Saegusa, H., Fujigasaki, H., Uchihara, T., Nagayama, S., Osanai, M., Mizusawa, H., and Tanabe, T. (2000) *J. Biol. Chem.*, **275**, 10893-10898

[30] Piedras-Renteria, E. S., Watase, K., Harata, N., Zhuchenko, O., Zoghbi, H. Y., Lee, C. C., and Tsien, R. W.

(2001) *J. Neurosci.*, **21**, 9185-9193

[31] Kubodera, T., Yokota, T., Ohwada, K., Ishikawa, K., Miura, H., Matsuoka, T., and Mizusawa, H. (2003) *Neurosci. Lett.*, **341**, 74-78

[32] Matsuyama, Z., Yanagisawa, N. K., Aoki, Y., Black, J. L. 3rd, Lennon, V. A., Mori, Y., Imoto, K., and Inuzuka, T. (2004) *Neurobiol. Dis.*, **17**, 198-204

[33] Kordasiewicz, H. B., Thompson, R. M., Clark, H. B., and Gomez, C. M. (2006) *Hum. Mol. Genet.*, **15**, 1587-1599

[34] Saegusa, H., Wakamori, M., Matsuda, Y., Wang, J., Mori, Y., Zong, S., and Tanabe, T. (2007) *Mol. Cell. Neurosci.*, **34**, 261-270

[35] Watase, K., Barrett, C. F., Miyazaki, T., Ishiguro, T., Ishikawa, K., Hu, Y., Unno, T., Sun, Y., Kasai, S., Watanabe, M., Gomez, C. M., Mizusawa, H., Tsien, R. W., and Zoghbi, H. Y. (2008) *Proc. Natl. Acad. Sci. U. S. A.*, **105**, 11987-11992

[36] Ishiguro, T., Ishikawa, K., Takahashi, M., Obayashi, M., Amino, T., Sato, N., Sakamoto, M., Fujigasaki, H., Tsuruta, F., Dolmetsch, R., Arai, T., Sasaki, H., Nagashima, K., Kato, T., Yamada, M., Takahashi, H., Hashizume, Y., and Mizusawa, H. (2010) *Acta Neuorpathol.*, **119**, 447-464

[37] Kordasiewicz, H. B., and Gomez, C. M. (2007) *Neurotherapeutics*, **4**, 285-294

[38] Smith, S., Giriat, I., Schmitt, A., and de Lange, T., (1998) *Science*, **282**, 1484-1487

[39] Chi, N. W., and Lodish, H. F. (2000) *J. Biol. Chem.*, **275**, 38437-38444

[40] Lyons, R. J., Deane, R., Lynch, D. K., Ye, Z. S., Sanderson, G. M., Eyre, H. J., Sutherland, G. R., and Daly, R. J. (2001) *J. Biol. Chem.*, **276**, 17172-17180

[41] Kaminker, P. G., Kim, S. H., Taylor, R. D., Zebarjadian, Y., Funk, W. D., Morin, G. B., Yaswen, P., and Campisi, J. (2001) *J. Biol. Chem.*, **276**, 35891-35899

[42] Barrick, D., Ferreiro, D. U., and Komives, E. A. (2008) *Curr. Opin. Struct. Biol.*, **18**, 27-34

[43] Waragai, M., Lammers, C. H., Takeuchi, S., Imafuku, I., Udagawa, Y., Kanazawa, I., Kawabata, M., Mouradian, M. M., and Okazawa, H. (1999) *Hum. Mol. Genet.*, **8**, 977-987

[44] Bae, J., Donigian, J. R., and Hsueh, A. J. (2003) *J. Biol. Chem.*, **278**, 5195-5204

[45] Chiang, Y. J., Nguyen, M. L., Gurunathan, S., Kaminker, P., Tessarollo, L., Campisi, J., and Hodes, R. J. (2006) *Mol. Cell Biol.*, **26**, 2037-2043

[46] Smith, S., and de Lange, T. (2000) *Curr. Biol.*, **10**, 1299-1302

[47] Huang, S. M., Mishina, Y. M., Liu, S., Cheung, A., Stegmeier, F., Michaud, G. A., Charlat, O., Wiellette, E., Zhang, Y., Wiessner, S., Hild, M., Shi, X., Wilson, C. J., Mickanin, C., Myer, V., Fazal, A., Tomlinson, R., Serluca, F., Shao, W., Cheng, H., Shultz, M., Rau, C., Schirle, M., Schlegl, J., Ghidelli, S., Fawell, S., Lu, C., Curtis, D., Kirschner, M. W., Lengauer, C., Finan, P. M., Tallarico, J. A., Bouwmeester, T., Porter, J. A., Bauer, A., and Cong, F. (2009) *Nature*, **461**, 614-620

[48] Fancy, S. P., Harrington, E. P., Yuen, T. J., Silbereis, J. C., Zhao, C., Baranzini, S. E., Bruce, C. C., Otero, J. J., Huang, E. J., Nusse, R., Franklin, R. J., and Rowitch, D. H. (2011) *Nat. Neurosci.*, **14**, 1009-1016

[49] Hibino, H., Pironkova, R., Onwumere, O., Rousset, M., Charnet, P., Hudspeth, A. J., and Lesage, F. (2003) *Proc. Natl. Acad. Sci. U. S. A.*, **100**, 307-312

[50] Xu, X., Lee, Y. J., Holm, J. B., Terry, M. D., Oswald, R. E., and Horne, W. A. (2011) *J. Biol. Chem.*, **286**, 9677-9687

[51] Subramanyam, P., Obermair, G. J., Baumgartner, S., Gebhart, M., Striessnig, J., Kaufmann, W. A., Geley, S, and Flucher, B. E. (2009) *Channels (Austin)*, **3**, 343-355

[52] Tadmouri, A., Kiyonaka, S., Barbado, M., Rousset, M., Fablet, K., Sawamura, S., Bahembera, E., Pernet-Galley, K., Arnoult, C., Miki, T., Sadoul, K., Gory-Faure, S., Lambrecht, C., Lesage, F., Akiyama, S., Khochbin, S., Baulande, S., Janssens, V., Andrieux, A., Dolmetsch, R., Ronjat, M., Mori, Y., and De Waard, M. (2012) *EMBO J.*, **31**, 3730-3744

[53] Niidome, T., Teramoto, T., Murata, Y., Tanaka, I., Seto, T., Sawada, K., Mori, Y., and Katayama, K. (1994) *Biochem. Biophys. Res. Commun.*, **203**, 1821-1827

[54] Wakamori, M., Yamazaki, K., Matsunodaira, H., Teramoto, T., Tanaka, I., Niidome, T., Sawada, K., Nishizawa, Y., Sekiguchi, N., Mori, E., Mori, Y., and Imoto, K. (1998) *J. Biol. Chem.*, **273**, 34857-34867

[55] Kiyonaka, S., Wakamori, M., Miki, T., Uriu, Y., Nonaka, M., Bito, H., Beedle, A. M., Mori, E., Hara, Y., De Waard, M., Kanagawa, M., Itakura, M., Takahashi, M., Campbell, K. P., and Mori, Y. (2007) *Nat.*

Neurosci., **10**, 691-701

[56] Kagawa, T., Ikenaka, K., Inoue, Y., Kuriyama, S., Tsujii, T., Nakao, J., Nakajima, K., Aruga, J., Okano, H., and Mikoshiba, K. (1994) *Neuron*, **13**, 427-442

General Conclusion

The first two chapters carried out to reveal physiological role of novel VDCC complexes in neurotransmission and suggested novel function of the VDCC β-subunit as a node of presynaptic protein assembly. The second two chapters carried out to reveal physiological role of VDCC complexes in neuronal disease conditions and suggested novel pathological mechanism involved with the disruption of VDCC functions.

Physical and functional interaction of the active zone protein CAST/ERC2 and the β-subunit of the voltage-dependent Ca^{2+} channel

In the nerve terminals, active zone protein CAST/ERC2 forms a protein complex with the other active zone proteins, and is thought to play an organizational and functional role in neurotransmitter release. This study demonstrates that CAST/ERC2 physically interacts with VDCC β-subunits and forms channelsomes at the presynaptic active zone. Moreover, CAST/ERC2 functionally modulates the opening of VDCCs via interacting β-subunit. Notably, this is the first report to show that the activation of VDCC is directly modified by an active zone protein. Thus, these findings suggest that the voltage-dependent Ca^{2+} channelsomes including CAST/ERC2 are required for efficient neurotransmission.

Functional impacts of Munc18-1 on gating properties of voltage-dependent Ca^{2+} channels

Coupling of presynaptic VDCCs with various active zone proteins is essential for neurotransmitter release in mammalian neuron. The study shows that Munc18-1, which is one of the presynaptic proteins, directly associates with VDCC α_1- and β-subunits and forms complexes. Functional characterization of Munc18-1 demonstrates that Munc18-1 negatively shifts the voltage-dependence of VDCC inactivation and inhibits Ca^{2+} entry into the cells. Moreover, the study suggests Munc18-1 functionally modulates VDCC function, competitive with syntaxin 1A. Therefore, the present study provides new insights into the molecular assembly to work for neurotransmitter release at presynaptic nerve terminal.

Rab3 interacting molecule 3 mutations associated with autism alter regulation of voltage-dependent Ca^{2+} channels.

Autism is a wide-spectrum neurodevelopmental disorder and it has been thought to be involved with synaptic disturbance. Our present study provide new insights that autism phenotypes are at least partly due to altered regulation of presynaptic VDCC currents and neurotransmitter release. We demonstrate that the mouse RIM3 mutant E176A and M259V, equivalent to the human autism mutation, alter RIM3 function in regulating VDCC currents. In addition, two RIM3 mutants partly suppress the neurotransmitter release and $[Ca^{2+}]_i$ elevation in PC12 cells. Hence, the present data suggest that functional alteration of RIM3 on calcium regulation may be relevant for the pathological mechanism of neurodevelopmental disorders caused by synaptic dysfunction.

Tankyrase contributes to the risk of spinocerebellar ataxia type 6 by binding of the C-terminal of voltage-dependent Ca^{2+} channels

SCA6 is one of the intractable neurodegenerative diseases related to polyQ expansion. In present study, we showed the possibility that tankyrase is a contributor to the pathogenic risk of SCA6. Tankyrase directly binds to the C-terminus of $Ca_V2.1$, and modulates Ca^{2+} channel function in a polyQ length-dependent manner. Moreover, we also demonstrate that VDCC β_4-subunit is translocated into nucleus by the elongation of polyQ in $Ca_V2.1$. These results indicate that the impairment of channel-tankyrase complex formation and dysfunction in Ca^{2+} channels are implicated in the SCA6 pathogenesis. Therefore, functional modulators of tankyrase may have therapeutic potentials for SCA6.

List of Publications

- Research articles -

[1] Physical and functional interaction of the active zone protein CAST/ERC2 and the β-subunit of the voltage-dependent Ca^{2+} channel.

Shigeki Kiyonaka, Hiroshi Nakajima, **Yoshinori Takada**, Yamato Hida, Toshinori Yoshioka, Akari Hagiwara, Isao Kitajima, Yasuo Mori, and Toshihisa Ohtsuka.

J. Biochem., **152**, 149-159, 2012. (Chapter 1)

[2] Functional impact of Munc18-1 on gating properties of voltage-dependent Ca^{2+} channels.

Yoshinori Takada, Hiroshi Nakajima, Yoshitsugu Uriu, Shigeki Kiyonaka, and Yasuo Mori.

Manuscript in preparation. (Chapter 2)

[3] Rab3 interacting molecule 3 mutations associated with autism alter regulation of voltage-dependent Ca^{2+} channels.

Yoshinori Takada, Mitsuru Hirano, Shigeki Kiyonaka, Yoshifumi Ueda, Kazuma Yamaguchi, Keiko Nakahara, Masayuki X Mori, and Yasuo Mori.

Cell Calcium, **58**, 296-306, 2015. (Chapter 3)

[4] Tankyrase contributes to the risk of spinocerebellar ataxia type 6 by binding of the C-terminal of the voltage-dependent Ca^{2+} channels.

Yoshinori Takada, Kazuma Yamaguchi, Mitsuru Hirano, Masayuki X Mori, and Yasuo Mori.

Manuscript in preparation. (Chapter 4)

- Review articles -

[1] Molecular architecture of Ca^{2+} channel complexes in presynaptic active zones.

Akito Nakao, Mitsuru Hirano, **Yoshinori Takada**, Shigeki Kiyonaka, and Yasuo Mori.

In Stephens G; Mochida S, editor. *Modulation of presynaptic calcium channels*, Springer Publishing Group; Chapter 4, 79-99, 2013.

[2] Targeting TRPs in neurodegenerative disorders.

Yoshinori Takada, Tomohiro Numata, and Yasuo Mori.

Curr. Top. Med. Chem., **13**, 322-334, 2013.

- Japanese review articles -

[1] Calcium channels regulate neuronal function, gene expression, and development.

Akito Nakao, **Yoshinori Takada**, and Yasuo Mori.

Brain Nerve, **63**, 657-667, 2011.

[2] Ca^{2+}チャネルソーム

瓜生　幸嗣, 清中　茂樹, **高田　宜則**, 森　泰生

遺伝子医学MOOK, **19**, 210-219, 2011.

[3] TRP チャネル(キーワード解説)

高田　宜則, 森　泰生

日本薬理学雑誌, **139**, 39-40, 2012.

[4] 電位依存性チャネル

若森　実, 三木　崇文, 中尾　章人, **高田　宜則**, 森　泰生

脳神経科学イラストレイテッド, **3**, 185-192, 2013.